Journal of Magnetic Resonance Open 23 (2025) 100191

Contents lists available at ScienceDirect

Journal of Magnetic Resonance Open

journal homepage: www.sciencedirect.com/journal/journal-of-magnetic-resonance-open

Tutorial paper

Introduction to average Hamiltonian theory. II. Advanced examples

Andreas Brinkmann

Metrology, National Research Council Canada, 1200 Montreal Road, M-40 Ottawa, Ontario K1A 0R6, Canada

ARTICLE INFO

Keywords:
Average Hamiltonian theory
Decoupling
Recoupling
Rotational-echo double resonance (REDOR)
Lee–Goldburg (LG) homonuclear dipolar decoupling
Flip-Flop Lee–Goldburg (FFLG)
Frequency-switched Lee–Goldburg (FSLG)

ABSTRACT

Where the first part of our tutorial *Introduction to average Hamiltonian theory* (Brinkmann, 2016) introduced in detail the basic concepts and demonstrated the application to two composite radio-frequency (rf) pulses in nuclear magnetic resonance (NMR) spectroscopy, this second part will present in a comprehensive but educational manner two, more advanced examples for the application of average Hamiltonian theory in solid-state NMR spectroscopy, both to analyse and design rf pulse sequences: (i) The Rotational-Echo Double Resonance (REDOR) sequence, which recouples the heteronuclear dipolar coupling during sample rotation around an axis at the magic-angle of 54.74° with respect to the external static magnetic field. We will gradually increase the complexity of applying average Hamiltonian theory by first considering ideal, infinitesimally short rf pulses. Next, we will examine finite pulses with an rf phase of zero, and finally, we will explore finite pulses with arbitrary rf phases. In the latter case, if a first order average Hamiltonian proportional to heteronuclear longitudinal two-spin order ($2I_zS_z$) is desired, solutions for the choice of rf phases include the XY and MLEV type schemes. (ii) The Lee–Goldburg homonuclear dipolar decoupling sequence under static samples conditions and its improved successors, Flip-Flop Lee–Goldburg (FFLG) and Frequency-Switched Lee–Goldburg (FSLG).

1. Introduction

This tutorial paper is the second part of the *Introduction to average Hamiltonian theory*. It continues seamlessly where the first part left off [1]. It focusses on two, more advanced examples for the application of average Hamiltonian theory in solid-state nuclear magnetic resonance (NMR) spectroscopy both to analyse and design radio-frequency (rf) pulse sequences: (i) The REDOR pulse sequence [2,3] that achieves the *recoupling* of the heteronuclear dipolar coupling during magic-angle spinning (MAS) of the sample by suspending the averaging of the interaction by the sample rotation; (ii) The original Lee-Goldburg (LG) sequence [4,5] and its improvements Flip-Flop Lee-Goldburg (FFLG) [6,7] and Frequency-Switched Lee-Goldburg (FSLG) [8,9] that all achieve *decoupling* of the homonuclear dipolar coupling. These pulse sequences are examples of the vast number of decoupling and recoupling pulse sequences that have been developed over the last decades both for solution and solid-state NMR spectroscopy often with the help of average Hamiltonian theory [10–19]. In Part I, we discussed several alternative approaches for approximating solutions to the time-dependent Schrödinger equation for a spin system in the presence of rf pulses. These approaches include Floquet theory [20–22], the Fer expansion [23,24], and, more generally, numerical simulations [25–27].

As this tutorial paper continues Part I of the *Introduction to average Hamiltonian theory*, the fundamentals of quantum mechanics and average Hamiltonian theory that were presented in detail in there will not be repeated here, rather the reader is encouraged to consult Part I in parallel while reading Part II. Cross references to equations and sections in Part I will be indicated by the prefix "I-". For example, "Eq. (I-1)" and "section I-2.1" refer to Eq. (1) and Section 2.1 in Part I of the *Introduction to average Hamiltonian theory* [1].

The advanced examples in this paper are based on educational lectures on average Hamiltonian theory presented at different NMR conferences and solid-state NMR summerschools. In Section 2 of this tutorial first order average Hamiltonian theory is used to describe the REDOR heteronuclear recoupling sequences for three cases, gradually increasing in difficulty: (i) using ideal (infinitesimal short) rf pulses in Section 2.2, (ii) employing finite rf pulses with all rf phases set to zero in Section 2.3, and (iii) applying finite rf pulses with arbitrary rf phases in Section 2.4. Finally, in Section 3 the LG homonuclear decoupling sequence and its improvements FFLG and FSLG are analysed in first and second order average Hamiltonian theory

2. Rotational-Echo Double Resonance (REDOR)

2.1. Heteronuclear dipolar coupling

2.1.1. Hamiltonian in static solids

As described in detail in Appendix C.8.2 The nuclear spin Hamiltonian of the direct heteronuclear dipolar coupling in static solids

E-mail address: Andreas.Brinkmann@nrc-cnrc.gc.ca.

https://doi.org/10.1016/j.jmro.2025.100191
Received 8 November 2024; Received in revised form 30 January 2025; Accepted 7 February 2025
Available online 16 February 2025

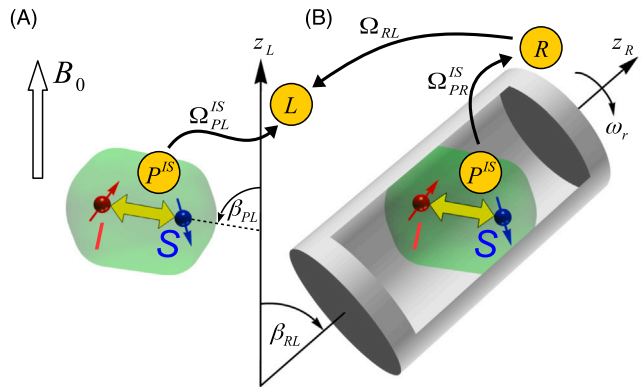

Fig. 1. (A) Visualization of two heteronuclear dipolar coupled spins I and S, where the principal axis system P^{IS} and laboratory reference frame L are depicted together with the Euler angles Ω_{PL}^{IS} relating the two reference frames. (B) Illustration of a heteronuclear dipolar coupled spin pair in an MAS NMR rotor together with the relevant reference frames, and connecting Euler angles.

between two nuclear spins I and S in the high-field approximation and in the interaction frame of the Zeeman interaction (i. e. the *rotating frame*, see section I-3.2), can be written in the following way:

$$H_{IS}^{\mathrm{DD}} = \omega_{IS}^{\mathrm{DD}}\, 2I_zS_z, \tag{1}$$

where the time-independent dipolar frequency $\omega_{IS}^{\mathrm{DD}}$ is obtained by transforming the tensor of the heteronuclear dipolar coupling from the principle axis system (PAS) denoted P^{IS} to the laboratory frame L as shown in Fig. 1(A):

$$\begin{aligned}\omega_{IS}^{\mathrm{DD}} &= b_{IS}\, D_{00}^{(2)}\big(\Omega_{PL}^{IS}\big)\\ &= b_{IS}\, d_{00}^{(2)}\big(\beta_{PL}^{IS}\big)\\ &= b_{IS}\, \frac{1}{2}\left(3\cos^2\beta_{PL}^{IS} - 1\right)\end{aligned} \tag{2}$$

where the Euler angles $\Omega_{PL}^{IS} = \{\alpha_{PL}^{IS}, \beta_{PL}^{IS}, \gamma_{PL}^{IS}\}$ define the relative orientation of the PAS and the laboratory frame. If we consider a powdered sample the Euler angles Ω_{PL}^{IS} are random variables, i. e. all possible orientations occur with equal probability. The only relevant angle β_{PL}^{IS} here encloses the internuclear vector between spins I and S and the external static magnetic field B_0. $D_{mm'}^{(l)}$ and $d_{mm'}^{(l)}$ are the elements of the Wigner D-matrix and the Wigner d-matrix, respectively [25,28]. At the *magic angle* $\theta = \arctan\sqrt{2} \approx 54.74°$ the Wigner d-matrix element $d_{00}^{(2)}$ vanishes, i. e. $d_{00}^{(2)}(\theta) = (3\cos^2\theta - 1)/2 = 0$. A more general discussion of suitable reference frames in solid-state NMR can be found in Appendix C.3.

As defined in Appendix C.8.2, the heteronuclear dipolar coupling constant b_{IS} is given by

$$b_{IS} = -\frac{\mu_0}{4\pi}\frac{\gamma_I\gamma_S\hbar}{r_{IS}^3}, \tag{3}$$

where in the Appendix examples of typical heteronuclear dipolar coupling constants are given, which are also depicted in Fig. 2.

2.1.2. Hamiltonian under magic-angle spinning

In magic-angle spinning (MAS) NMR the sample is rapidly rotated around an axis at the magic-angle of 54.74° with respect to the external static magnetic field. This is depicted in Fig. 1(B). In this case the Hamiltonian of the heteronuclear dipolar coupling becomes time dependent:

$$H_{IS}^{\mathrm{DD}}(t) = \omega_{IS}^{\mathrm{DD}}(t)\, 2I_zS_z, \tag{4}$$

where the time-dependent dipolar frequency $\omega_{IS}^{\mathrm{DD}}(t)$ is again obtained by transforming the tensor of the heteronuclear dipolar coupling from the PAS P^{IS} to the laboratory frame L. However, it is useful to

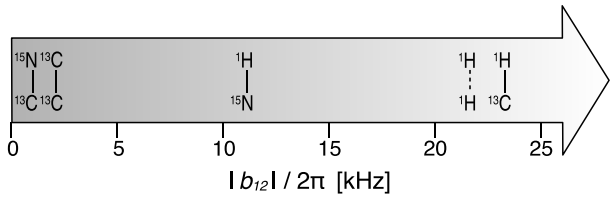

Fig. 2. Examples of homo- and heteronuclear dipolar coupling constants b_{12} between two spins labelled 1 and 2 are depicted. The examples correspond to typical one-bond internuclear distances (^{13}C–^{15}N,^{13}C–^{13}C, ^{15}N–^{1}H and ^{13}C–^{1}H) and the ^{1}H···^{1}H internuclear distance in a CH_2 group.

introduce an intermediate step the transformation into the rotor frame R as shown in Fig. 1(B):

$$\omega_{IS}^{\mathrm{DD}}(t) = b_{IS}\sum_{m=-2}^{2} D_{0m}^{(2)}\big(\Omega_{PR}^{IS}\big)\, D_{m0}^{(2)}\big(-\omega_r t, \theta, 0\big), \tag{5}$$

where the Euler angles $\Omega_{PR}^{IS} = \{\alpha_{PR}^{IS}, \beta_{PR}^{IS}, \gamma_{PR}^{IS}\}$ define the relative orientation of the PAS and the rotor frame. In powdered samples the Euler angles Ω_{PR}^{IS} are random variables. The Euler angles $\Omega_{RL} = \{-\omega_r t, \theta, 0\}$ describe the transformation from the rotor frame to the laboratory frame, where ω_r is the sample spinning frequency and $\theta = \arctan\sqrt{2} \approx 54.74°$ is the magic angle enclosing the rotation axis and the external static magnetic field [14,19,25,29]. A more general discussion of the transformations into suitable reference frames for the description of MAS experiments can be found in Appendix C.10.

Using the definition of the Wigner D-matrix [25,28], the time-dependent dipolar frequency may be further simplified:

$$\begin{aligned}\omega_{IS}^{\mathrm{DD}}(t) &= \sum_{m=-2}^{2}\frac{1}{2}\Omega^{(m)}\exp\{\mathrm{i}\, m(\omega_r t - \gamma_{PR}^{IS})\}\\ &= \sum_{m=1}^{2}\Omega^{(m)}\cos\big(m(\omega_r t - \gamma_{PR}^{IS})\big)\\ &= \omega^{(1)}(t) + \omega^{(2)}(t),\end{aligned} \tag{6}$$

where the time-dependent and time-independent dipolar frequency coefficients $\omega^{(m)}(t)$ and $\Omega^{(m)}$ have been introduced, respectively. The sum over $m = -2, -1, 0, 1, 2$ has been replaced by the sum over $m = 1, 2$, where the property $d_{00}^{(2)}(\theta) = (3\cos^2\theta - 1)/2 = 0$ for $\theta = \arctan\sqrt{2} \approx 54.74°$ has been exploited. The real coefficients $\omega^{m}(t)$ and Ω^{m} are defined as

$$\Omega^{(m)} = 2\, b_{IS}\, d_{0m}^{(2)}\big(\beta_{PR}^{IS}\big) d_{m0}^{(2)}(\theta) \tag{7}$$

$$\omega^{(m)}(t) = \Omega^{(m)}\cos\big(m(\omega_r t - \gamma_{PR}^{IS})\big) \tag{8}$$

with $\Omega^{(-m)} = \Omega^{(m)}$ and $\omega^{(-m)} = \omega^{(m)}$. For $m = 1, 2$ these coefficients are explicitly given by:

$$\Omega^{(1)} = -\frac{1}{\sqrt{2}}\, b_{IS}\sin\big(2\beta_{PR}^{IS}\big) \qquad \Omega^{(2)} = \frac{1}{2}\, b_{IS}\sin^2\big(\beta_{PR}^{IS}\big) \tag{9}$$

$$\omega^{(1)}(t) = \Omega^{(1)}\cos\big(\omega_r t - \gamma_{PR}^{IS}\big) \qquad \omega^{(2)}(t) = \Omega^{(2)}\cos\big(2(\omega_r t - \gamma_{PR}^{IS})\big). \tag{10}$$

Fig. 3 shows the time dependence of the dipolar frequencies $\omega^{(1)}(t)$ and $\omega^{(2)}(t)$ for a single crystallite orientation, i. e. for a single specific set of Euler angles $\Omega_{PR}^{IS} = \{\alpha_{PR}^{IS}, \beta_{PR}^{IS}, \gamma_{PR}^{IS}\}$, over two rotational periods. $\omega^{(1)}(t)$ is periodic with a single rotor period $\tau_r = 2\pi/\omega_r$, whereas $\omega^{(2)}(t)$ is periodic with half a rotor period $\tau_r/2$. Furthermore, the ratio of the amplitudes of $\omega^{(1)}(t)$ and $\omega^{(2)}(t)$ is given by $\sqrt{2}$. The following time symmetries can be derived from Eq. (10):

$$\omega^{(1)}(t + \frac{\tau_r}{2}) = -\omega^{(1)}(t) \qquad \omega^{(2)}(t + \frac{\tau_r}{2}) = \omega^{(2)}(t) \tag{11}$$

$$\omega^{(1)}(t + \tau_r) = \omega^{(1)}(t) \qquad \omega^{(2)}(t + \tau_r) = \omega^{(2)}(t) \tag{12}$$

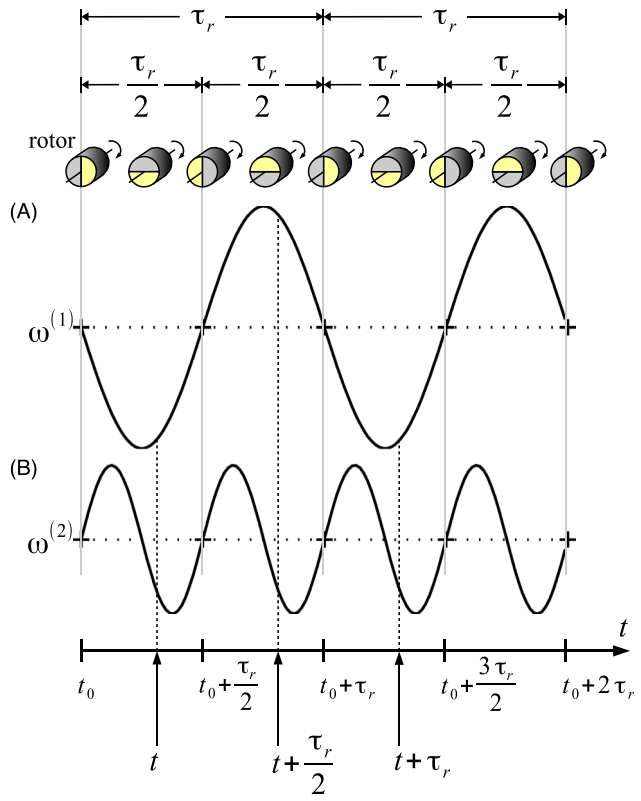

Fig. 3. Time dependence of the heteronuclear dipolar coupling under MAS. Two rotational periods and the corresponding positions of the rotor are depicted on the top. The evolution of the dipolar frequency coefficients $\omega^{(1)}(t)$ and $\omega^{(2)}(t)$ as a function of time is shown in panels (A) and (B), respectively.

2.1.3. Propagator

As depicted in Fig. I-1, in order to calculate the evolution of a spin-system ensemble from time point $t_a = 0$ to time point $t_b = t$ under the heteronuclear dipolar coupling Hamiltonian $H_{IS}^{\mathrm{DD}}(t)$ defined in Eq. (4) during an MAS experiment, the propagator $U(t,0)$ needs to be determined by solving the Schrödinger equation (I-5) for the propagator. Although, the Hamiltonian $H_{IS}^{\mathrm{DD}}(t)$ is time-dependent, it commutes with itself at all time points in the interval $[0,t]$. As discussed in section I-2.2 and depicted in the flowchart Fig. I-2 this is the *inhomogeneous* case in the sense of Maricq and Waugh [30], and the propagator for a single crystallite orientation Ω_{PR}^{IS} can be derived analytically according to Eq. (I-8):

$$\begin{aligned} U(t,0) &= \exp\left\{-\mathrm{i}\int_0^t \mathrm{d}t'\; H_{IS}^{\mathrm{DD}}(t')\right\} \\ &= \exp\left\{-\mathrm{i}\,2\,I_z S_z \int_0^t \mathrm{d}t'\; \omega_{IS}^{\mathrm{DD}}(t')\right\} \\ &= \exp\left\{-\mathrm{i}\,2\,I_z S_z\,\Phi(t,0)\right\}, \end{aligned} \tag{13}$$

where the phase $\Phi(t,0)$ has been introduced:

$$\begin{aligned} \Phi(t,0) &= \int_0^t \mathrm{d}t'\; \omega_{IS}^{\mathrm{DD}}(t') \\ &= \int_0^t \mathrm{d}t'\; \left\{\omega^{(1)}(t) + \omega^{(2)}(t)\right\} \\ &= \frac{b_{IS}}{2\omega_r}\Big\{ -2\sqrt{2}\sin\left(2\beta_{PR}^{IS}\right)\cos\left(\frac{\omega_r t}{2} - \gamma_{PR}^{IS}\right)\sin\left(\frac{\omega_r t}{2}\right) \\ &\qquad + \sin^2\left(\beta_{PR}^{IS}\right)\cos\left(\omega_r t - 2\gamma_{PR}^{IS}\right)\sin\left(\omega_r t\right)\Big\} \end{aligned} \tag{14}$$

Consider two spin-½ nuclei I and S during an MAS experiment, evolving under the heteronuclear dipolar coupling Hamiltonian Eq. (4). Furthermore, assume they are prepared such that the initial density operator at time point $t_a = 0$ is given by I-spin x-magnetization, i. e. $\rho(0) = I_x$. With the help of the propagator Eq. (13) the density operator at a later time point $t_b = t$ can be calculated using Eq. (I-12):

$$\begin{aligned} \rho(t) &= U(t,0)\,\rho(0)\,U^{\dagger}(t,0) \\ &= \exp\left\{-\mathrm{i}\,2\,I_z S_z\,\Phi(t,0)\right\}\, I_x\, \exp\left\{\mathrm{i}\,2\,I_z S_z\,\Phi(t,0)\right\} \\ &= I_x\,\cos\left(\Phi(t,0)\right) + 2I_y S_z\,\sin\left(\Phi(t,0)\right), \end{aligned} \tag{15}$$

where we have used the property of spin-½ nuclei that in the $(I_x, 2I_yS_z, 2I_zS_z)$ operator subspace, the *heteronuclear longitudinal two-spin order* operator $2I_zS_z$ induces a rotation in the $(I_x, 2I_yS_z)$-plane [31,32].

The time-dependent I-spin NMR signal $S(t;\Omega_{PR}^{IS})$ for a single crystallite orientation Ω_{PR}^{IS} can be obtained by calculating the normalized trace of the product of the density operator $\rho(t)$ and the signal detection operator I^+:

$$\begin{aligned} S(t;\Omega_{PR}^{IS}) &= \frac{\mathrm{Tr}\left\{I^+\rho(t)\right\}}{\mathrm{Tr}\left\{I_x^2\right\}} \\ &= \cos\left(\Phi(t,0)\right). \end{aligned} \tag{16}$$

In a powder sample the final I-spin signal is obtained by averaging over all possible orientations Ω_{PR}^{IS}:

$$S(t) = \left\langle \cos\left(\Phi(t,0)\right)\right\rangle_{\Omega_{PR}^{IS}} \tag{17}$$

Fig. 4 shows examples of the calculated time-dependent I-spin signal $S(t)$, or *free induction decay* (FID) and its Fourier transformed spectrum $S(\Omega)$ for a two (I, S)-spin system in a powdered sample with a heteronuclear dipolar coupling constant of $b_{IS}/2\pi$ = 950 Hz, which corresponds to a typical ^{13}C–^{15}N internuclear distance of 147.7 pm. The first column shows the first 20 ms of the FID without any additional line-broadening applied, whereas the second column shows the full FID used for Fourier transformation, where additional line broadening has been applied. The bottom row (J)–(L) shows the results for a static sample, in which case the spectrum (L) shows the typical *Pake doublet* or *Pake pattern* of a heteronuclear dipolar coupled spin-½ [33]. The distance between the two inner discontinuities is equal to the dipolar coupling constant $b_{IS}/2\pi$.

The remaining rows in Fig. 4 show from bottom to top results calculated under MAS with increasing spinning frequencies of 100, 400 and 4000 Hz, respectively. At 100 Hz MAS frequency $\omega_r \ll b_{IS}$ applies, and the time signal $S(t)$ depicted in (G) and (H) shows pronounced rotational echoes occurring every rotational period τ_r. During each rotational period the signal $S(t)$ is strongly modulated by the heteronuclear diplar coupling through the phase $\Phi(t,0)$ in Eq. (14). The rotational echoes translate into *spinning sidebands* in the spectrum $S(\Omega)$ shown in (J) separated by the sample spinning frequency and centred around the *centerband* at 0 as no I-spin isotropic chemical shift has been considered in these calculations. It should be noted that although the pattern of the sidebands resembles the static Pake pattern the match is not exact, especially with increasing spinning frequencies. The amplitudes of the spinning sidebands can be determined by expanding Eq. (16) together with Eq. (14) in a Fourier series of the spinning frequency ω_r and calculating the Fourier coefficients [29].

At MAS frequency of 400 Hz, $\omega_r < b_{IS}$ applies, where b_{IS}/ω_r is in the order of 2. The rotational echoes in $S(t)$ move closer together in time as τ_r decreases as can be seen in panels (D) and (E), and less signal modulation occurs during each rotational period. The spectrum $S(\Omega)$ shown in (F) contains only a few sidebands, where the centerband becomes the signal with the highest intensity.

Finally in the fast spinning regime at 4000 kHz MAS frequency is depicted in the top row (A)–(C). In this case $\omega_r \gg b_{IS}$ is valid, resulting in a spectrum $S(\Omega)$ showing solely the centerband at 0. Correspondingly, no modulation due to the heteronuclear dipolar coupling is visible in the time signal $S(t)$ shown in (A), the rotational echoes have merged into a constant signal (if no additional line broadening is applied),

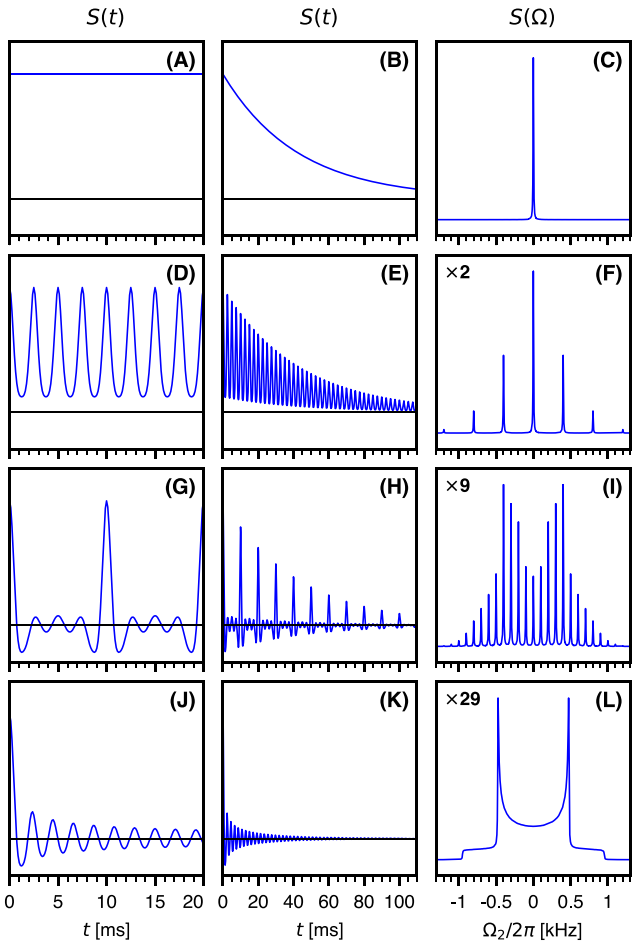

Fig. 4. Calculated FIDs $S(t)$ (first two columns) and their corresponding Fourier transformed spectra $S(\Omega)$ (last column) for a two (I, S)-spin system in a powdered sample with a heteronuclear dipolar coupling constant of $b_{IS}/2\pi = 950$ Hz. To the FIDs $S(t)$ shown in the first column no additional line broadening was applied, whereas to the FIDs $S(t)$ shown in the second column 7.5 Hz exponential line broadening was applied. The results were calculated, from bottom to top, under static (J)–(L) and MAS conditions with spinning frequencies of (G)–(I): 100 Hz, (D)–(F): 400 Hz and (A)–(C): 4000 Hz. All calculations were performed using the Mathematica [34] package *SpinDynamica* [35].

corresponding to an exponentially decaying signal in (B) if exponential line broadening is used. The effect of the heteronuclear dipolar coupling has been averaged out by the rapid sample spinning. All spectra $S(\Omega)$ in the right column of Fig. 4 indicate their individual scaling factor. It is evident that MAS increases tremendously both the resolution and sensitivity of the I-spin spectra.

2.1.4. Average Hamiltonian

For educational interest's sake, average Hamiltonian theory may be applied to the time-dependent periodic Hamiltonian Eq. (4) of the heteronuclear dipolar coupling. Consulting the third column in Fig. (I-7) and section I-3.3, enables us to calculate the first order average Hamiltonian for the heteronuclear dipolar coupling under MAS over one rotational period $T = \tau_r$:

$$\bar{H}_{IS}^{DD(1)} = \frac{1}{\tau_r}\int_0^{\tau_r} \mathrm{d}t\; H_{IS}^{DD}(t) = 2I_zS_z\frac{1}{\tau_r}\int_0^{\tau_r}\mathrm{d}t\;\omega_{IS}^{DD}(t) = 0 \tag{18}$$

However, as discussed above, the heteronuclear dipolar coupling Hamiltonian commutes with itself (and any chemical shift Hamiltonian) at different time points. As a result, even all higher order average Hamiltonians disappear over one rotational period $[0, \tau_r]$ and the overall effective Hamiltonian Eq. (I-29) is zero:

$$\bar{H}_{IS}^{DD} = \bar{H}_{IS}^{DD(1)} + \bar{H}_{IS}^{DD(2)} + \cdots = 0 \tag{19}$$

As a result, the propagator over one rotational period is unity:

$$U(\tau_r, 0) = \mathbb{1} \tag{20}$$

This result is not surprising, as evolution of the transverse I-spin magnetization under the heteronuclear dipolar coupling is refocussed at the end of each rotational period resulting in the rotational echoes in the time signal $S(t)$ discussed in the previous section. This result also highlights that average Hamilton theory can only be applied over multiples of the time period of the Hamiltonian, for example here multiples of the rotational period τ_r under MAS. It does not allow for results to be obtained at intermediate time points during the time period. Hence, average Hamiltonian theory fails to predict the occurrence of spinning sidebands in MAS spectra. However, as we will see in the following section average Hamiltonian theory is a powerful tool to calculate the density operator at multiples of the period of the basic building block of an applied rf pulse sequence.

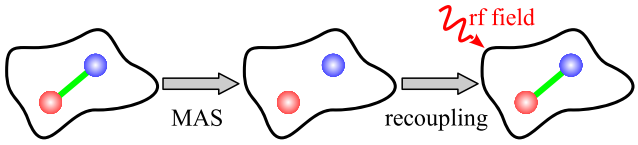

Fig. 5. Principle of heteronuclear dipolar recoupling in MAS NMR.

2.2. REDOR with ideal pulses

Most realistic applications of solid-state NMR in disordered solids require MAS to attenuate the effects of the anisotropic spin interactions in order to achieve high spectral resolution and sensitivity, as we have seen by the example of the heteronuclear dipolar coupling in the previous section. However, anisotropic spin interactions contain information about the molecular structure, e. g., the direct dipolar coupling depends upon the internuclear distance. Therefore, it is often desirable to temporarily *recouple* certain anisotropic spin interactions by applying pulse schemes of resonant rf fields to the nuclear spins, in order to suspend the averaging effect of the magic-angle rotation over a limited time interval. This is depicted in Fig. 5 for the recoupling of the heteronuclear dipolar coupling.

These rf schemes are called *recoupling pulse sequences*. The recoupling of dipolar couplings by rf pulse sequences is called *dipolar recoupling*, specifically *homonuclear dipolar recoupling* and *heteronuclear dipolar recoupling* for the cases of homonuclear and heteronuclear dipolar couplings, respectively.

In general, to achieve heteronuclear dipolar recoupling in a heteronuclear two-spin system I and S, an rf pulse sequence can be applied either to *both* spin species or to *solely one* of the two spin species. The archetypal heteronuclear recoupling sequence in solid-state NMR that is applied to both spin species is the Hartmann-Hahn cross polarization (CP) scheme [36,37], which is widely employed in solid-state NMR for the enhancement of signals from nuclei with small gyromagnetic ratios and is an essential component of high-resolution NMR in solids. The combination of CP and MAS is referred to as CP-MAS [38,39]. Two of the most successful (and oldest) heteronuclear recoupling methods in MAS NMR that involve application of rf fields to only one of the two spin species are rotary resonance recoupling (R^3) [40,41] and rotational-echo double-resonance NMR (REDOR) [2,3]. In this section we will introduce the basic concept of REDOR employing ideal rf pulses and describe in detail how to apply first-order average Hamiltonian theory to understand how this pulse sequence achieves heteronuclear dipolar recoupling under MAS. In the following

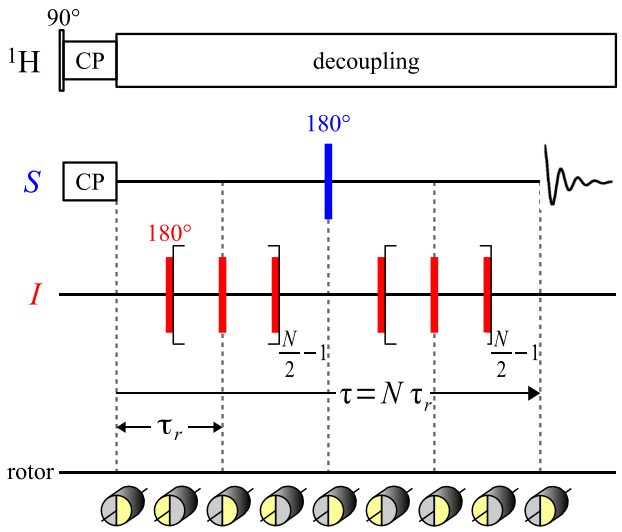

Fig. 6. Rf pulse sequence that employs REDOR as heteronuclear recoupling sequence while the abundant protons are decoupled.

section this will be extended to REDOR using (realistic) finite rf pulses and the connection between REDOR and R^3 will elucidated generalizing previous work by Naito et al. [42] and Jaroniec et al. [43].

Fig. 6 shows a typical rf pulse sequence applied to a heteronuclear I and S spin system during MAS that employs REDOR as heteronuclear recoupling sequence while the abundant protons are decoupled. A common case is represented by $S = {}^{13}$C and $I = {}^{15}$N. Firstly, enhanced S-spin transverse magnetization is generated by transferring magnetization from the protons by CP. Secondly, the S-spins are subjected to a spin-echo of duration τ prior to the signal detection period, where τ is equal to an even integer number of rotational periods, $\tau = N\tau_r$. During the spin-echo duration on the I-spins the REDOR recoupling sequence is applied, in which discrete 180° pulses are applied every half rotational period.

The essential building block of the REDOR sequence, two 180° pulse every half rotational period, is shown in Fig. 7, where we first will consider the case depicted in Fig. 7(A), i. e. assuming the 180° pulses with phase 0 are ideal pulses that are infinitesimal short. The starting time point of the sequence block is denoted t_0, the time point of the first and second 180_x pulse are denoted t_1 and t_2, respectively, where $\tau_r = t_2 - t_0$, $\tau_r/2 = t_2 - t_1$ and $\tau_r/2 = t_1 - t_0$.

2.2.1. Hamiltonian

Consider a heteronuclear two-spin system I and S in the presence of the heteronuclear dipolar coupling and the REDOR pulse sequence in Fig. 7(A) applied to the I-spins during MAS. In the high-field approximation, the Hamiltonian at time point t is given by the sum of the Hamiltonian $H_{\rm rf}(t)$, Eqs. (I-16) and (C.22), of the interaction of the I-spins with the on-resonance rf field and the internal spin Hamiltonian $H_{\rm int}(t)$, see Appendix C.4. Since we are ultimately interested to determine the spin-echo amplitude of the S-spins as a function of the duration τ during which the REDOR sequence is applied, as shown in Fig. 6, we need solely consider the Hamiltonian $H_{IS}^{\rm DD}(t)$, Eq. (4), of the heteronuclear dipolar coupling as contribution to $H_{\rm int}(t)$, and may ignore both the I- and S-spin chemical shifts:

$$\begin{aligned} H(t) &= H_{\rm rf}(t) + H_{\rm int}(t) \\ &= \underbrace{\omega_{\rm nut}(t)\, I_x}_{H_A(t)} + \underbrace{\omega_{IS}^{\rm DD}(t)\, 2I_zS_z}_{H_B(t)}, \end{aligned} \tag{21}$$

where a phase of $\phi = 0$ was assumed for all rf pulses as shown in Fig. 7(A). Furthermore, the Hamiltonian has been split into two parts

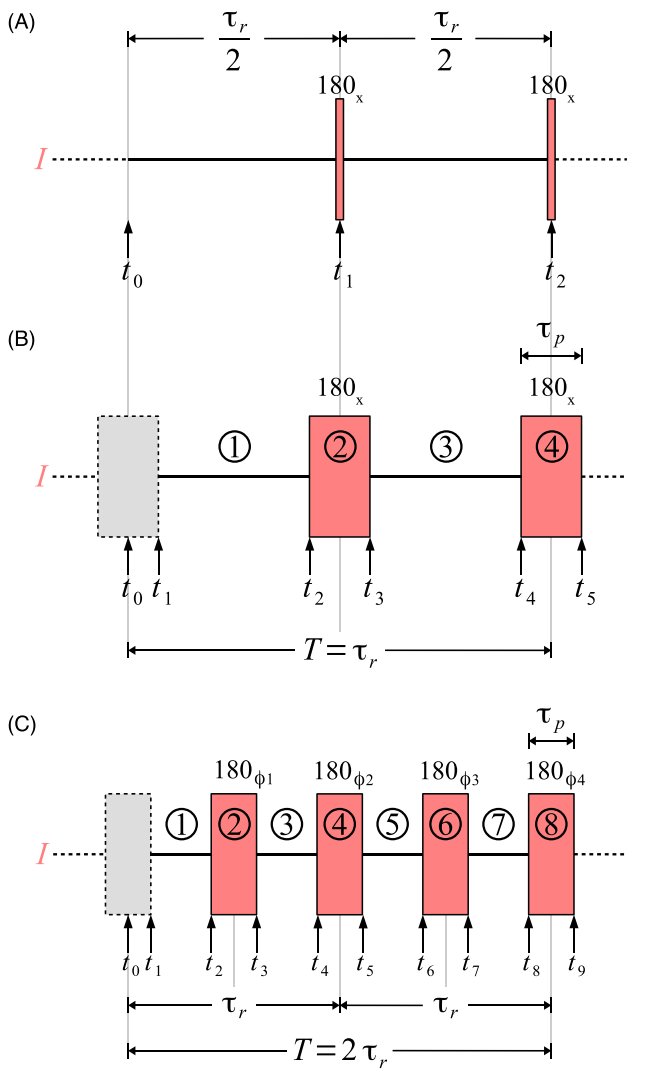

Fig. 7. Building blocks of the REDOR sequence analysed by average Hamiltonian theory in this paper, employing (A) ideal (infinitesimal short) 180_x pulses, (B) finite 180_x pulses, and (C) finite 180° pulses with arbitrary rf phases $\phi_1, \ldots, \phi_4$.

$H_A(t)$ and $H_B(t)$, which will allow to transform $H(t)$ into the interaction frame of $H_A(t)$ before the application of average Hamiltonian theory as described in section I-3.2. $H_A(t) = H_{\rm rf}(t)$ corresponds to the time-dependent Hamiltonian of the interaction with the rf field and $H_B(t) = H_{IS}^{\rm DD}(t)$ is the time-dependent Hamiltonian of the heteronuclear dipolar coupling. Both Hamiltonians are periodic in time with the rotational period τ_r:

$$H_A(t+\tau_r) = H_A(t) \qquad H_B(t+\tau_r) = H_B(t) \tag{22}$$

Hence, consulting the summary sheet of average Hamiltonian theory Fig. I-7, we see that the steps outlined in the last column apply in this case. For the different time periods during the REDOR pulse sequence in Fig. 7(A) $H_A(t)$ and $H_B(t)$ are explicitly given by:

$$H_A(t) = \begin{cases} 0 & \text{for} \quad t_0 \le t < t_1 \text{ or } t_1 < t < t_2 \\ \omega_{\rm nut}^{\infty} I_x & \text{for} \quad t = t_1 \text{ or } t = t_2 \end{cases} \tag{23}$$

and

$$H_B(t) = \begin{cases} \omega_{IS}^{\rm DD}(t)\, 2I_zS_z & \text{for} \quad t_0 \le t < t_1 \text{ or } t_1 < t < t_2 \\ 0 & \text{for} \quad t = t_1 \text{ or } t = t_2, \end{cases} \tag{24}$$

where $\omega_{\rm nut}^{\infty}$ denotes the infinitely large rf nutation frequency of the ideal pulses. In addition, as the pulses are considered to be ideal

and infinitesimal short, the heteronuclear dipolar coupling is neglected during the rf pulses.

2.2.2. Rf propagator

In order to transform the Hamiltonian $H(t)$ in Eq. (21) into the interaction frame of the rf field Hamiltonian $H_A(t)$, we need to calculate the rf propagator solving the corresponding Schrödinger equation (I-50). This is straightforward, as we have assumed ideal the rf pulses:

$$U_A(t,t_0) = \begin{cases} \mathbb{1} & \text{for} \quad t_0 \le t < t_1 \\ R_x(\pi) & \text{for} \quad t = t_1 \\ R_x(\pi) & \text{for} \quad t_1 < t < t_2 \\ R_x(2\pi) = -\mathbb{1} & \text{for} \quad t = t_2, \end{cases} \tag{25}$$

where $R_x(\beta)$ is the operator for the rotation of the I-spins through the angle β about the x-axis, as defined in section I-2.4. Note how the propagators in the last row are the accumulated two $R_x(\pi)$ rotations. For the transformation into the interaction frame, we also need to calculate the adjoint of the rf propagator:

$$U_A^{\dagger}(t,t_0) = \begin{cases} \mathbb{1} & \text{for} \quad t_0 \le t < t_1 \\ R_x(-\pi) & \text{for} \quad t = t_1 \\ R_x(-\pi) & \text{for} \quad t_1 < t < t_2 \\ -\mathbb{1} & \text{for} \quad t = t_2. \end{cases} \tag{26}$$

2.2.3. Interaction frame Hamiltonian

With the help of the rf propagators calculated in the previous section, we can now transform the Hamiltonian $H(t)$ into the interaction frame of $H_A(t)$ as shown in Eq. (I-56):

$$\begin{aligned} \tilde{H}_B(t) &= U_A(t,t_0)^{\dagger}\, H_B(t)\, U_A(t,t_0) \\ &= \begin{cases} \omega_{IS}^{\mathrm{DD}}(t)\, 2I_zS_z & \text{for} \quad t_0 \le t < t_1 \\ \omega_{IS}^{\mathrm{DD}}(t)\, 2R_x(-\pi)I_zR_x(\pi)S_z & \text{for} \quad t_1 < t < t_2 \end{cases} \\ &= \begin{cases} \omega_{IS}^{\mathrm{DD}}(t)\, 2I_zS_z & \text{for} \quad t_0 \le t < t_1 \\ -\omega_{IS}^{\mathrm{DD}}(t)\, 2I_zS_z & \text{for} \quad t_1 < t < t_2. \end{cases} \end{aligned} \tag{27}$$

2.2.4. First order average Hamiltonian and propagator

With the help of the interaction frame Hamiltonian in Eq. (27) we can now calculate the first order average Hamiltonian according to Eq. (I-30):

$$\begin{aligned} \bar{H}_B^{(1)} &= \frac{1}{T}\int_{t_0}^{t_2} \mathrm{d}t\, \tilde{H}(t) \\ &= \bar{\omega}_{IS}^{(z)}\, 2I_zS_z \end{aligned} \tag{28}$$

where we have introduced the time-independent amplitude $\bar{\omega}_{IS}^{(z)}$ of the recoupled heteronuclear dipolar interaction proportional to the I_zS_z spin operator, which is given by

$$\begin{aligned} \bar{\omega}_{IS}^{(z)} &= \frac{1}{\tau_r}\left\{\int_{t_0}^{t_1} \mathrm{d}t\, \omega_{IS}^{\mathrm{DD}}(t) - \int_{t_1}^{t_2} \mathrm{d}t\, \omega_{IS}^{\mathrm{DD}}(t)\right\} \\ &= \frac{1}{\tau_r}\int_{t_0}^{t_1} \mathrm{d}t\left\{\omega_{IS}^{\mathrm{DD}}(t) - \omega_{IS}^{\mathrm{DD}}(t+\frac{\tau_r}{2})\right\} \\ &= \frac{2}{\tau_r}\int_{t_0}^{t_1} \mathrm{d}t\, \omega^{(1)}(t), \end{aligned} \tag{29}$$

where we have used the rotational symmetries Eqs. (11) and (12). We can further simplify the result using the definition of $\omega^{(1)}(t)$ in Eq. (10):

$$\begin{aligned} \bar{\omega}_{IS}^{(z)} &= \Omega^{(1)}\, \frac{2}{\tau_r}\int_{t_0}^{t_0+\tau_r/2} \mathrm{d}t\, \cos\left(\omega_r t - \gamma_{PR}^{IS}\right) \\ &= -\frac{2}{\pi}\Omega^{(1)}\sin\left(\omega_r t_0 - \gamma_{PR}^{IS}\right) \\ &= \frac{\sqrt{2}}{\pi} b_{IS}\sin\left(2\beta_{PR}^{IS}\right)\sin\left(\omega_r t_0 - \gamma_{PR}^{IS}\right) \end{aligned} \tag{30}$$

As a result the first order average Hamiltonian in Eq. (28) is given by

$$\bar{H}_B^{(1)} = \frac{\sqrt{2}}{\pi} b_{IS}\sin\left(2\beta_{PR}^{IS}\right)\sin\left(\omega_r t_0 - \gamma_{PR}^{IS}\right)\, 2I_zS_z. \tag{31}$$

We note here that not only is the amplitude of the first order average Hamiltonian proportional to the dipolar coupling constant b_{IS} but also depends on the starting time point of the REDOR block t_0. Therefore, if the difference of the starting time points of the two periods of REDOR irradiation on the I-spins during the S-spin-echo shown in Fig. 6 is not equal to an integer multiple of the rotation period τ_r, the spin-echo amplitude becomes encoded by the position of the rotor, the basis of *rotor-encoded spectroscopy* introduced and extensively studied by the group of Spiess [44,45]. This principle also can be used to scale the recoupled heteronuclear dipolar Hamiltonian [46].

The REDOR basic rf pulse sequence block depicted in Fig. 7 is cyclic, therefore, the rf propagator over one rotational period is equal to unity,

$$U_A(t_2,t_0) = U_A(t_0+\tau_r,t_0) = -\mathbb{1}, \tag{32}$$

the propagator in first order average Hamiltonian theory over an integer multiples of the rotational period $\tau = N\tau_r$ of REDOR recoupling as shown in Fig. 6 according to Eq. (I-70):

$$\begin{aligned} U(t_0+\tau,t_0) &= \exp\{-\mathrm{i}\bar{H}_B^{(1)}\tau\} \\ &= \exp\{-\mathrm{i}\,\bar{\omega}_{IS}^{(z)}\tau\, 2I_zS_z\} \end{aligned} \tag{33}$$

As shown in Fig. 6 in an MAS experiment employing the REDOR sequence, the S-spin-echo intensity is recorded as a function of the duration τ during which the REDOR sequence is applied. The spin-echo intensity for a single crystallite orientation as a function of τ is given by:

$$\begin{aligned} S(\tau;\Omega_{PR}^{IS}) &= \frac{\mathrm{Tr}\left\{I_x\, U(t_0+\tau,t_0)\, I_x\, U^{\dagger}(t_0+\tau,t_0)\right\}}{\mathrm{Tr}\left\{I_x^2\right\}} \\ &= \cos\left(\bar{\omega}_{IS}^{(z)}\tau\right) \end{aligned} \tag{34}$$

where in order to arrive at the result in Eq. (34) the same transformation steps were performed as to arrive at the results in Eqs. (15) and (16). In a powder sample the final S-spin signal as a function of the duration τ of the REDOR sequence is obtained by averaging over all possible orientations Ω_{PR}^{IS}:

$$S(\tau) = \left\langle\cos\left(\bar{\omega}_{IS}^{(z)}\tau\right)\right\rangle_{\Omega_{PR}^{IS}} \tag{35}$$

As discussed in Section 2.1.2 in a powdered sample the orientations Ω_{PR}^{IS} are random variables. The powdered averaging can be achieved numerically by summing the intensities $S(\tau;\Omega_{PR}^{IS})$ for a single crystallite orientation over a defined set of orientations Ω_{PR}^{IS} [27], or by attempting to solve the following integral analytically:

$$\left\langle\ldots\right\rangle_{\Omega_{PR}^{IS}} = \frac{1}{4\pi}\int_0^{2\pi}\mathrm{d}\gamma_{PR}^{IS}\int_0^{\pi}\mathrm{d}\beta_{PR}^{IS}\,\sin\beta_{PR}^{IS}\ldots \tag{36}$$

Mueller et al. [47–49] elegantly expressed the solution to the integral in Eqs. (35) and (36) with the help of Bessel functions:

$$S(\tau) = \frac{\pi}{2\sqrt{2}}\, J_{-1/4}\left(\frac{\sqrt{2}}{2\pi}\, b_{IS}\,\tau\right) J_{1/4}\left(\frac{\sqrt{2}}{2\pi}\, b_{IS}\,\tau\right), \tag{37}$$

where $J_\nu(z)$ denotes Bessel functions of the first kind with in general integer or fractional parameter ν and in general complex argument z [50,51].

Fig. 8 shows the result of calculating $S(\tau)$ for three different dipolar coupling constants $b_{IS}/2\pi$ = 850, 950 and 1050 Hz, corresponding to ^{13}C–^{15}N internuclear distances of 153.3, 147.7 and 142.9 pm, respectively. As the dipolar coupling constant increases, the extrema of the modulation curve move closer together. This enables the determination of internuclear distances and REDOR has been successfully applied over the last 35 years to determine distances between a wide range of pairs of different nuclei, including spin-1/2 and quadrupolar nuclei [13,52–55].

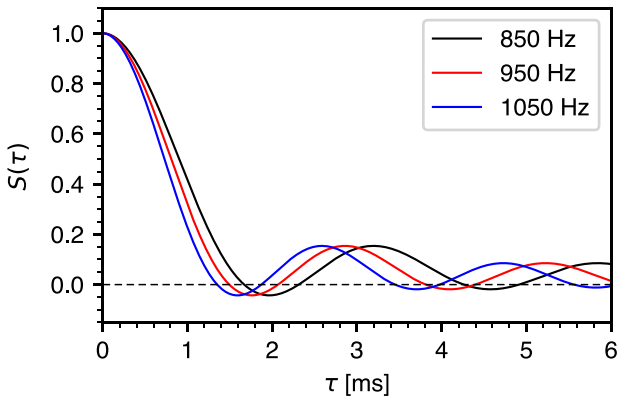

Fig. 8. Calculated S-spin-echo amplitudes $S(\tau)$, Eq. (37), for different values of the heteronuclear dipolar coupling constant $b_{IS}/2\pi$ as a function of the duration τ during which the REDOR sequence with ideal pulses is applied.

2.3. REDOR with finite pulses and rotary resonance recoupling

In the previous section we have discussed the REDOR sequence employing ideal rf pulses in first order average Hamiltonian theory. In this section, the goal is to extend this description to realistic, finite rf pulses. The modified basic building block the REDOR pulse sequence employing rf pulses of finite duration is shown in Fig. 7(B). The duration and nutation frequency of the 180° rf pulses is denoted τ_p and ω_{nut}, respectively, and the following relation is fulfilled:

$$\omega_{\text{nut}}\tau_p = \pi. \tag{38}$$

It is useful to introduce the fraction f of the total duration of the two rf pulses and the rotational period:

$$f = \frac{2\tau_p}{\tau_r}, \qquad \text{hence } 0 \le f \le 1 \tag{39}$$

Furthermore, it will become useful to express both the pulse duration τ_p and the nutation frequency ω_{nut} as a function of the fraction f and the rotational period τ_r and the spinning frequency ω_r:

$$\tau_p = \frac{f\tau_r}{2} = \frac{f\pi}{\omega_r} \qquad \text{and} \qquad \omega_{\text{nut}} = \frac{2\pi}{f\tau_r} = \frac{\omega_r}{f}, \tag{40}$$

where the latter implies that $1/f$ corresponds to the ratio of the nutation frequency of the rf-field and the spinning frequency

Fig. 7(B) specifies in detail the labelling of time points t_0 to t_5 and sequence segments ①–④ during the basic building block of the REDOR sequence employing finite rf pulses. For consistency with the case of ideal rf pulses shown in Fig. 7(A), t_0 is chosen as the *reference time point*. However, the average Hamiltonian and propagator will be calculated over the interval $[t_1, t_5]$ with $\tau_r = t_5 - t_1$. The following equations, express the different time points t_1 to t_5 as a function of t_0, the rotational period τ_r and the fraction f:

$$t_1 = t_0 + \frac{\tau_p}{2} \qquad = t_0 + f\frac{\tau_r}{4} \tag{41}$$

$$t_2 = t_0 + \frac{\tau_r}{2} - \frac{\tau_p}{2} = t_0 + \frac{\tau_r}{2} - f\frac{\tau_r}{4} \tag{42}$$

$$t_3 = t_0 + \frac{\tau_r}{2} + \frac{\tau_p}{2} = t_0 + \frac{\tau_r}{2} + f\frac{\tau_r}{4} \tag{43}$$

$$t_4 = t_0 + \tau_r - \frac{\tau_p}{2} \qquad = t_0 + \tau_r - f\frac{\tau_r}{4} \tag{44}$$

$$t_5 = t_0 + \tau_r + \frac{\tau_p}{2} \qquad = t_0 + \tau_r + f\frac{\tau_r}{4} \tag{45}$$

2.3.1. Hamiltonian

The Hamiltonians $H_A(t)$ and $H_B(t)$ in Eq. (21) during REDOR employing finite rf pulses can be written as

$$H_A(t) = \begin{cases} 0 & \text{for} \quad t_1 \le t < t_2 \text{ or } t_3 \le t < t_4 \\ \omega_{\text{nut}} I_x & \text{for} \quad t_2 \le t < t_3 \text{ or } t_4 \le t \le t_5 \end{cases} \tag{46}$$

and

$$H_B(t) = \omega_{IS}^{\text{DD}}(t)\, 2I_z S_z. \tag{47}$$

2.3.2. Rf propagator

In a second step we need to calculate the propagator $U_A(t, t_1)$ for the rf Hamiltonian $H_A(t)$ in Eq. (46). The propagator during the four time blocks ①–④ is given by:

$$U_A(t, t_1) = \begin{cases} \mathbb{1} & \text{for} \quad t_1 \le t < t_2 \\ R_x\left(\omega_{\text{nut}}(t - t_2)\right) & \text{for} \quad t_2 \le t < t_3 \\ R_x(\pi) & \text{for} \quad t_3 \le t < t_4 \\ R_x\left(\omega_{\text{nut}}(t - t_4)\right) R_x(\pi) & \text{for} \quad t_4 \le t \le t_5. \end{cases} \tag{48}$$

It is helpful to introduce time-dependent nutation angles $\beta_{②}(t)$ and $\beta_{④}(t)$ during the pulse sequence blocks ② and ④,

$$\beta_{②}(t) = \omega_{\text{nut}}(t - t_2) \tag{49}$$

$$\beta_{④}(t) = \omega_{\text{nut}}(t - t_4), \tag{50}$$

where the following relation applies as the nutation frequency ω_{nut} is the same during time blocks ② and ④:

$$\beta_{④}(t + \frac{\tau_r}{2}) = \beta_{②}(t) \tag{51}$$

With the help of Eqs. (49) and (50) the expression in the propagator can be simplified:

$$U_A(t, t_1) = \begin{cases} \mathbb{1} & \text{for} \quad t_1 \le t < t_2 \\ R_x\left(\beta_{②}(t)\right) & \text{for} \quad t_2 \le t < t_3 \\ R_x(\pi) & \text{for} \quad t_3 \le t < t_4 \\ R_x(\pi) R_x\left(\beta_{④}(t)\right) & \text{for} \quad t_4 \le t \le t_5. \end{cases} \tag{52}$$

Finally, for the transformation into the interaction frame we also need to calculate the adjoint of the rf propagator:

$$U_A^{\dagger}(t, t_1) = \begin{cases} \mathbb{1} & \text{for} \quad t_1 \le t < t_2 \\ R_x\left(-\beta_{②}(t)\right) & \text{for} \quad t_2 \le t < t_3 \\ R_x(-\pi) & \text{for} \quad t_3 \le t < t_4 \\ R_x\left(-\beta_{④}(t)\right) R_x(-\pi) & \text{for} \quad t_4 \le t \le t_5. \end{cases} \tag{53}$$

2.3.3. Interaction frame Hamiltonian

We can now employ the rf propagator $U_A(t, t_1)$ calculated in the previous section to transform the Hamiltonian into the interaction frame of rf field Hamiltonian $H_A(t)$ according to Eq. (I-56):

$$\begin{aligned} \tilde{H}_B(t) &= U_A(t, t_1)^{\dagger}\, H_B(t)\, U_A(t, t_1) \\ &= \omega_{IS}^{\text{DD}}(t)\, 2S_z \begin{cases} I_z & \text{for} \quad t_1 \le t < t_2 \\ R_x\left(-\beta_{②}(t)\right) I_z R_x\left(\beta_{②}(t)\right) & \text{for} \quad t_2 \le t < t_3 \\ -I_z & \text{for} \quad t_3 \le t < t_4 \\ -R_x\left(-\beta_{④}(t)\right) I_z R_x\left(\beta_{④}(t)\right) & \text{for} \quad t_4 \le t \le t_5 \end{cases} \\ &= \omega_{IS}^{\text{DD}}(t)\, 2S_z \begin{cases} I_z & \text{for} \quad t_1 \le t < t_2 \\ I_z \cos\beta_{②}(t) + I_y \sin\beta_{②}(t) & \text{for} \quad t_2 \le t < t_3 \\ -I_z & \text{for} \quad t_3 \le t < t_4 \\ -I_z \cos\beta_{④}(t) - I_y \sin\beta_{④}(t) & \text{for} \quad t_4 \le t \le t_5, \end{cases} \end{aligned} \tag{54}$$

where we have used $R_x(\pi) I_z R_x(-\pi) = -I_z$ and $R_x(\beta) I_z R_x(-\beta) = I_z \cos\beta - I_y \sin\beta$.

2.3.4. First order average Hamiltonian and propagator

After we have determined the interaction frame Hamiltonian in Eq. (54), it is now time to calculate the first order average Hamiltonian

according to Eq. (I-30):

$$\begin{aligned}\bar{H}_B^{(1)} &= \frac{1}{T}\int_{t_1}^{t_5} \mathrm{d}t\ \tilde{H}(t)\\ &= \underbrace{\frac{1}{\tau_r}\int_{t_1}^{t_2} \mathrm{d}t\ \tilde{H}_B(t)}_{\int①} + \underbrace{\frac{1}{\tau_r}\int_{t_2}^{t_3} \mathrm{d}t\ \tilde{H}_B(t)}_{\int②} + \underbrace{\frac{1}{\tau_r}\int_{t_3}^{t_4} \mathrm{d}t\ \tilde{H}_B(t)}_{\int③}\\ &\quad + \underbrace{\frac{1}{\tau_r}\int_{t_4}^{t_5} \mathrm{d}t\ \tilde{H}_B(t)}_{\int④}\end{aligned} \tag{55}$$

where the integral over the complete time interval $[t_1, t_5]$ was split into 4 separate integrals $\int_①$, $\int_②$, $\int_③$ and $\int_④$. In a first step the sum $\int_① + \int_③$ can straightforwardly be calculated:

$$\begin{aligned}\int_① + \int_③ &= 2I_zS_z\ \frac{1}{\tau_r}\left\{\int_{t_1}^{t_2}\mathrm{d}t\ \omega_{IS}^{\mathrm{DD}}(t) - \int_{t_3}^{t_4}\mathrm{d}t\ \omega_{IS}^{\mathrm{DD}}(t)\right\}\\ &= 2I_zS_z\ \frac{1}{\tau_r}\int_{t_1}^{t_2}\mathrm{d}t\left\{\omega_{IS}^{\mathrm{DD}}(t) - \omega_{IS}^{\mathrm{DD}}(t+\frac{\tau_r}{2})\right\}\\ &= 2I_zS_z\ \frac{2\Omega^{(1)}}{\tau_r}\int_{t_1}^{t_2}\mathrm{d}t\ \cos\left(\omega_r t - \gamma_{PR}^{IS}\right)\\ &= 2I_zS_z\ \frac{2\Omega^{(1)}}{\omega_r\tau_r}\left\{\sin\left(\omega_r t_2 - \gamma_{PR}^{IS}\right) - \sin\left(\omega_r t_1 - \gamma_{PR}^{IS}\right)\right\},\end{aligned} \tag{56}$$

where we have used the rotational symmetries Eqs. (11) and (12) in the same way as in Eq. (29). In addition to $\omega_r\tau_r = 2\pi$, we can use the following identities derived from Eqs. (41) and (42),

$$\omega_r t_2 = \omega_r t_0 - f\frac{\pi}{2} + \pi \tag{57}$$

$$\omega_r t_1 = \omega_r t_0 + f\frac{\pi}{2}, \tag{58}$$

in order to simplify Eq. (56), leading to the following result:

$$\begin{aligned}\int_① + \int_③ &= -2I_zS_z\ \frac{\Omega^{(1)}}{\pi}\left\{\sin\left(\omega_r t_0 - \gamma_{PR}^{IS} - f\frac{\pi}{2}\right)\right.\\ &\qquad\left. + \sin\left(\omega_r t_0 - \gamma_{PR}^{IS} + f\frac{\pi}{2}\right)\right\}\\ &= -2I_zS_z\ \frac{2}{\pi}\Omega^{(1)}\cos\left(f\frac{\pi}{2}\right)\sin\left(\omega_r t_0 - \gamma_{PR}^{IS}\right),\end{aligned} \tag{59}$$

where we have used the identity $\sin(\alpha+\beta) + \sin(\alpha-\beta) = 2\cos\beta\sin\alpha$. In a second step the sum $\int_② + \int_④$ needs to be calculated, employing again the rotational symmetries Eqs. (11) and (12) and the relation of the time-dependent nutation angles Eq. (51):

$$\begin{aligned}\int_② + \int_④ &= 2I_zS_z\ \frac{1}{\tau_r}\left\{\int_{t_1}^{t_2}\mathrm{d}t\ \omega_{IS}^{\mathrm{DD}}(t)\left\{I_z\cos\beta_②(t) + I_y\sin\beta_②(t)\right\}\right.\\ &\qquad\left. - \int_{t_3}^{t_4}\mathrm{d}t\ \omega_{IS}^{\mathrm{DD}}(t)\left\{I_z\cos\beta_④(t) + I_y\sin\beta_④(t)\right\}\right\}\\ &= 2I_zS_z\ \frac{1}{\tau_r}\int_{t_1}^{t_2}\mathrm{d}t\left\{\omega_{IS}^{\mathrm{DD}}(t)\left\{I_z\cos\beta_②(t) + I_y\sin\beta_②(t)\right\}\right.\\ &\qquad\left.\omega_{IS}^{\mathrm{DD}}(t+\frac{\tau_r}{2})\left\{I_z\cos\beta_④(t+\frac{\tau_r}{2})\right.\right.\\ &\qquad\left.\left. + I_y\sin\beta_④(t+\frac{\tau_r}{2})\right\}\right\}\\ &= 2S_z\ \frac{1}{\tau_r}\int_{t_2}^{t_3}\mathrm{d}t\left\{\omega_{IS}^{\mathrm{DD}}(t) - \omega_{IS}^{\mathrm{DD}}(t+\frac{\tau_r}{2})\right\}\\ &\qquad\times\left\{I_z\cos\beta_②(t) + I_y\sin\beta_②(t)\right\}\\ &= 2S_z\ \frac{2}{\tau_r}\int_{t_2}^{t_3}\mathrm{d}t\ \omega^{(1)}(t)\left\{I_z\cos\beta_②(t) + I_y\sin\beta_②(t)\right\}.\end{aligned} \tag{60}$$

Calculation of the integral in the last row of Eq. (60) can be performed separately for the terms proportional to I_z and I_y, respectively. The term proportional to I_z can be transformed in the following way:

$$\begin{aligned}&\frac{2}{\tau_r}\int_{t_2}^{t_3}\mathrm{d}t\ \omega^{(1)}(t)\cos\beta_②(t)\\ &\quad= \frac{2\Omega^{(1)}}{\tau_r}\int_{t_2}^{t_3}\mathrm{d}t\ \cos\left(\omega_r t - \gamma_{PR}^{IS}\right)\cos\left(\frac{\omega_r}{f}(t-t_2)\right)\\ &\quad= \frac{2\Omega^{(1)}}{\tau_r}\int_0^{\tau_p}\mathrm{d}t'\ \cos\left(\omega_r(t'+t_2) - \gamma_{PR}^{IS}\right)\cos\left(\frac{\omega_r}{f}t'\right)\\ &\quad= -\frac{2\Omega^{(1)}}{\tau_r}\int_0^{f\pi/\omega_r}\mathrm{d}t'\ \cos\left(\omega_r t' + \omega_r t_0 - \gamma_{PR}^{IS} - f\frac{\pi}{2}\right)\cos\left(\frac{\omega_r}{f}t'\right)\\ &\quad= -\frac{2}{\pi}\Omega^{(1)}\ \frac{f^2\cos(f\pi/2)}{1-f^2}\ \sin\left(\omega_r t_0 - \gamma_{PR}^{IS}\right)\end{aligned} \tag{61}$$

where we have used the relationship

$$\omega_r t_2 = \omega_r t_0 + \pi - f\frac{\pi}{2}. \tag{62}$$

The term proportional to I_y may be simplified in a similar fashion:

$$\begin{aligned}&\frac{2}{\tau_r}\int_{t_2}^{t_3}\mathrm{d}t\ \omega^{(1)}(t)\sin\beta_②(t)\\ &\quad= \frac{2\Omega^{(1)}}{\tau_r}\int_{t_2}^{t_3}\mathrm{d}t\ \cos\left(\omega_r t - \gamma_{PR}^{IS}\right)\sin\left(\frac{\omega_r}{f}(t-t_2)\right)\\ &\quad= -\frac{2\Omega^{(1)}}{\tau_r}\int_0^{f\pi/\omega_r}\mathrm{d}t'\ \cos\left(\omega_r t' + \omega_r t_0 - \gamma_{PR}^{IS} - f\frac{\pi}{2}\right)\sin\left(\frac{\omega_r}{f}t'\right)\\ &\quad= -\frac{2}{\pi}\Omega^{(1)}\ \frac{f\cos(f\pi/2)}{1-f^2}\ \cos\left(\omega_r t_0 - \gamma_{PR}^{IS}\right)\end{aligned} \tag{63}$$

Collecting all results from Eqs. (59)–(63), the final first order average Hamiltonian may be written as:

$$\bar{H}_B^{(1)} = \bar{\omega}_{IS}^{(z)}(f)\ 2I_zS_z + \bar{\omega}_{IS}^{(y)}(f)\ 2I_yS_z, \tag{64}$$

where the time-independent amplitudes $\bar{\omega}_{IS}^{(z)}$ and $\bar{\omega}_{IS}^{(y)}$ are given by

$$\begin{aligned}\bar{\omega}_{IS}^{(z)}(f) &= -\frac{2}{\pi}\Omega^{(1)}\ \cos(f\pi/2) \qquad \sin\left(\omega_r t_0 - \gamma_{PR}^{IS}\right)\\ &\quad - \frac{2}{\pi}\Omega^{(1)}\ \frac{f^2\cos(f\pi/2)}{1-f^2}\ \sin\left(\omega_r t_0 - \gamma_{PR}^{IS}\right)\\ &= -\frac{2}{\pi}\Omega^{(1)}\ \frac{\cos(f\pi/2)}{1-f^2} \qquad \sin\left(\omega_r t_0 - \gamma_{PR}^{IS}\right)\\ &= \frac{\sqrt{2}}{\pi}b_{IS} \quad \varsigma^{(z)}(f) \qquad \sin\left(2\beta_{PR}^{IS}\right)\sin\left(\omega_r t_0 - \gamma_{PR}^{IS}\right)\end{aligned} \tag{65}$$

and

$$\begin{aligned}\bar{\omega}_{IS}^{(y)}(f) &= -\frac{2}{\pi}\Omega^{(1)}\ \frac{f\cos(f\pi/2)}{1-f^2}\ \cos\left(\omega_r t_0 - \gamma_{PR}^{IS}\right)\\ &= \frac{\sqrt{2}}{\pi}b_{IS} \quad \varsigma^{(y)}(f) \qquad \sin\left(2\beta_{PR}^{IS}\right)\cos\left(\omega_r t_0 - \gamma_{PR}^{IS}\right),\end{aligned} \tag{66}$$

where we have defined the two scaling factors $\varsigma^{(z)}(f)$ and $\varsigma^{(y)}(f)$:

$$\varsigma^{(z)}(f) = \frac{\cos(f\pi/2)}{1-f^2} \tag{67}$$

$$\varsigma^{(y)}(f) = \frac{f\cos(f\pi/2)}{1-f^2} \tag{68}$$

Fig. 9 depicts both scaling factors as a function of the fraction f of the duration of the rf pulses and the rotational period.

With the help of the time-independent amplitudes $\bar{\omega}_{IS}^{(z)}(f)$ and $\bar{\omega}_{IS}^{(y)}(f)$ in Eqs. (65) and (66) the general complete first order average Hamiltonian Eq. (64) can be written as:

$$\begin{aligned}\bar{H}_B^{(1)} = \frac{\sqrt{2}}{\pi}b_{IS}\sin\left(2\beta_{PR}^{IS}\right)\Big\{&\ \varsigma^{(z)}(f)\ \sin\left(\omega_r t_0 - \gamma_{PR}^{IS}\right)\ 2I_zS_z\\ &+ \varsigma^{(y)}(f)\ \cos\left(\omega_r t_0 - \gamma_{PR}^{IS}\right)\ 2I_yS_z\Big\}\end{aligned} \tag{69}$$

In a first step to discuss the implications of Eq. (69), it is insightful to examine the two extreme cases of (i) ideal pulses that are infinitesimal

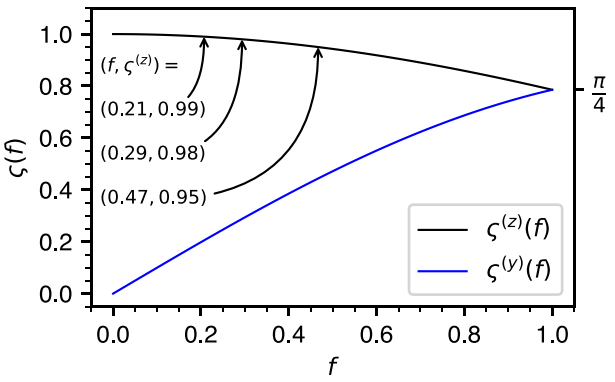

Fig. 9. Scaling factors $\varsigma^{(z)}(f)$ and $\varsigma^{(y)}(f)$ defined in Eqs. (67) and (68), respectively, as a function of the pulse fraction f defined in Eq. (39).

short ($f = 0$) and (ii) a sequence that employs a constant, windowless rf field ($f = 1$).

In the first case (i), $f = 0$, we obtain the following expressions for the factors containing the fraction f and the time-independent amplitudes $\bar{\omega}_{IS}^{(z)}$ and $\bar{\omega}_{IS}^{(y)}$:

$$\varsigma^{(z)}(0) = 1 \quad \Rightarrow \quad \bar{\omega}_{IS}^{(z)}(0) = \frac{\sqrt{2}}{\pi} b_{IS} \sin\left(2\beta_{PR}^{IS}\right) \sin\left(\omega_r t_0 - \gamma_{PR}^{IS}\right) \tag{70}$$

$$\varsigma^{(y)}(0) = 0 \quad \Rightarrow \quad \bar{\omega}_{IS}^{(y)}(0) = 0. \tag{71}$$

As expected in the case of $f = 0$ we obtain in Eqs. (70) and (71) the same result as previously in Eq. (30) with the resulting first order average Hamiltonian

$$\bar{H}_B^{(1)}(f = 0) = \frac{\sqrt{2}}{\pi} b_{IS} \sin\left(2\beta_{PR}^{IS}\right) \sin\left(\omega_r t_0 - \gamma_{PR}^{IS}\right) 2I_z S_z \tag{72}$$

being identical to Eq. (31).

The second case (ii), $f = 1$, corresponds to applying a constant windowless rf field with the nutation frequency equal to the spinning frequency, $\omega_{\text{nut}} = \omega_r$, see Eq. (40). This exactly resembles rotary resonance recoupling (R^3) at the $n = 1$ resonance condition [40,41]. For $f = 1$ we obtain:

$$\varsigma^{(z)}(1) = \frac{\pi}{4} \quad \Rightarrow \quad \bar{\omega}_{IS}^{(z)}(1) = \frac{b_{IS}}{2\sqrt{2}} \sin\left(2\beta_{PR}^{IS}\right) \sin\left(\omega_r t_0 - \gamma_{PR}^{IS}\right) \tag{73}$$

$$\varsigma^{(y)}(1) = \frac{\pi}{4} \quad \Rightarrow \quad \bar{\omega}_{IS}^{(y)}(1) = \frac{b_{IS}}{2\sqrt{2}} \sin\left(2\beta_{PR}^{IS}\right) \cos\left(\omega_r t_0 - \gamma_{PR}^{IS}\right) \tag{74}$$

and the resulting first order average Hamiltonian

$$\bar{H}_B^{(1)}(f = 1) = \frac{b_{IS}}{2\sqrt{2}} \sin\left(2\beta_{PR}^{IS}\right) \left\{ \sin\left(\omega_r t_0 - \gamma_{PR}^{IS}\right) 2I_z S_z + \cos\left(\omega_r t_0 - \gamma_{PR}^{IS}\right) 2I_y S_z \right\}. \tag{75}$$

We have seen that in the case that all rf pulses have the same phase 0, REDOR with infinitesimal short pulses, REDOR with finite pulses and rotary resonance recoupling at the $n = 1$ resonance condition are just specific manifestations of the same general recoupling mechanism. Interestingly, Levitt et al. had suggested that the unmodulated rf field during R^3 could be replaced by discrete 180° pulses every half rotor period [41], which is identical to the original REDOR sequence [2,3].

In the case of a general value for the fraction f the propagator under the REDOR sequence with finite rf pulses is given by

$$U(t_1 + \tau, t_1) = \exp\{-\mathrm{i}\bar{H}_B^{(1)}\tau\} = \exp\left\{ -\mathrm{i}\,\tau \left\{ \bar{\omega}_{IS}^{(z)}(f)\, 2I_z S_z + \bar{\omega}_{IS}^{(y)}(f)\, 2I_y S_z \right\} \right\}, \tag{76}$$

where the propagator in the second row corresponds to a rotation in the spin-1/2 $(I_x, 2I_y S_z, 2I_z S_z)$ operator subspace around an axis in the $(2I_y S_z, 2I_z S_z)$-plane enclosing an angle of $\psi(f)$ with the $2I_z S_z$-axis and a rotation angle of $\bar{\omega}_{IS}^{\text{eff}}(f)\,\tau$, where the angle $\psi(f)$ and the effective amplitude $\bar{\omega}_{IS}^{\text{eff}}(f)$ are given by:

$$\psi(f) = \arctan\left(\frac{\bar{\omega}_{IS}^{(y)}(f)}{\bar{\omega}_{IS}^{(z)}(f)} \right) \tag{77}$$

$$\bar{\omega}_{IS}^{\text{eff}}(f) = \sqrt{\bar{\omega}_{IS}^{(y)}(f)^2 + \bar{\omega}_{IS}^{(z)}(f)^2}. \tag{78}$$

The effective amplitudes $\bar{\omega}_{IS}^{\text{eff}}(f)$ for the two cases (i) $f = 0$, ideal pulses and $f = 1$, windowless rf field (R^3, $n = 1$ condition) are given by:

$$\bar{\omega}_{IS}^{\text{eff}}(0) = \left|\bar{\omega}_{IS}^{(z)}(0)\right| = \frac{\sqrt{2}}{\pi} \left| b_{IS} \sin\left(2\beta_{PR}^{IS}\right) \sin\left(\omega_r t_0 - \gamma_{PR}^{IS}\right) \right| \tag{79}$$

$$\bar{\omega}_{IS}^{\text{eff}}(1) = \sqrt{\bar{\omega}_{IS}^{(y)}(1)^2 + \bar{\omega}_{IS}^{(z)}(1)^2} = \frac{1}{2\sqrt{2}} \left| b_{IS} \sin\left(2\beta_{PR}^{IS}\right) \right| \tag{80}$$

We note that $\bar{\omega}_{IS}^{\text{eff}}(1)$ for a constant, windowless rf field, which is equivalent to the R^3 $n = 1$ resonance condition, does neither depend on the powder angle γ_{PR}^{IS} nor on the starting time point t_0 of the pulse sequence. In this case a pulse sequence is referred to as being *γ-encoded* [14,56–58]. This property leads to more pronounced oscillations in the dephasing curves as will be discussed below.

With the help of the definitions Eqs. (77) and (78) the propagator in Eq. (76) can be written as:

$$U(t_1 + \tau, t_1) = R_x(-\psi(f))\, \exp\{-\mathrm{i}\,\bar{\omega}_{IS}^{\text{eff}}(f)\tau\, 2I_z S_z\}\, R_x(\psi(f)). \tag{81}$$

The S-spin-echo intensity under a REDOR sequence of duration τ for a single crystallite orientation can be calculated according to Eq. (34), where the I-spin rotation operator $R_x(\psi(f))$ commutes with the I_x spin operator:

$$S(\tau; f; \Omega_{PR}^{IS}) = \frac{\mathrm{Tr}\left\{ I_x\, U(t_1 + \tau, t_1)\, I_x\, U^{\dagger}(t_1 + \tau, t_1) \right\}}{\mathrm{Tr}\left\{ I_x^2 \right\}} = \cos\left(\bar{\omega}_{IS}^{\text{eff}}(f)\,\tau\right) \tag{82}$$

Analogous to Eq. (35) the final S-spin signal intensity in a powdered sample as a function of the duration τ of the REDOR sequence is obtained by averaging over all possible orientations Ω_{PR}^{IS}:

$$S(\tau, f) = \left\langle \cos\left(\bar{\omega}_{IS}^{\text{eff}}(f)\,\tau\right) \right\rangle_{\Omega_{PR}^{IS}} \tag{83}$$

Naturally, in the case of $f = 0$ the signal intensity is identical to Eq. (37):

$$S(\tau, 0) = \frac{\pi}{2\sqrt{2}} J_{-1/4}\left(\frac{\sqrt{2}}{2\pi} b_{IS}\,\tau \right) J_{1/4}\left(\frac{\sqrt{2}}{2\pi} b_{IS}\,\tau \right) \tag{84}$$

More interestingly, in the case of a constant windowless rf field ($f = 1$), i. e. R^3 at the $n = 1$ resonance condition, the integral in Eq. (83) together with Eqs. (80) and (36) can be analytically expressed compactly with the help of the Lommel function [51] as shown in Appendix A:

$$S(\tau, 1) = -\frac{1}{4} s_{-1,1/2}\left(\frac{1}{2\sqrt{2}} b_{IS}\,\tau \right), \tag{85}$$

where $s_{\nu,\mu}(z)$ denotes the Lommel function with in general integer or fractional parameters ν and μ and in general complex argument z [51]. Although the use of the Lommel function in Eq. (85) leads to the most appealing and neat expression, we show in Appendix A that alternatively, the Lommel function may be expressed with the help of the hypergeometric, Anger or Weber functions [51]. Furthermore, as shown, the Lommel function can also be expressed with the help of the Fresnel cosine and sine integrals [50]. Previously, Pileio et al. have shown that the double-quantum filtered efficiency as a function of the duration of the application of a γ-encoded homonuclear dipolar recoupling sequence can be expressed employing Fresnel cosine and sine integrals [59]. We expect that the use of the Lommel function will be significantly more elegant for this purpose as well.

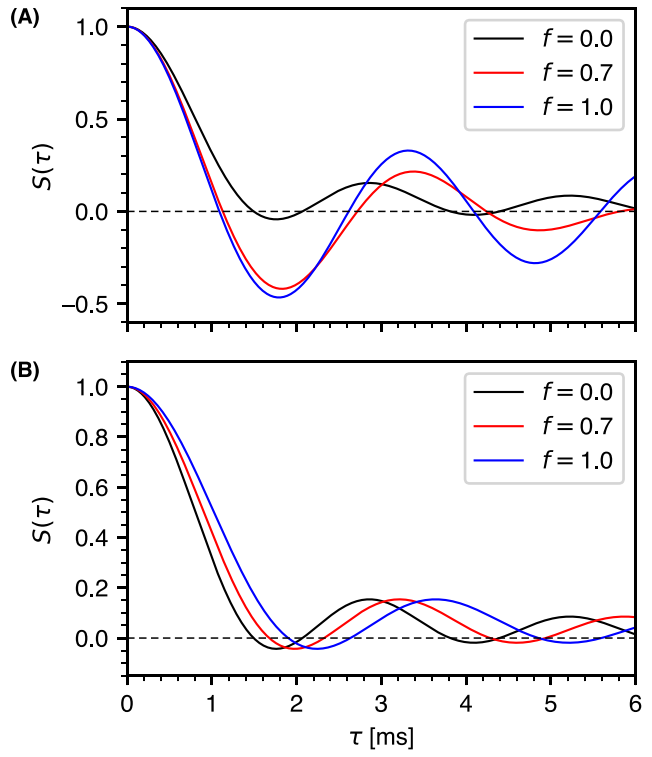

Fig. 10. Calculated S-spin-echo amplitudes $S(\tau)$ for different values of the pulse fraction f as a function of the duration τ during which the REDOR sequence with ideal pulses is applied. (A) Employing finite 180_x pulses, $S(\tau)$ according to Eq. (83). (B) Employing finite 180° pulses with a sequence of phases such that the resulting average Hamiltonian is solely proportional to $2I_zS_z$, resulting in $S(\tau)$ according to Eq. (152).

Fig. 10(A) shows the result of calculating $S(\tau, f)$ for a dipolar coupling constant $b_{IS}/2\pi = 950$ Hz and three different values $f = 0.0$, 0.7 and 1.0. Clearly visible are the more pronounced oscillations in the case of $f = 1.0$ stemming from the fact that pulse sequence becomes γ-encoded as it resembles rotary resonance recoupling at the $n = 1$ resonance condition. For decreasing values of f the oscillations become less pronounced until at $f = 0$ they are least clearly visible. Fig. 10(A) illustrates why in general γ-encoded dipolar recoupling sequences are desirable: the stronger oscillations allow for a more exact determination of internuclear distances.

2.4. REDOR with finite pulses employing a sequence of rf phases

In the previous section we have extended the discussion of the REDOR heteronuclear dipolar recoupling sequence to the use of finite rf pulses that all employ the same zero rf phase. The resulting first order average Hamiltonian Eq. (69) contains terms proportional to the spin operators $2I_zS_z$ and $2I_yS_z$, where their individual amplitude depends on the fraction f of the rotational period that is occupied by the rf pulses. The reader will know that in practise the 180° pulses during the REDOR sequence employ a sequence of rf phases such as the XY-4 sequence, 0°, 90°, 0°, 90°, to improve the stability of the sequence with respect to rf offset and rf amplitude errors [60–63]. However, in addition such a sequence of phases leads to a simplified first order average Hamiltonian solely proportional to the heteronuclear longitudinal two-spin-order operator $2I_zS_z$ [43].

In this section, rather than analysing a given, existing sequence of rf phases for the REDOR rf pulses, the goal is to start with the rf phases as variables and to use first order average Hamiltonian theory to find solutions for the sequence of phases that result in the desired form of the first order average Hamiltonian solely proportional to the $2I_zS_z$ heteronuclear longitudinal two-spin order operator. This problem is closely related to compensating a train of 180° pulses in proton decoupling or the Carr-Purcell Meiboom-Gill (CPMG) sequence [64,65] with respect to rf offset and amplitude errors [60–63,66–70].

As shown in Fig. 7(C) we consider two basic building blocks of the REDOR sequence employing a total of 4 180° pulses with arbitrary rf phases ϕ_1–ϕ_4. The use of two basic building blocks rather than just a single one proves necessary to achieve the first order average Hamiltonian solely being proportional to $2I_zS_z$. Fig. 7(C) shows the definitions of time points t_0 to t_9 and sequence segments ①–⑧ during the two basic building blocks of the REDOR sequence. The definitions of time points t_1 to t_5 with respect to t_0 is identical to Eqs. (41)–(45). In addition, we can express the time points t_6 to t_9 in the following way:

$$t_6 = t_0 + \frac{3\tau_r}{2} - f\frac{\tau_r}{4} \tag{86}$$

$$t_7 = t_0 + \frac{3\tau_r}{2} + f\frac{\tau_r}{4} \tag{87}$$

$$t_8 = t_0 + 2\tau_r - f\frac{\tau_r}{4} \tag{88}$$

$$t_9 = t_0 + 2\tau_r + f\frac{\tau_r}{4} \tag{89}$$

To enhance the accessibility of the following calculations, readers are encouraged to first review the results presented in Eq. (125), which is the outcome of applying first-order average Hamiltonian theory to the REDOR sequence employing finite pulses with arbitrary rf phases. Afterwards, they can return to this section for a deeper understanding.

2.4.1. Hamiltonian

The Hamiltonian Eq. (21) during REDOR pulse sequence assuming an rf phase of $\phi = 0$ for all rf pulses can be modified to accommodate general rf pulse phases with the help of Eq. (I-16):

$$\begin{aligned} H(t) &= H_{\mathrm{rf}}(t) + H_{\mathrm{int}}(t) \\ &= \underbrace{\omega_{\mathrm{nut}}(t)\, R_z\big(\phi(t)\big)\, I_x\, R_z\big(-\phi(t)\big)}_{H_A(t)} + \underbrace{\omega_{IS}^{\mathrm{DD}}(t)\, 2I_zS_z}_{H_B(t)}, \end{aligned} \tag{90}$$

where $\phi(t)$ denotes the time-dependent rf phase during the basic REDOR sequence block in Fig. 7(C), which spans a total of two rotational periods, $T = 2\tau_r$. As a result $H_A(t)$ and $H_B(t)$ are periodic in time with periods $2\tau_r$ and τ_r, respectively. However that implies that both are periodic in time with $2\tau_r$:

$$H_A(t + 2\tau_r) = H_A(t) \qquad H_B(t + 2\tau_r) = H_B(t). \tag{91}$$

The piecewise time-independent Hamiltonian $H_A(t)$ of the interaction with the rf field is given by:

$$H_A(t) = \begin{cases} 0 & \text{for} \quad \begin{array}{l} t_1 \le t < t_2 \text{ or } t_3 \le t < t_4 \text{ or} \\ t_5 \le t < t_6 \text{ or } t_7 \le t < t_8 \end{array} \\ \omega_{\mathrm{nut}}\, R_z(\phi_1)\, I_x\, R_z(-\phi_1) & \text{for} \quad t_2 \le t < t_3 \\ \omega_{\mathrm{nut}}\, R_z(\phi_2)\, I_x\, R_z(-\phi_2) & \text{for} \quad t_4 \le t < t_5 \\ \omega_{\mathrm{nut}}\, R_z(\phi_3)\, I_x\, R_z(-\phi_3) & \text{for} \quad t_6 \le t < t_7 \\ \omega_{\mathrm{nut}}\, R_z(\phi_4)\, I_x\, R_z(-\phi_4) & \text{for} \quad t_8 \le t \le t_9, \end{cases} \tag{92}$$

and the time-dependent Hamilton of the heteronuclear dipolar interaction is given by:

$$H_B(t) = \omega_{IS}^{\mathrm{DD}}(t)\, 2I_zS_z. \tag{93}$$

2.4.2. Rf propagator

With the help of the rf Hamiltonian $H_A(t)$ in Eq. (92) we can calculate the propagator $U_A(t, t_1)$ that will be used to transform the Hamiltonian Eq. (90) into the interaction frame of the rf field. However as shown in Fig. 7(C) we have to consider the 8 different blocks ①–⑧ in the sequence when setting up $U_A(t, t_1)$. To improve the readability of the equations from this point forward, we introduce two new symbols

$U_A^{①④}(t,t_1)$ and $U_A^{⑤⑧}(t,t_1)$ that denote the *total accumulated* propagators of the rf field from time point t_1 up to a time point t in the time intervals $[t1,t5[$ and $[t5,t9]$, respectively:

$$U_A(t,t_1) = \begin{cases} U_A^{①④}(t,t_1) & \text{for } t_1 \le t < t_5 \\ U_A^{⑤⑧}(t,t_1) & \text{for } t_5 \le t \le t_9 \end{cases} \tag{94}$$

The propagator $U_A^{①④}(t,t_1)$ is given by

$$U_A^{①④}(t,t_1) = \begin{cases} \mathbb{1} & \text{for } t_1 \le t < t_2 \\ R_z(\phi_1)R_x\left(\beta_{②}(t)\right)R_z(-\phi_1) & \text{for } t_2 \le t < t_3 \\ R_z(\phi_1)R_x(\pi)R_z(-\phi_1) & \text{for } t_3 \le t < t_4 \\ R_z(\phi_2)R_x\left(\beta_{④}(t)\right)R_z(-\phi_2) & \\ \quad \times R_z(\phi_1)R_x(\pi)R_z(-\phi_1) & \text{for } t_4 \le t < t_5. \end{cases} \tag{95}$$

and can be simplified to

$$U_A^{①④}(t,t_1) = \begin{cases} \mathbb{1} & \text{for } t_1 \le t < t_2 \\ R_z(\phi_1)R_x\left(\beta_{②}(t)\right)R_z(-\phi_1) & \text{for } t_2 \le t < t_3 \\ R_x(\pi)R_z(-2\phi_1) & \text{for } t_3 \le t < t_4 \\ R_x(\pi)R_z(-\phi_2)R_x\left(\beta_{④}(t)\right)R_z(-2\phi_1+\phi_2) & \text{for } t_4 \le t < t_5, \end{cases} \tag{96}$$

where in the third and fourth row the rotation operator $R_x(\pi)$ was moved to the front, which allowed to collect the z-rotations at the end. We have used the time-dependent nutation angles $\beta_{②}(t)$ and $\beta_{④}(t)$ that have been introduced in Eqs. (49) and (50), respectively. For the pulse sequence blocks ⑥ and ⑧, the corresponding time-dependent nutation angles $\beta_{⑥}(t)$ and $\beta_{⑧}(t)$ may be defined:

$$\beta_{⑥}(t) = \omega_{\text{nut}}(t - t_6) \tag{97}$$

$$\beta_{⑧}(t) = \omega_{\text{nut}}(t - t_8), \tag{98}$$

where analogous to Eq. (51), they may be expressed as a function of $\beta_{②}(t)$:

$$\beta_{⑥}(t+\tau_r) = \beta_{②}(t) \tag{99}$$

$$\beta_{⑧}(t+\frac{3\tau_r}{2}) = \beta_{②}(t) \tag{100}$$

For the propagator $U_A^{⑤⑧}(t,t_1)$ we obtain:

$$U_A^{⑤⑧}(t,t_1) = \begin{cases} R_z(-2\phi_1+2\phi_2) & \text{for } t_5 \le t < t_6 \\ R_z(\phi_3)R_x\left(\beta_{⑥}(t)\right) & \\ \quad \times R_z(-2\phi_1+2\phi_2-\phi_3) & \text{for } t_6 \le t < t_7 \\ R_x(\pi)R_z(-2\phi_1+2\phi_2-2\phi_3) & \text{for } t_7 \le t < t_8 \\ R_x(\pi)R_z(-\phi_4)R_x\left(\beta_{⑧}(t)\right) & \\ \quad \times R_z(-2\phi_1+2\phi_2-2\phi_3+\phi_4) & \text{for } t_8 \le t \le t_9. \end{cases} \tag{101}$$

It will prove useful in the next section to introduce abbreviations for the accumulated phases in rows 2 and 4 in both Eqs. (96) and (101):

$$\chi_{②} = \phi_1 \tag{102}$$

$$\chi_{④} = 2\phi_1 - \phi_2 \tag{103}$$

$$\chi_{⑥} = 2\phi_1 - 2\phi_2 + \phi_3 \tag{104}$$

$$\chi_{⑧} = 2\phi_1 - 2\phi_2 + 2\phi_3 - \phi_4 \tag{105}$$

where the first line has solely been added for completeness. In addition to providing more clarity in writing the equations it shows how the case of four 180° rf pulses with arbitrary phases can be extended to adding further pulses. Here, we will not repeat Eqs. (96) and (101) using these abbreviations, however, for the transformation into the interaction frame we need the adjoint of both propagators, $U_A^{①④}(t,t_1)$ and $U_A^{⑤⑧}(t,t_1)$:

$$U_A^{\dagger①④}(t,t_1) = \begin{cases} \mathbb{1} & \text{for } t_1 \le t < t_2 \\ R_z(\chi_{②})R_x\left(-\beta_{②}(t)\right)R_z(-\phi_1) & \text{for } t_2 \le t < t_3 \\ R_z(\chi_{②}+\phi_1)R_x(-\pi) & \text{for } t_3 \le t < t_4 \\ R_z(\chi_{④})R_x\left(-\beta_{④}(t)\right)R_z(\phi_2)R_x(-\pi) & \text{for } t_4 \le t < t_5. \end{cases} \tag{106}$$

and

$$U_A^{\dagger⑤⑧}(t,t_1) = \begin{cases} R_z(\chi_{④}-\phi_2) & \text{for } t_5 \le t < t_6 \\ R_z(\chi_{⑥})R_x\left(-\beta_{⑥}(t)\right)R_z(-\phi_3) & \text{for } t_6 \le t < t_7 \\ R_z(\chi_{⑥}+\phi_3)R_x(-\pi) & \text{for } t_7 \le t < t_8 \\ R_z(\chi_{⑧})R_x\left(-\beta_{⑧}(t)\right)R_z(\phi_4)R_x(-\pi) & \text{for } t_8 \le t \le t_9. \end{cases} \tag{107}$$

We note that with using the abbreviations χ_1–χ_4 rows 2 and 4 in both Eqs. (106) and (107) have a similar form. Furthermore, as the Hamiltonian $H_B(t)$ of the heteronuclear dipolar interaction Eq. (93) is proportional to I_z, row 1 in both (106) and (107) does not change I_z and row 3 in both (106) and (107) simply inverts I_z.

2.4.3. Interaction frame Hamiltonian

The propagators $U_A^{\dagger①④}(t,t_1)$ and $U_A^{\dagger⑤⑧}(t,t_1)$ calculated in the previous section can now be used to transform the Hamiltonian into the interaction frame of the rf field. The transformation into the interaction frame is performed according to Eq. (I-56). For clarity the interaction frame Hamiltonian $\tilde{H}_B(t)$ will also be separated into two parts:

$$\begin{aligned} \tilde{H}_B(t) &= U_A(t,t_1)^\dagger\, H_B(t)\, U_A(t,t_1) \\ &= \begin{cases} U_A^{\dagger①④}(t,t_1)\, H_B(t)\, U_A^{①④}(t,t_1) & \text{for } t_0 \le t < t_5 \\ U_A^{\dagger⑤⑧}(t,t_1)\, H_B(t)\, U_A^{⑤⑧}(t,t_1) & \text{for } t_5 \le t \le t_9 \end{cases} \qquad (108) \\ &= \begin{cases} \tilde{H}_B^{①④}(t) & \text{for } t_0 \le t < t_5 \\ \tilde{H}_B^{⑤⑧}(t) & \text{for } t_5 \le t \le t_9. \end{cases} \qquad (109) \end{aligned}$$

Here we will as an example show the transformation for a time point t in the interval $[t_4,t_5[$, which corresponds to the last lines in $U_A^{①④}(t,t_1)$ and $U_A^{\dagger①④}(t,t_1)$ in Eqs. (96) and (106), respectively. For $t_4 \le t < t_5$:

$$\begin{aligned} &\tilde{H}_B^{①④}(t) \\ &\quad = \omega_{IS}^{\text{DD}}(t)\, 2S_z\, R_z(\chi_{④})R_x\left(-\beta_{④}(t)\right) \\ &\qquad \times \underbrace{R_z(\phi_2)R_x(-\pi)}\, I_z\, R_x(\pi)R_z(-\phi_2)\, R_x\left(\beta_{④}(t)\right)\, R_z(-\chi_{④}) \\ &\quad = -\omega_{IS}^{\text{DD}}(t)\, 2S_z\, R_z(\chi_{④})\, R_x\left(-\beta_{④}(t)\right)\, I_z\, R_x\left(\beta_{④}(t)\right)\, R_z(-\chi_{④}) \\ &\quad = -\omega_{IS}^{\text{DD}}(t)\, 2S_z\, \underbrace{R_z(\chi_{④})\left\{I_z\cos\beta_{④}(t) + I_y\sin\beta_{④}(t)\right\}}\, R_z(-\chi_{④}) \\ &\quad = -\omega_{IS}^{\text{DD}}(t)\, 2S_z\, \left\{I_z\cos\beta_{④}(t) + \left\{I_y\cos\chi_{④} - I_x\sin\chi_{④}\right\}\sin\beta_{④}(t)\right\}, \end{aligned} \tag{110}$$

In a similar way as in the Eq. (110) the other rows in the interaction frame Hamiltonians $\tilde{H}_B^{①④}(t)$ and $\tilde{H}_B^{⑤⑧}(t)$ can be calculated, resulting in

$$\tilde{H}_B^{①④}(t) = \omega_{IS}^{\text{DD}}(t)\, 2S_z \times \begin{cases} I_z & \text{for } t_1 \le t < t_2 \\ I_z\cos\beta_{②}(t) & \\ \quad + \left\{I_y\cos\chi_{②} - I_x\sin\chi_{②}\right\}\sin\beta_{②}(t) & \text{for } t_2 \le t < t_3 \\ -I_z & \text{for } t_3 \le t < t_4 \\ -I_z\cos\beta_{④}(t) & \\ \quad - \left\{I_y\cos\chi_{④} - I_x\sin\chi_{④}\right\}\sin\beta_{④}(t) & \text{for } t_4 \le t < t_5 \end{cases} \tag{111}$$

and

$$\tilde{H}_B^{⑤⑧}(t) = \omega_{IS}^{\mathrm{DD}}(t)\, 2S_z \times \begin{cases} I_z & \text{for } t_5 \le t < t_6 \\ I_z \cos\beta_{⑥}(t) & \\ \quad + \{I_y \cos\chi_{⑥} - I_x \sin\chi_{⑥}\} \sin\beta_{⑥}(t) & \text{for } t_6 \le t < t_7 \\ -I_z & \text{for } t_7 \le t < t_8 \\ -I_z \cos\beta_{⑧}(t) & \\ \quad - \{I_y \cos\chi_{⑧} - I_x \sin\chi_{⑧}\} \sin\beta_{⑧}(t) & \text{for } t_8 \le t \le t_9. \end{cases} \quad (112)$$

2.4.4. First order average Hamiltonian and propagator

After the interaction frame Hamiltonians $\tilde{H}_B^{①④}(t)$ and $\tilde{H}_B^{⑤⑧}(t)$ have been determined in the previous section, the first order average Hamiltonian over the complete interval $[t_1, t_9]$ with duration $T = 2\tau_r$ can be calculated according to

$$\bar{H}_B^{(1)} = \frac{1}{T}\int_{t_1}^{t_5} \mathrm{d}t\ \tilde{H}(t) = \sum_{k=1}^{8} \underbrace{\frac{1}{2\tau_r}\int_{t_k}^{t_{k+1}} \mathrm{d}t\ \tilde{H}_B(t)}_{\int_{⑥}}, \quad (113)$$

where the integral over $[t_1, t_9]$ was split into 8 separate intergrals denoted $\int_{⑥}$ with $k = 1...8$. In a first step the sum of the odd numbered integrals $\int_{①}$, $\int_{③}$, $\int_{⑤}$ and $\int_{⑦}$ is calculated analogous to Eqs. (56)–(59) in Section 2.3.4, where the final result is identical to Eq. (59) and given by

$$\int_{①} + \int_{③} + \int_{⑤} + \int_{⑦} = -2I_z S_z\, \frac{2}{\pi}\Omega^{(1)} \cos(f\pi/2) \sin\big(\omega_r t_0 - \gamma_{PR}^{IS}\big). \quad (114)$$

The even numbered integrals $\int_{②}$, $\int_{④}$, $\int_{⑥}$ and $\int_{⑧}$ are more elaborate to calculate compared to Section 2.3.4, as the rf pulses have the general phases ϕ_1–ϕ_4. However, the introduction of $\chi_{②}$–$\chi_{⑧}$ in Eqs. (111) and (112) allows to write the sum in the following way:

$$\int_{②} + \int_{④} + \int_{⑥} + \int_{⑧} = 2S_z \sum_{k=2,4,6,8} \frac{(-1)^{1+\frac{k}{2}}}{2\tau_r} \int_{t_k}^{t_{k+1}} \mathrm{d}t\ \omega_{IS}^{\mathrm{DD}}(t) \big\{ I_z \cos\beta_{⑥}(t) + \{I_y \cos\chi_{⑥} - I_x \sin\chi_{⑥}\} \sin\beta_{⑥}(t) \big\}, \quad (115)$$

where we note that the term proportional to $\cos\beta_{⑥}(t)$ does not depend on the rf phases and therefore its integral can be calculated in a similar way as in Eqs. (60) and (61). The term proportional to $\sin\beta_{⑥}(t)$ depends on the different rf phases, hence, in order to calculate its integral the terms have to be collected in the following way:

$$\int_{②} + \int_{④} + \int_{⑥} + \int_{⑧} = 2S_z I_z\, \Omega^{(1)} \frac{2}{\pi} \frac{f^2 \cos(f\pi/2)}{f^2 - 1} \sin\big(\omega_r t_0 - \gamma_{PR}^{IS}\big) + 2S_z \frac{1}{2\tau_r} \underbrace{\int_{t_2}^{t_3} \mathrm{d}t\, \sin\beta_{②}(t) \Big\{ \omega_{IS}^{\mathrm{DD}}(t) \big[I_y c_1 - I_x s_1\big] - \omega_{IS}^{\mathrm{DD}}(t + \frac{\tau_r}{2}) \big[I_y c_2 - I_x s_2\big] \Big\}}_{\int_{⑤}}, \quad (116)$$

where we have introduced another shorthand notation:

$$c_1 = \cos\chi_{②} + \cos\chi_{⑥} \quad (117)$$

$$s_1 = \sin\chi_{②} + \sin\chi_{⑥} \quad (118)$$

$$c_2 = \cos\chi_{④} + \cos\chi_{⑧} \quad (119)$$

$$s_2 = \sin\chi_{④} + \sin\chi_{⑧}. \quad (120)$$

The integral $\int_{⑤}$ can be simplified using the time symmetry relations Eqs. (11) and (12):

$$\int_{⑤} = 2S_z\, \frac{1}{4}\big[I_y(c_1 + c_2) - I_x(s_1 + s_2)\big]\, \frac{2}{\tau_r} \int_{t_2}^{t_3} \mathrm{d}t\ \omega^{(1)}(t) \sin\beta_{②}(t) + 2S_z\, \frac{1}{4}\big[I_y(c_1 - c_2) - I_x(s_1 - s_2)\big]\, \frac{2}{\tau_r} \int_{t_2}^{t_3} \mathrm{d}t\ \omega^{(2)}(t) \sin\beta_{②}(t) \quad (121)$$

The integral over time of $\omega^{(1)}(t)\sin\beta_{②}(t)$ in the first row was already determined earlier in Eq. (63). The time integral over $\omega^{(2)}(t)\sin\beta_{②}(t)$ in the second row can be solved in the following way:

$$\begin{aligned} &\frac{2}{\tau_r}\int_{t_2}^{t_3} \mathrm{d}t\ \omega^{(2)}(t)\sin\beta_{②}(t) \\ &= \frac{2\Omega^{(2)}}{\tau_r}\int_{t_2}^{t_3} \mathrm{d}t\ \cos\big(2(\omega_r t - \gamma_{PR}^{IS})\big) \sin\big(\frac{\omega_r}{f}(t - t_2)\big) \\ &= \frac{2\Omega^{(2)}}{\tau_r}\int_{0}^{f\pi/\omega_r} \mathrm{d}t'\ \cos\big(\,2\omega_r t' + 2(\omega_r t_0 - \gamma_{PR}^{IS}) - f\pi\,\big) \sin\big(\frac{\omega_r}{f}t'\big) \\ &= \frac{2}{\pi}\Omega^{(2)}\, \frac{f\cos(f\pi)}{1 - 4f^2}\, \cos\big(2(\omega_r t_0 - \gamma_{PR}^{IS})\big), \end{aligned} \quad (122)$$

where we have used the relationship

$$2\omega_r t_2 = 2\omega_r t_0 - f\pi + 2\pi. \quad (123)$$

With the help of the result in Eq. (122) the integral $\int_{⑤}$ can be simplified to

$$\int_{⑤} = -2S_z\, \frac{1}{4}\big[I_y(c_1 + c_2) - I_x(s_1 + s_2)\big] \times \frac{2}{\pi}\Omega^{(1)}\, \frac{f\cos(f\pi/2)}{1 - f^2}\, \cos\big(\omega_r t_0 - \gamma_{PR}^{IS}\big) + 2S_z\, \frac{1}{4}\big[I_y(c_1 - c_2) - I_x(s_1 - s_2)\big] \times \frac{2}{\pi}\Omega^{(2)}\, \frac{f\cos(f\pi)}{1 - 4f^2}\, \cos\big(2(\omega_r t_0 - \gamma_{PR}^{IS})\big) \quad (124)$$

Collecting all results from Eqs. (114), (116) and (124), the final first order average Hamiltonian may be written as:

$$\bar{H}_B^{(1)} = \bar{\omega}_{IS}^{(z)}(f)\, 2I_z S_z + \sum_{m=1}^{2} \Big\{ \bar{\omega}_{IS}^{(x,m)}(f)\, 2I_x S_z + \bar{\omega}_{IS}^{(y,m)}(f)\, 2I_y S_z \Big\}, \quad (125)$$

where the time-independent amplitudes are given by

$$\bar{\omega}_{IS}^{(z)}(f) = \frac{\sqrt{2}}{\pi} b_{IS}\ \ \varsigma^{(z)}(f) \sin\big(2\beta_{PR}^{IS}\big) \cos\big(\omega_r t_0 - \gamma_{PR}^{IS}\big) \quad (126)$$

$$\bar{\omega}_{IS}^{(x,1)}(f) = -\frac{s_1 + s_2}{4}\frac{\sqrt{2}}{\pi} b_{IS}\, \varsigma^{(xy,1)}(f) \sin\big(2\beta_{PR}^{IS}\big) \cos\big(\omega_r t_0 - \gamma_{PR}^{IS}\big) \quad (127)$$

$$\bar{\omega}_{IS}^{(y,1)}(f) = \frac{c_1 + c_2}{4}\frac{\sqrt{2}}{\pi} b_{IS}\, \varsigma^{(xy,1)}(f) \sin\big(2\beta_{PR}^{IS}\big) \cos\big(\omega_r t_0 - \gamma_{PR}^{IS}\big) \quad (128)$$

$$\bar{\omega}_{IS}^{(x,2)}(f) = -\frac{s_1 - s_2}{4}\ \ \frac{1}{\pi} b_{IS}\, \varsigma^{(xy,2)}(f) \sin^2\big(\beta_{PR}^{IS}\big) \cos\big(2(\omega_r t_0 - \gamma_{PR}^{IS})\big) \quad (129)$$

$$\bar{\omega}_{IS}^{(y,2)}(f) = \frac{c_1 - c_2}{4}\ \ \frac{1}{\pi} b_{IS}\, \varsigma^{(xy,2)}(f) \sin^2\big(\beta_{PR}^{IS}\big) \cos\big(2(\omega_r t_0 - \gamma_{PR}^{IS})\big), \quad (130)$$

where $\varsigma^{(z)}(f)$ has been defined in Eq. (67) and $\bar{\omega}_{IS}^{(z)}(f)$ in Eq. (126) is identical to the expression in Eq. (65). In addition, $\varsigma^{(xy,1)}(f)$ and $\varsigma^{(xy,2)}(f)$ are given by

$$\varsigma^{(xy,1)}(f) = \varsigma^{(y)}(f), \qquad \text{see Eq. (68)} \quad (131)$$

$$\varsigma^{(xy,2)}(f) = \frac{f\cos(f\pi)}{1 - 4f^2} \quad (132)$$

As a result, the final general first order average Hamiltonian Eq. (125) can be written as:

$$\begin{aligned}\bar{H}_B^{(1)} = \; & \frac{\sqrt{2}}{\pi} b_{IS}\, \varsigma^{(z)}(f)\, \sin\left(2\beta_{PR}^{IS}\right) \sin\left(\omega_r t_0 - \gamma_{PR}^{IS}\right)\, 2I_zS_z \\ & + \frac{\sqrt{2}}{\pi} b_{IS}\, \varsigma^{(xy,1)}(f)\, \sin\left(2\beta_{PR}^{IS}\right) \cos\left(\omega_r t_0 - \gamma_{PR}^{IS}\right) \\ & \qquad \times 2S_z \left[a^{(y,1)}\, I_y - a^{(x,1)}\, I_x\right] \\ & + \frac{1}{\pi} b_{IS}\, \varsigma^{(xy,2)}(f)\, \sin^2\left(\beta_{PR}^{IS}\right) \cos\left(2(\omega_r t_0 - \gamma_{PR}^{IS})\right) \\ & \qquad \times 2S_z \left[a^{(y,2)}\, I_y - a^{(x,2)}\, I_x\right], \end{aligned} \tag{133}$$

where we have defined the coefficients:

$$a^{(x,1)} = \frac{1}{4}(s_1 + s_2) \tag{134}$$

$$a^{(y,1)} = \frac{1}{4}(c_1 + c_2) \tag{135}$$

$$a^{(x,2)} = \frac{1}{4}(s_1 - s_2) \tag{136}$$

$$a^{(y,2)} = \frac{1}{4}(c_1 - c_2) \tag{137}$$

The term proportional to $2I_zS_z$ in Eq. (133) is identical to the one in Eq. (69). To check the overall consistency of the result in Eq. (133) for general rf phases ϕ_1–ϕ_4 with the result in Eq. (69) for $\phi_1 = \phi_2 = \phi_3 = \phi_4 = 0$, we need to evaluate the factor c_1, c_2, s_1 and s_2 for this case, which can be easily done using the definitions in Eqs. (117)–(120) and (102)–(105):

$$a^{(x,1)} = 0 \qquad \text{for } \phi_1 = \phi_2 = \phi_3 = \phi_4 = 0 \tag{138}$$

$$a^{(y,1)} = 1 \qquad \text{for } \phi_1 = \phi_2 = \phi_3 = \phi_4 = 0 \tag{139}$$

$$a^{(x,2)} = 0 \qquad \text{for } \phi_1 = \phi_2 = \phi_3 = \phi_4 = 0 \tag{140}$$

$$a^{(y,2)} = 0 \qquad \text{for } \phi_1 = \phi_2 = \phi_3 = \phi_4 = 0. \tag{141}$$

Hence in the case that the rf phase of all 180° pulses are set to zero, as expected, Eq. (133) transforms into Eq. (69).

Eq. (133) is a general and powerful result as it enables us to choose the phases ϕ_1–ϕ_4 in such a way that we *design* the first order average Hamiltonian of the REDOR sequence with finite rf pulses to have the properties we desire. As discusses in the introduction of this section, a desirable first order average Hamiltonian is solely proportional to the longitudinal two-spin order operator $2I_zS_z$. One advantage of this type of average Hamiltonian is that the terms $2I_zS_z$ commute for different spin pairs. This means the evolution of the heteronuclear spin system can be described as the superposition of the evolution of isolated spin pairs.

In order to achieve an first order average Hamiltonian solely proportional to $2I_zS_z$ the phases ϕ_1–ϕ_4 must be chosen such that the coefficients of the terms proportional to $2I_xS_z$ and $2I_yS_z$ in Eq. (133) disappear, i. e. $a^{(x,1)} = a^{(y,1)} = a^{(x,2)} = a^{(y,2)} = 0$. Using the definitions in Eqs. (117)–(120) and (102)–(105) this can be achieved if the following conditions are fulfilled:

$$\cos\phi_1 + \cos\left(2\phi_1 - 2\phi_2 + \phi 3\right) = 0 \tag{142}$$

and

$$\cos\left(2\phi_1 - \phi_2\right) + \cos\left(2\phi_1 - 2\phi_2 + 2\phi_3 - \phi_4\right) = 0 \tag{143}$$

and

$$\sin\phi_1 + \sin\left(2\phi_1 - 2\phi_2 + \phi 3\right) = 0 \tag{144}$$

and

$$\sin\left(2\phi_1 - \phi_2\right) + \sin\left(2\phi_1 - 2\phi_2 + 2\phi_3 - \phi_4\right) = 0. \tag{145}$$

Solving this system of equations involving trigonometric functions is difficult in general. However, it is straightforward to employ a computer to scan the phases ϕ_1–ϕ_4 in constant increments in a nested loop and check if the conditions in Eqs. (142)–(145) are fulfilled and evaluate the coefficients in Eqs. (134)–(137).

Table 1 shows the result of stepping all phases by an increment of $\pi/4$ (45°) in a nested loop. According to Eq. (I-66), the total propagator over the basic REDOR block in Fig. 7(C) is a product of the rf propagator and the average Hamiltonian propagator. Therefore, Table 1 also lists the rf propagator $U_A(t_1 + T, t_1)$. As discussed in section I-3.3, preferably, the basic REDOR block is cyclic, i. e. $U_A(t_1 + T, t_1) = \pm\mathbb{1}$. This condition is straightforwardly fulfilled if all phases ϕ_1–ϕ_4 are zero, however, for arbitrary values for the phases ϕ_1–ϕ_4, the rf propagator $U_A(t_1 + T, t_1)$ needs to be calculated explicitly.

Table 1
Results for the coefficients $a^{(x,1)}$, $a^{(y,1)}$, $a^{(x,2)}$ and $a^{(y,2)}$ in Eqs. (138)–(141) for sets of rf phases $\phi_1, \ldots, \phi_4$ of the 180° pulses in the basic REDOR building block shown in Fig. 7(C).

ϕ_1	0	0	0	0	0	0	0	0
ϕ_2	0	π	$\pi/2$	0	π	$\pi/2$	$\pi/4$	$3\pi/4$
ϕ_3	0	0	$\pi/2$	π	π	0	$-\pi/2$	$\pi/2$
ϕ_4	0	π	0	π	0	$\pi/2$	$-\pi/4$	$-3\pi/4$
$a^{(x,1)}$	0	0	$-1/2$	0	0	0	0	0
$a^{(y,1)}$	1	0	$1/2$	0	0	0	0	0
$a^{(x,2)}$	0	0	0	0	0	0	0	0
$a^{(y,2)}$	0	1	0	0	0	0	0	0
$U_A(t_1+T,t_1)$	$\mathbb{1}$	$\mathbb{1}$	$\mathbb{1}$	$\mathbb{1}$	$\mathbb{1}$	$-\mathbb{1}$	$R_z(\pi)$	$R_z(\pi)$

The first column of Table 1 recapitulates the results for $\{\phi_1, \phi_2, \phi_3, \phi_4\} = \{0, 0, 0, 0\}$ shown in Eqs. (138)–(141). The second column shows the results for an intuitive choice for the sequence of phases given by $\{\phi_1, \phi_2, \phi_3, \phi_4\} = \{0, \pi, 0, \pi\}$. However, as it turns out $a^{(y,2)}$ is not zero for this choice of phases, an undesirable result.

Highlighted in yellow in Table 1 are three fundamental choices for the phase sequence $\{\phi_1, \phi_2, \phi_3, \phi_4\}$ for which all coefficients fulfil (i) $a^{(x,1)} = a^{(y,1)} = a^{(x,2)} = a^{(y,2)} = 0$ and (ii) $U_A(t_1 + T, t_1) = \pm\mathbb{1}$. Interestingly, two choices are $\{\phi_1, \phi_2, \phi_3, \phi_4\} = \{0, 0, \pi, \pi\}$ and $\{0, \pi, \pi, 0\}$, which resemble the phases in the basic building blocks of the MLEV sequences used for the train of 180° pulses in broadband heteronuclear decoupling or the CPMG sequence [66–69]. Furthermore, the third solution $\{\phi_1, \phi_2, \phi_3, \phi_4\} = \{0, \pi/2, 0, \pi/2\}$ corresponds to the XY-4 phase sequence [60,61,70] that is both used in the CPMG sequence and has together with its extensions, the XY-8 and XY-16 sequences, commonly been the choice for the rf phases of the pulses in the REDOR sequence. Both the MLEV and XY type of phase sequences were originally constructed to compensate a series of 180° pulses with respect to rf resonance offsets and rf amplitude errors [60–63,66–70].

The cyclicity restriction $U_A(t_1 + T, t_1) = \pm\mathbb{1}$ can be slightly lifted and solutions be permitted, in which the rf propagator corresponds to an overall z-rotation, $U_A(t_1 + T, t_1) = R_z(2\pi/k)$, where k is an integer, as repeating this pulse sequence block k-times results in an overall cyclic pulse sequence again. An abundant number of solutions resulting in an overall z-rotation can be found, Table 1 includes two of the simplest solutions of this kind with $U_A(t_1 + T, t_1) = R_z(\pi)$.

If the phase sequence $\{\phi_1, \phi_2, \phi_3, \phi_4\}$ is chosen such that all coefficients disappear, $a^{(x,1)} = a^{(y,1)} = a^{(x,2)} = a^{(y,2)} = 0$, the first order average Hamiltonian in Eq. (125) simplifies to

$$\bar{H}_B^{(1)} = \bar{\omega}_{IS}^{(z)}(f)\, 2I_zS_z, \tag{146}$$

where $\bar{\omega}_{IS}^{(z)}(f)$ is given in Eq. (126). The resulting first order average Hamiltonian can be written as:

$$\bar{H}_B^{(1)} = \frac{\sqrt{2}}{\pi} b_{IS}\, \varsigma^{(z)}(f)\, \sin\left(2\beta_{PR}^{IS}\right) \sin\left(\omega_r t_0 - \gamma_{PR}^{IS}\right)\, 2I_zS_z, \tag{147}$$

which is solely proportional to $2I_zS_z$ as the average Hamiltonian Eq. (31) of the original REDOR sequence with indefinitely short pulses with phase zero. However, the amplitudes $\bar{\omega}_{IS}^{(z)}(f)$ in Eq. (126) for the case of finite pulses are scaled compared to the amplitudes $\bar{\omega}_{IS}^{(z)}$ in Eq. (30) for indefinitely short pulses:

$$\bar{\omega}_{IS}^{(z)}(f) = \varsigma^{(z)}(f)\, \bar{\omega}_{IS}^{(z)}, \tag{148}$$

where limits of the scaling factor $\varsigma^{(z)}(f)$ for $f \to 0$ and $f \to 1$ have be shown above in Eqs. (70) and (73), respectively.

In case the basic REDOR pulse sequence block of duration T is cyclic, the propagator in first order average Hamiltonian theory over

a duration $\tau = NT$ that is an integer multiple of T is given by

$$U(t_0+\tau,t_0) = \exp\{-\mathrm{i}\bar{H}_B^{(1)}\tau\} = \exp\{-\mathrm{i}\,\bar{\omega}_{IS}^{(z)}(f)\,\tau\,2I_zS_z\} \quad (149)$$

analogous to the case of infinitely short pulses shown in Eq. (33). Similarly, the S-spin-echo intensity under a REDOR sequence of duration τ for a single crystallite orientation is given by:

$$S(\tau;f;\Omega_{PR}^{IS}) = \cos\left(\bar{\omega}_{IS}^{(z)}(f)\,\tau\right) \quad (150)$$

In a powder sample the final S-spin signal as a function of the duration τ of the REDOR sequence is obtained by averaging over all possible orientations Ω_{PR}^{IS}:

$$S(\tau,f) = \left\langle \cos\left(\bar{\omega}_{IS}^{(z)}(f)\,\tau\right)\right\rangle_{\Omega_{PR}^{IS}} \quad (151)$$

Similarly to the case of REDOR with ideal pulses the integral in Eq. (151) can be expressed using the Bessel functions:

$$S(\tau,f) = \frac{\pi}{2\sqrt{2}}\,J_{-1/4}\left(\varsigma^{(z)}(f)\frac{\sqrt{2}}{2\pi}\,b_{IS}\,\tau\right)J_{1/4}\left(\varsigma^{(z)}(f)\frac{\sqrt{2}}{2\pi}\,b_{IS}\,\tau\right) \quad (152)$$

Fig. 10(B) shows the result of calculating $S(\tau,f)$ in Eqs. (151) and (152) for a dipolar coupling constant $b_{IS}/2\pi = 950$ Hz and three different values $f = 0.0$, 0.7 and 1.0. Unlike in the case depicted in (A), for all values of f the graphs have the identical overall shape, solely the frequency of the oscillations decreases slightly when moving from $f = 0$ to $f = 1$. As a result if the REDOR sequence employing pulses of finite length is used, i. e. basically in all experimentally realistic cases, is used to determine heteronuclear dipolar couplings, and hence heteronuclear internuclear distances, the factor f has to be taken into account in the analysis, otherwise the resulting heteronulcear dipolar couplings appear weaker than they really are, leading to an overestimate in the internuclear distances [43].

A recent review by Ladizhansky et al. covers further developments of the REDOR pulse sequence [19]: In frequency-selective REDOR (FS-REDOR) [71], selective 180° pulses are used to generate the spin-echo, which allows to select specific heteronuclear spin pairs in multiple spin systems. Gullion and Schaefer achieved scaling of the recoupled heteronuclear dipolar coupling Hamiltonian by shifting one of the 180° pulses in the basic REDOR block referred to as Shifted-REDOR (S-REDOR) experiment [2,3]. This principle can be used to implement a *constant-time* version of the REDOR pulse sequence similar to the one shown in Fig. 6, in which the total recoupling time period τ is fixed and the spin-echo amplitude is recorded as function of the time-offset of every other 180° pulse from their original position [2,3]. This implementation resembles the dipolar and chemical shift (DIPSHIFT) correlation experiment [72–74]. Furthermore, as discussed below Eq. (31) in rotor-encoded spectroscopy [44,45] the two REDOR I-spin irradiation blocks during the S-spin-echo shown in Fig. 6 are shifted with respect to each other. The same principle can be used to scale the recoupled heteronuclear dipolar Hamiltonian [46]. As we have seen above, the conventional implementation of REDOR with two 180° pulses per rotational period requires the nutation frequency of the rf field to be at least equal to the sample rotation frequency, see Eq. (40), which might be difficult to achieve at fast sample spinning when the REDOR sequence is applied to nuclei with small gyromagnetic ratios such as ^{15}N. Jain et al. introduced the deferred rotational echo double resonance (DEDOR) sequence, in which two 180° pulses are applied per 3 rotational periods, reducing the minimum rf field requirement by a factor of 1/3 [75].

Although REDOR has been successfully employed to recouple heteronuclear dipolar couplings and determine distances between nuclei of which one type is protons [46,76–78], it is arguably not the ideal choice in dense proton networks, as for realistic, finite pulses REDOR also recouples the homonuclear dipolar ^{1}H···^{1}H couplings if applied to the ^{1}H nuclei. As superior alternative, especially for this application, Brinkmann and Kentgens have presented the symmetry-based rf pulse sequence SR4$_1^2$, which generates the desirable first order average Hamiltonian proportional to heteronuclear longitudinal two-spin-order ($2I_zS_z$), while decoupling the homonuclear proton dipolar interactions [79,80].

3. Lee-Goldburg homonuclear dipolar decoupling

In the second part of this tutorial paper we direct our attention to another important example for the application of average Hamiltonian theory in solid-state NMR, the design of rf pulse sequences that decouple the homonuclear dipolar coupling, especially targeting the strong homonuclear ^{1}H···H^1 dipolar couplings, enabling the recording of well-resolved ^{1}H NMR spectra in the solid-state. In static solids several homonuclear decoupling techniques have been developed. The original Lee-Goldburg (LG) scheme for homonuclear decoupling applies unmodulated rf irradiation off resonance on the ^{1}H, so as to satisfy the *Lee-Goldburg condition* [4,5]. This sequence will be discussed in detail in this section employing average Hamiltonian theory. However, because of its relatively poor performance, this technique has been superseded by more effective schemes including WAHUHA (WHH-4) [81], MREV-8 [82–84], BR-24, BR-52 [85], and BLEW-48 [86]. Furthermore, in order to improve the homonuclear decoupling performance, Mehring and Waugh suggested the Flip-Flop Lee-Goldburg (FFLG) experiment, in which a tilted rf coil is employed to alternate the direction of the effective field satisfying the Lee-Goldburg condition by applying simultaneously a constant magnetic field with alternating signs along the z-axis together with an rf field along the x-axis with rf phases alternating between 0 and π [6,7]. The same can be achieved by switching the frequency of the rf field in a phase-continuous way, resulting in the Frequency-Switched Lee-Goldburg (FSLG) sequence by Levitt and co-workers [8,9]. The aspects that lead to the improved performance of the FSLG sequence (and therefore the FFLG sequence) is discussed in detail below. The switching of the rf frequency may be implemented using linear ramps of the rf phase, resulting in the Phase-Modulated Lee-Goldburg (PMLG) sequence [87–89], which has been further improved resulting in the LG4 sequence [90,91]. The above sequences can be combined with MAS (combined multiple pulse NMR and magic angle spinning, CRAMPS) resulting in significantly improved ^{1}H spectral resolution [92]. Rather than using average Hamiltonian theory, the DUMBO ("decoupling using mind-boggling optimization") sequence has been developed by numerical optimization using a two-spin system [93,94]. Furthermore, a highly successful approach has been the direct optimization of this type of sequence directly on the NMR spectrometer, which led to the eDUMBO sequence, since imperfections in the experimental setup are inherently included in the optimization [95]. Recently, Paruzzo and Emsley, published an excellent, comprehensive comparison study and detailed experimental protocol covering the LG, WHH-4, MREV-8, BR-24, FSLG/PMLG, DUMBO, eDUMBO and LG4 homonuclear decoupling sequences [96].

3.1. Hamiltonians of the chemical shift and homonuclear dipolar coupling

In order to analyse both the LG and FFLG/FSLG homonuclear decoupling sequences using average Hamiltonian theory, we consider for simplicity a homonuclear two-spin-1/2 system with spins labelled I_j and I_k., respectively. In a static solid the nuclear spin Hamiltonian is comprised of the chemical shift and direct homonuclear dipolar coupling interactions, which are presented in detail in Appendices C.7 and C.8.1, respectively.

3.1.1. Chemical shift

The combined Hamiltonian for the Zeeman and chemical shift interactions for spin I_j in the high-field approximation and in the rotating

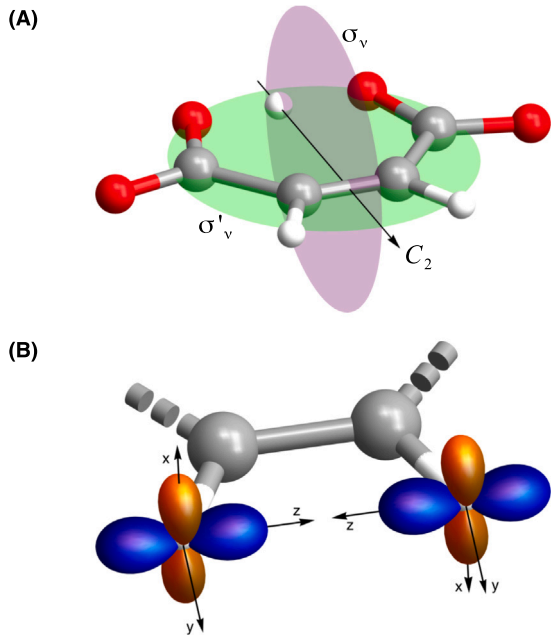

Fig. 11. (A) Molecular structure of the hydrogen maleate anion in the geometry optimized crystal structure of potassium hydrogen maleate [97]. The twofold symmetry axis C_2 and the two mirror planes σ_v and σ_v' for the C_{2v} symmetry of the hydrogen maleate anion are shown. (B) Ovaloids representing the CSA tensors, i. e. the anisotropic components of the full chemical shift tensors, of the two CH protons. The colours orange and blue represent positive and negative chemical shift values, respectively. The principal axis of the chemical shift tensors as determined by Achlama et al. are depicted [98]. The principal values are given by $(\delta_{XX}, \delta_{YY}, \delta_{ZZ}) = (9.2, 7.0, 4.3)$ ppm [98], where the original chemical shift referencing with respect to solid adamantane was converted to neat TMS [99,100]. The isotropic, anisotropic chemical shifts and asymmetry parameter are given by $(\delta_{\text{iso}}, \delta_{\text{aniso}}, \eta) = (6.8\text{ ppm}, -2.5\text{ ppm}, 0.87)$, respectively. The homonuclear ^{1}H–^{1}H homonuclear dipolar coupling constant is given by $b_{jk}/2\pi = -9400$ Hz, corresponding to an internuclear distance of $r_{jk} = 233.8$ pm. (For interpretation of the references to colour in this figure legend, the reader is referred to the web version of this article.)

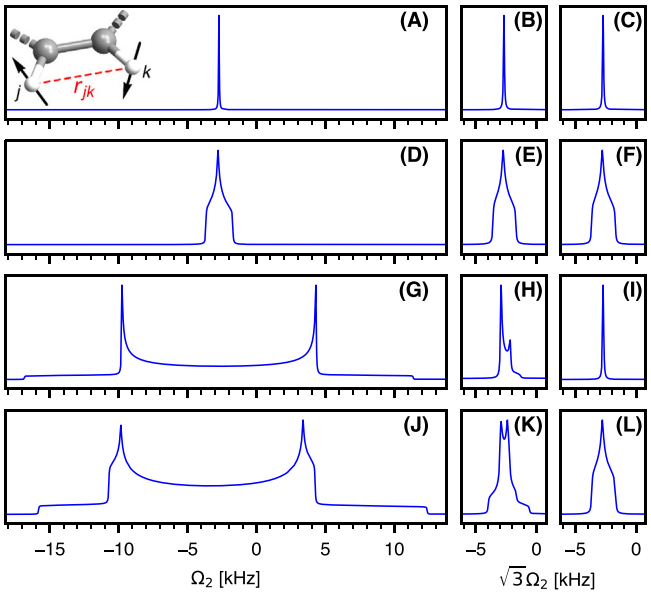

Fig. 12. Numerically simulated spectra of the two-^{1}H spin system depicted in the small inset on the top and fully in Fig. 11(B) at an external field of 9.4 T and static sample conditions: first row (A)–(C) solely considering the isotropic chemical shift; second row (D)–(F) including the isotropic and anisotropic chemical shifts; third row (G)–(I) considering the isotropic chemical shift and the homonuclear dipolar coupling; fourth row (J)–(L) including all spin interactions, i. e. the isotropic, anisotropic chemical shifts and the homonuclear dipolar coupling. first column (A), (D), (G), (J) without the application of an rf field during acquisition; second column (B), (E), (H), (K) under constant rf irritation at the LG condition employing an effective rf field of $\omega_{\text{eff}}/2\pi = 100$ kHz; third column (C), (F), (I), (L) under FSLG irradiation using an effective rf field of $\omega_{\text{eff}}/2\pi = 100$ kHz. All numerical simulations were performed using the *Simpson* package version 4.2.3 [103–105] using a ^{1}H Larmor frequency of $\omega_0/2\pi = -400$ MHz and 50 Hz exponential line broadening.

frame is given in Eq. (C.35) and can be written as:

$$H_j^{\text{Z,CS}} = \omega_j^{\text{CS}}\, I_{jz} = \omega_j^{\text{CS}}\, T_{10}^j, \tag{153}$$

where T_{10}^j is the 0th component of the irreducible spherical spin tensor of rank 1 for spin I_j as defined in Table C.1 and we have introduced the chemical shift frequency

$$\omega_j^{\text{CS}} = \Omega_j^{\text{iso}} + \omega_j^{\text{CSA}}, \tag{154}$$

where the isotropic chemical shift frequency Ω_j^{iso} is defined in Eq. (C.34), and the chemical shift anisotropy (CSA) frequency ω_j^{CSA} is defined as

$$\omega_j^{\text{CSA}} = [A_{20}^{\text{CS}}]^L = \sum_{m=-2}^{2} [A_{2m}^{\text{CS}}]^P D_{m0}^{(2)}(\Omega_{PL}^j), \tag{155}$$

where $[A_{20}^{\text{CS}}]^L$ and $[A_{2m}^{\text{CS}}]^P$ are components of the 2nd rank CSA tensor in the laboratory frame and PAS, respectively, listed in Table C.2. The Euler angles $\Omega_{PL}^j = \{\alpha_{PL}^j, \beta_{PL}^j, \gamma_{PL}^j\}$ define the relative orientation of the PAS and the laboratory frame and are random variables in a powdered sample.

As an example Fig. 11 depicts the CSA tensors of the two CH protons in potassium hydrogen maleate (KHM) as ovaloids according to Mueller and co-workers [101]. Fig. 12(A) and (D) show numerically simulated ^{1}H spectra of the two-^{1}H spin system of the two CH groups in a powdered sample of KHM, (A) solely considering the isotropic chemical shift and (D) including both the isotropic and anisotropic chemical shifts. As shown in Fig. 11(A) the two CH groups are symmetry related and therefore the ^{1}H spectra only show a single resonance line, where panel (D) shows a typical CSA powder pattern [102].

3.1.2. Homonuclear dipolar coupling

As described in detail in Appendix C.8.1 The nuclear spin Hamiltonian of the direct homonuclear dipolar coupling in static solids between two nuclear spins I_j and I_k in the high-field approximation and in the rotating frame is given by:

$$H_{jk}^{\text{DD}} = \omega_{jk}^{\text{DD}} \frac{1}{\sqrt{6}} \left(2I_{jz}I_{kz} - \frac{1}{2}\left(I_j^- I_k^+ + I_j^+ I_k^-\right)\right) = \omega_{jk}^{\text{DD}}\, T_{20}^{jk}, \tag{156}$$

where T_{20}^{jk} is the 0th component of the irreducible spherical spin tensor of rank 2 for the two spins I_j and I_k as defined in Table C.1. Analogous to the steps described in Section 2.1.1, the time-independent dipolar frequency ω_{jk}^{DD} is obtained by transforming the tensor of the homonuclear dipolar coupling from the PAS to the laboratory frame:

$$\omega_{jk}^{\text{DD}} = \sqrt{6}\, b_{jk}\, D_{00}^{(2)}(\Omega_{PL}^{jk}) = \sqrt{6}\, b_{jk}\, d_{00}^{(2)}(\beta_{PL}^{jk}) = \sqrt{6}\, b_{jk}\, \frac{1}{2}\left(3\cos^2\beta_{PL}^{jk} - 1\right), \tag{157}$$

where the Euler angles $\Omega_{PL}^{jk} = \{\alpha_{PL}^{jk}, \beta_{PL}^{jk}, \gamma_{PL}^{jk}\}$ define the relative orientation of the PAS and the laboratory frame and are random variables in a powdered sample. We note that for simplicity we have used different sets of Euler angles Ω_{PL}^j and Ω_{PL}^{jk} to describe the transformation from the PAS directly to the laboratory frame for the CSA tensor for spin

I_j and the homonuclear dipolar coupling, respectively. In practise, to perform numerical powder averaging it proves often useful to introduce an intermediate reference frame, the *molecular frame*, fixed on the molecule into which all interactions are transformed first from their respective PAS. In a second step the interactions are transformed from the molecular frame to the laboratory frame, where the corresponding Euler angles are random variables in a powder. This is described in more detail in Appendix C.3.

As defined in Appendix C.8.1, the homonuclear dipolar coupling constant b_{jk} is given by

$$b_{jk} = -\frac{\mu_0}{4\pi}\frac{\gamma_I^2\hbar}{r_{jk}^3}, \tag{158}$$

where in the Appendix examples of typical homonuclear dipolar coupling constants are given, which are also depicted in Fig. 2.

Fig. 12(G) shows the numerically simulated ^{1}H powder pattern of the two-^{1}H spin system in KHM shown in Fig. 11 including the homonuclear dipolar coupling and the isotropic chemical shift. The spectrum resembles the typical Pake doublet of a homonuclear dipolar coupled spin-1/2 pair [33]. The distance between the two inner discontinuities is equal to $3/2 \times b_{jk}/2\pi$, i. e. 1.5 times the the homonuclear dipolar coupling constant. Furthermore, in Fig. 12(J), the result of a numerical simulation including in addition the CSA tensors of the two CH protons are shown. The spectrum clearly shows the effect of the *tensor interplay* [106] between the homonuclear and CSA interactions.

3.2. Lee-Goldburg (LG) homonuclear decoupling

In this section we will introduce the original Lee-Goldburg sequence and use first-order average Hamiltonian theory to understand how it achieves homonuclear dipolar decoupling. Furthermore, the limitations of this sequence will become evident in the second-ordered average Hamiltonian, which can be overcome by the FFLG and FSLG sequences discussed in the following section.

Fig. 13(A) shows the basic building block of the LG sequence: Continuous, windowless, rf irradiation is applied to the I-spins with a nutation frequency ω_{nut} and frequency offset Δ. As shown in Fig. 14, if the rf phase is chosen to be $\phi = 0$, this results in an effective field with effective nutation frequency ω_{eff}, where the vector of the rotation axis lies in the xz-plane and encloses the angle θ with the z-axis. ω_{eff} and θ are given in Eqs. (I-22) and (I-23), respectively, but are repeated here for clarity:

$$\omega_{\text{eff}} = \sqrt{\omega_{\text{nut}}^2 + \Delta^2} \tag{159}$$

$$\theta = \arctan(\omega_{\text{nut}}/\Delta), \tag{160}$$

where the *Lee-Goldburg condition* is fulfilled if ω_{nut} and Δ are chosen such that θ is equal to the magic angle, i. e. $\theta = \arctan\sqrt{2} \approx 54.74°$.

The starting time point of the LG irradiation is denoted t_0 and for the purpose of the analysis by average Hamiltonian theory, a sequence of length $T = \tau_c$ is considered, such that $\omega_{\text{eff}}\,\tau_c = 2\pi$ and end time point is given by $t_2 = t_1 + T$.

3.2.1. Hamiltonian

The Hamiltonian of the homonuclear two-spin system I_j and I_k in the presence of the LG irradiation is time-independent in the rotating frame and contains the contribution H_{rf} from the interaction with the rf field and the contribution H_{int} from the internal spin interactions, consisting of the chemical shift and homonuclear dipolar interactions, Eqs. (153) and (156), respectively:

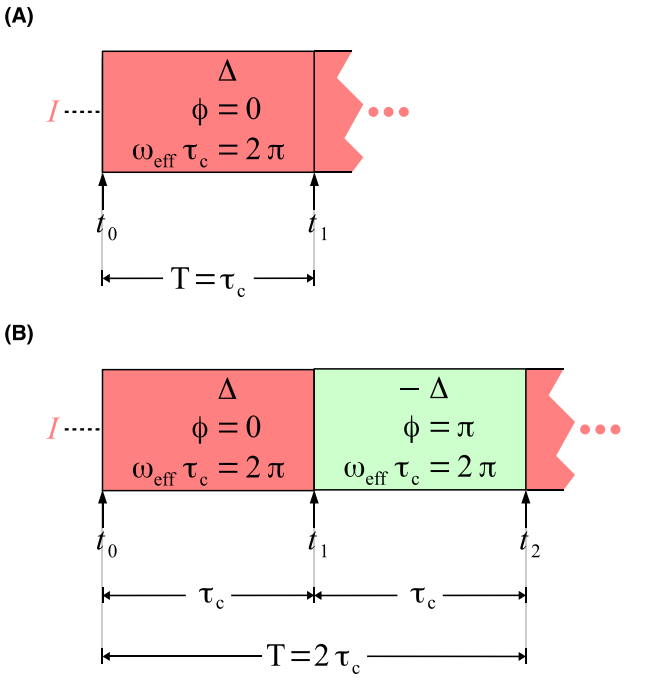

Fig. 13. Building blocks of the (A) Lee-Goldburg (LG) and (B) Frequency-Switched Lee-Goldburg (FSLG) homonuclear recoupling sequences, where Δ and $-\Delta$ are the rf frequency offsets, $\phi = 0, \pi$ the rf phases, ω_{eff} the effective nutation frequency and τ_c the duration of the elementary cycles.

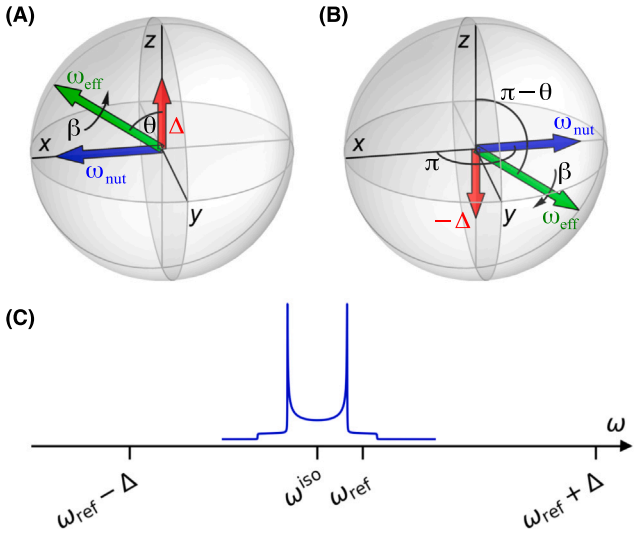

Fig. 14. Details of the rf field settings during the LG and FSLG pulse sequences: (A) At a phase of $\phi = 0$ the positive rf frequency offset Δ of the rf field and the nutation frequency ω_{nut} are chosen such that the resulting effective field encloses the magic angle $\theta = \arctan\sqrt{2}$ with the positive z-axis. (B) At the same nutation frequency ω_{nut} together with the negative rf frequency offset $-\Delta$ and rf phase $\phi = \pi$, the resulting effective field encloses the angle $\pi - \theta_m$ with the positive z-axis. (C) Depiction of the relevant rf frequencies in relation to the NMR spectrum.

$$\begin{aligned} H &= H_{\text{rf}} + H_{\text{int}} \\ &= \underbrace{\Delta I_z + \omega_{\text{nut}} I_x}_{H_A} + \underbrace{\omega_j^{\text{CS}} T_{10}^j + \omega_k^{\text{CS}} T_{10}^k}_{H_B^{\text{CS}}} + \underbrace{\omega_{jk}^{\text{DD}} T_{20}^{jk}}_{H_B^{\text{DD}}}, \end{aligned} \tag{161}$$

where the Hamiltonian has been split into three parts H_A, H_B^{CS}, and H_B^{DD} which will enable us to transform H into the interaction frame of H_A before the application of average Hamiltonian theory as described in section (I-3.2).

As described in detail in section I-2.4, the rf Hamiltonian of an off-resonance rf field can be expressed with the help of the effective nutation frequency ω_{eff}, see Eq. (I-24):

$$H_A = \omega_{\text{eff}}\, R_y(\theta)\, I_z\, R_y(-\theta), \tag{162}$$

where $R_x(\beta)$, $R_y(\beta)$ and $R_z(\beta)$ are the operators for the rotation of the I-spins about the x-, y- and z-axis, respectively, as defined in section I-2.4, however here using the total spin angular momentum operators:

$$I_x = I_{jx} + I_{kx} \qquad I_y = I_{jy} + I_{ky} \qquad I_z = I_{jz} + I_{kz}. \tag{163}$$

We noted above that the Hamiltonian in Eq. (161) is time-independent and therefore according to the discussion in I-2.2 the propagator can be calculated directly using Eq. (I-7). However, this requires to determine the matrix exponential of the Hamiltonian, which is in general not analytically possible even for a two-spin-1/2 system, but needs a numerical approach. Furthermore, a numerical approach cannot provide the physically intuitive insight into the operating principles of pulse sequences that average Hamiltonian theory can provide.

3.2.2. Rf propagator

In order to transform the Hamiltonian H in Eq. (161) into the interaction frame of the rf field Hamiltonian H_A, we need to calculate the rf propagator, which is straightforward based on Eq. (I-25):

$$U_A(t,t_0) = R_y(\theta) R_z\big(\omega_{\text{eff}}(t-t_0)\big) R_y(-\theta) \tag{164}$$

In addition, we need the adjoint of the rf propagator for the transformation into the interaction frame:

$$\begin{aligned} U_A^\dagger(t,t_0) &= R_y(\theta) R_z\big(-\omega_{\text{eff}}(t-t_0)\big) R_y(-\theta) \\ &= R_y(\theta) R\big(\Omega_{\text{eff}}\big), \end{aligned} \tag{165}$$

where $R(\Omega)$ denotes the rotation by the rf field through the three Euler angles $\Omega = \{\alpha, \beta, \gamma\}$ [25,107]:

$$R(\Omega) = R_z(\alpha)\, R_y(\beta)\, R_y(\gamma). \tag{166}$$

Hence the Euler angles Ω_{eff} ion Eq. (165) are given by

$$\Omega_{\text{eff}} = \big\{-\omega_{\text{eff}}(t-t_0), -\theta, 0\big\} \tag{167}$$

3.2.3. Interaction frame Hamiltonian

As the original Hamiltonian H in Eq. (161) contains contributions from two spin interactions, the chemical shift H_B^{CS} and homonuclear dipolar coupling H_B^{DD}, the total interaction frame Hamiltonian $\tilde{H}_B(t)$ will also be written as the sum of those two contributions transformed into the interactions frame:

$$\tilde{H}_B(t) = \tilde{H}_B^{DD}(t) + \tilde{H}_B^{CS}(t) \tag{168}$$

where $\tilde{H}_B^{DD}(t)$ and $\tilde{H}_B^{CS}(t)$ are the time-dependent interaction frame Hamiltonians of the homonuclear dipolar and chemical shift interactions, respectively.

Homonuclear dipolar coupling. Firstly, the time-dependent interaction frame Hamiltonian of the homonuclear dipolar interaction can be generated employing the propagator $U_A^\dagger(t,t_0)$ of Eq. (165):

$$\begin{aligned} \tilde{H}_B^{DD}(t) &= U_A(t,t_0)^\dagger\, H_B^{DD}\, U_A(t,t_0) \\ &= \omega_{jk}^{DD}\, R_y(\theta) R\big(\Omega_{\text{eff}}\big)\, T_{20}^{jk}\, R\big(-\Omega_{\text{eff}}\big) R_y(-\theta) \\ &= \omega_{jk}^{DD}\, R_y(\theta) \Big(\sum_{\mu=-2}^{2} T_{2\mu}^{jk}\, D_{\mu 0}^{(2)}\big(\Omega_{\text{eff}}\big) \Big) R_y(-\theta) \\ &= \omega_{jk}^{DD}\, R_y(\theta) \Big(\sum_{\mu=-2}^{2} T_{2\mu}^{jk}\, \exp\big(\mathrm{i}\,\mu\,\omega_{\text{eff}}(t-t_0)\big)\, d_{\mu 0}^{(2)}(-\theta) \Big) R_y(-\theta) \end{aligned} \tag{169}$$

where we have used the rotation properties of the irreducible spherical spin tensor T_λ^{jk} of rank λ [25,107] together with the definitions of the Wigner-D and Wigner-d matrices $D_{mm'}^{(l)}$ and $d_{mm'}^{(l)}$, respectively [25,28].

Chemical shift. Secondly, the time-dependent interaction frame Hamiltonian of the chemical shift interaction can be generated using the propagator $U_A^\dagger(t,t_0)$ of Eq. (165):

$$\begin{aligned} \tilde{H}_B^{CS}(t) &= U_A(t,t_0)^\dagger\, H_B^{CS}\, U_A(t,t_0) \\ &= \sum_{l=j,k} \omega_l^{CS}\, R_y(\theta) R\big(\Omega_{\text{eff}}\big)\, T_{10}^{l}\, R\big(-\Omega_{\text{eff}}\big) R_y(-\theta) \\ &= \sum_{l=j,k} \omega_l^{CS}\, R_y(\theta) \Big(\sum_{\mu=-1}^{1} T_{1\mu}^{l}\, D_{\mu 0}^{(1)}\big(\Omega_{\text{eff}}\big) \Big) R_y(-\theta) \\ &= \sum_{l=j,k} \omega_l^{CS}\, R_y(\theta) \Big(\sum_{\mu=-1}^{1} T_{1\mu}^{l}\, \exp\big(\mathrm{i}\,\mu\,\omega_{\text{eff}}(t-t_0)\big)\, d_{\mu 0}^{(1)}(-\theta) \Big) R_y(-\theta) \end{aligned} \tag{170}$$

3.2.4. First order average Hamiltonian and propagator

Analogous to the interaction frame Hamiltonian Eq. (168), the first order average Hamiltonian under LG irradiation will be written as the sum of the first order average Hamiltonian of the homonuclear dipolar and chemical shift interactions:

$$\bar{H}_B^{(1)} = \bar{H}_B^{DD(1)} + \bar{H}_B^{CS(1)}, \tag{171}$$

where the first order average Hamiltonians are calculated according to Eq. (I-30).

Homonuclear dipolar coupling: The first order average Hamiltonian of the homonuclear dipolar coupling is given by:

$$\begin{aligned} \bar{H}_B^{DD(1)} &= \frac{1}{T} \int_{t_0}^{t_1} \mathrm{d}t\; \tilde{H}_B^{DD}(t) \\ &= \omega_{jk}^{DD}\, R_y(\theta) \Big(\sum_{\mu=-2}^{2} T_{2\mu}^{jk}\, d_{\mu 0}^{(2)}(-\theta)\, \frac{1}{T} \int_0^T \mathrm{d}t'\; \exp\big(\mathrm{i}\,\mu\,\omega_{\text{eff}}\, t'\big) \Big) R_y(-\theta), \end{aligned} \tag{172}$$

where without loss of generality we have chosen $t_0 = 0$ and $t_1 = T$ to simplify the result. The integral over the duration of the LG irradiation can be evaluated in the following way:

$$\begin{aligned} \frac{1}{T} \int_0^T \mathrm{d}t'\; \exp\big(\mathrm{i}\,\mu\,\omega_{\text{eff}}\, t'\big) &= -\frac{\mathrm{i}}{2\pi\mu} \Big[\exp\big(\mathrm{i}\,\mu\,\omega_{\text{eff}}\, t'\big) \Big]_0^{\tau_c} \\ &= \frac{\mathrm{i}}{2\pi\mu} \Big(1 - \exp\big(\mathrm{i}\,2\pi\mu\big) \Big) \\ &= \begin{cases} 0 & \text{for} \quad \mu \neq 0 \\ 1 & \text{for} \quad \mu = 0, \end{cases} \end{aligned} \tag{173}$$

where the case $\mu = 0$ can be easily calculated using the limit of $\mu \to 0$ (in spite of μ being integer) together with the approximations $\cos\alpha \approx 1$ and $\sin\alpha \approx \alpha$ for small $\alpha \ll 1$. We are left with the simplified expression

$$\begin{aligned} \bar{H}_B^{DD(1)} &= \omega_{jk}^{DD}\, R_y(\theta)\, T_{20}^{jk}\, d_{00}^{(2)}(-\theta)\, R_y(-\theta) \\ &= 0, \end{aligned} \tag{174}$$

where, we have used the property of the Wigner d-matrix element $d_{00}^{(2)}(\pm\theta) = (3\cos^2\theta - 1)/2 = 0$ at the magic angle $\theta = \arctan\sqrt{2}$, as has been previously discussed in Section 2.1.1. The result Eq. (174) is the reason the original LG sequence is referred to as a homonuclear dipolar decoupling sequence. We note that the rotation and averaging of the 2nd rank spin tensor by the rf field is analogous to the rotation and averaging of the 2nd rank spatial tensor during MAS, see Section 2.1.2 and Appendix C.10.

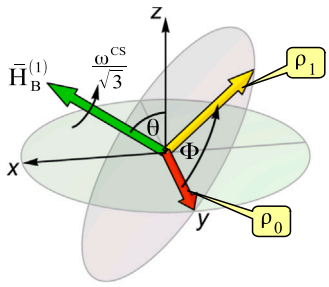

Fig. 15. Illustration of the trajectory of a starting y-magnetization vector under the first order average Hamiltonian under a LG or FSLG pulse sequence. The magnetization vector rotates in a plane whose normal encloses the angle $\theta = \arctan\sqrt{2}$ with the positive z-axis, where the accumulated phase is given by $\Phi = \omega^{CS}\tau/\sqrt{3}$.

Chemical shift: The first order average Hamiltonian of the chemical shift interactions is given by:

$$\begin{aligned}\bar{H}_B^{CS(1)} &= \frac{1}{T}\int_{t_0}^{t_1} \mathrm{d}t\ \tilde{H}_B^{CS}(t)\\ &= \sum_{l=j,k}\omega_l^{CS}\ R_y(\theta)\Bigg(\sum_{\mu=-1}^{1} T_{1\mu}^{l}\ d_{\mu 0}^{(1)}(-\theta)\\ &\qquad\qquad \times \frac{1}{T}\int_0^T \mathrm{d}t'\ \exp\left(\mathrm{i}\,\mu\,\omega_{\mathrm{eff}}\,t'\right)\Bigg) R_y(-\theta)\\ &= \sum_{l=j,k}\omega_l^{CS}\ R_y(\theta)\ T_{10}^{l}\ d_{00}^{(1)}(-\theta)\ R_y(-\theta)\\ &= R_y(\theta)\Bigg(\sum_{l=j,k}\frac{1}{\sqrt{3}}\ \omega_l^{CS}\ T_{10}^{l}\Bigg) R_y(-\theta),\end{aligned} \tag{175}$$

where, we have used $d_{00}^{(1)}(\theta) = \cos\theta = 1/\sqrt{3}$ at the magic angle $\theta = \arctan\sqrt{2}$. The last line has the same form as the original Hamiltonian of the chemical shift interaction Eq. (153) scaled by $1/\sqrt{3}$ and rotated around the y-axis in the rotating frame by the magic angle $\theta = \arctan\sqrt{2}$.

Propagator: The duration $T = \tau_c$ of the basic building block of the LG sequence shown in Fig. 13 was chosen such that $\omega_{\mathrm{eff}}\,\tau_c = 2\pi$, hence the rf propagator Eq. (164) over that time interval is cyclic:

$$U_A(t_1, t_0) = U_A(t_0 + \tau_c, t_0) = \mathbb{1}. \tag{176}$$

Therefore, the propagator in first order average Hamiltonian theory over a duration $\tau = NT$, where N is an integer, of LG irradiation is given by

$$\begin{aligned}U(t_0+\tau, t_0) &= \exp\{-\mathrm{i}\bar{H}_B^{(1)}\tau\}\\ &= \exp\{-\mathrm{i}\bar{H}_B^{CS(1)}\tau\}\\ &= R_y(\theta)\,R_z\Bigg(\sum_{l=j,k}\frac{1}{\sqrt{3}}\,\omega_l^{CS}\tau\Bigg)\,R_y(-\theta)\end{aligned} \tag{177}$$

according to Eq. (I-70). The propagator in Eq. (177) corresponds to the evolution of the spin density operator under the chemical shift Hamiltonian that is scaled by the factor of $1/\sqrt{3}$ around an axis that is parallel to the effective field, i. e. an axis that encloses an angle $\theta = \arctan\sqrt{2}$ with the positive z-axis. This evolution is depicted in Fig. 15 for the evolution of a starting density operator $\rho_0 = I_y$ depicted in red under the first order average Hamiltonian depicted in green by an angle Φ into the resulting density operator ρ_1 shown in yellow. The evolution corresponds to a rotation in the plane that is orthogonal to the direction of the effective field.

Fig. 12(B) and (E) show the result of numerically simulating the spectra of the two-^{1}H spin system in KHM shown in Fig. 11 in the presence of LG irradiation, including (B) solely the isotropic chemical shift and (E) including both the isotropic and anisotropic chemical shifts. Note, the frequency axis Ω_2 of the spectra has been scaled by the factor of $\sqrt{3}$, compensating for the scaling of the chemical shift Hamiltonian by the factor of $1/\sqrt{3}$ in Eqs. (175) and (177). As a result the spectra in panels (B) and (E) of Fig. 12 resemble the spectra in panels (A) and (D), respectively, which were simulated without LG irritation.

Interestingly, when the homonuclear dipolar ^{1}H$\cdots^1$H coupling is included in the simulations, the results shown in Fig. 12(H) and (K) cannot be predicted by first order average Hamiltonian theory alone, as the resulting spectral lineshapes do not resemble the results in panels (B) and (E), as would be expected for perfect homonuclear decoupling performance, but are typical second-order lineshapes, indicating contributions from the commutator of the homonuclear dipolar coupling and the isotropic chemical shift in (H) and contributions from the commutator of the homonuclear dipolar coupling and the full chemical shift tensor in (K). In the following section we will briefly discuss those contributions in second order average Hamiltonian theory.

3.2.5. Second order average Hamiltonian

In this section we will discuss briefly the second order average Hamiltonian under LG irradiating, which can be calculated using the interaction frame Hamiltonian $\tilde{H}_B(t)$ given in Eq. (168) according to Eq. (I-31):

$$\begin{aligned}\bar{H}_B^{(2)} &= \frac{1}{2\mathrm{i}T}\int_{t_0}^{t_1}\mathrm{d}t\int_{t_0}^{t}\mathrm{d}t'\ [\tilde{H}_B(t), \tilde{H}_B(t')]\\ &= \frac{1}{2\mathrm{i}T}\int_{t_0}^{t_1}\mathrm{d}t\int_{t_0}^{t}\mathrm{d}t'\Big\{\ [\tilde{H}_B^{CS}(t), \tilde{H}_B^{DD}(t')] + [\tilde{H}_B^{DD}(t), \tilde{H}_B^{CS}(t')]\\ &\qquad + [\tilde{H}_B^{CS}(t), \tilde{H}_B^{CS}(t')] + [\tilde{H}_B^{DD}(t), \tilde{H}_B^{DD}(t')]\Big\},\end{aligned} \tag{178}$$

where in the second line we had to consider the commutators between pairs of interactions. In general these commutators do not vanish as they contain pairwise commutators between the irreducible spherical spin operators $T_{1\mu}^{j}$, $T_{1\mu'}^{k}$, and $T_{2\mu''}^{jk}$, with $\mu, \mu' = -1, 0, 1$ and $\mu'' = -2, -1, 0, 1, 2$, which follows from the interaction frame Hamiltonians Eqs. (169) and (170). The second-order lineshapes visible in panels (H) and (K) of Fig. 12 are mostly the results of commutators between the chemical shift interaction and the homonuclear dipolar coupling. A more detailed discussion of the second order average Hamiltonian under LG homonuclear decoupling can be found in Appendix B.

3.3. Flip-Flop and Frequency-Switched Lee-Goldburg (FFLG and FSLG) homonuclear decoupling

As we have seen in the previous section, the use of simple LG homonuclear decoupling results in ^{1}H resonances that are affected by second order cross terms between the homonuclear dipolar coupling and the chemical shift interactions. As was introduced in section I-3.1 there is a basic design principle for the rf pulse sequence to eliminate terms in second order average Hamiltonian theory: If we can design the rf pulse sequence such that the interaction frame Hamiltonian is symmetric over the time interval during which the sequence is applied, all even order average Hamiltonian terms vanish, see Eq. (I-38). This principle was first exploited by Mansfield when designing the MREV-8 homonuclear decoupling sequence [82–84].

Furthermore, Mehring and Waugh achieved the same for the LG experiment by concatenating a block of LG irradiation with a second block during which the direction of the effective field is inverted, referring to it as the Flip-Flop Lee-Goldburg (FFLG) experiment [6]. The principle is shown in Fig. 13(B): One basic LG building block of duration τ_c with nutation frequency ω_{nut}, frequency offset Δ and rf phase $\phi = 0$ is followed by a second block with the same nutation frequency, but frequency offset $-\Delta$ and rf phase $\phi = \pi$. Therefore the direction of the effective field is inverted during the second LG block as shown in

Fig. 14(B). As explained above, in the original FFLG implementation the switching of the frequency offset was achieved by a pulsed magnetic field along the z-axis (referred to a *video field*) [6,7], whereas in the Frequency-Switched Lee-Goldburg (FSLG) implementation Levitt and co-workers switched the offset of the rf field phase-continuously exploiting direct digital synthesis of the rf signal [8,9]. The relevant spectral and rf frequencies during an FSLG experiment are depicted in Fig. 14, where the Pake doublet of a homonuclear dipolar coupled spin-1/2 pair is shown at the isotropic chemical shift frequency ω^{iso}. In addition, the positions of the rf reference frequency ω_{ref}, and the positions of the resonance offsets $\omega_{\mathrm{ref}} \pm \Delta$ are indicated.

Fig. 13 shows the labelling of the time points t_0 to t_2 during the basic building block of total duration T of the FSLG sequence, which consists of two concatenated blocks of LG irradiation of duration τ_c, resulting in $T = 2\tau_c$. The offset Δ is inverted and the rf phase is switched to $\phi = \pi$ during the second block of LG irradiation. The nutation frequency ω_{nut} and rf offset Δ are chosen such that as described above the LG condition is fulfilled. i. e. $\theta = \arctan\sqrt{2}$ with θ defined in Eq. (160). Furthermore, $\omega_{\mathrm{eff}}\,\tau_c = 2\pi$ with ω_{eff} defined in Eq. (159).

3.3.1. Hamiltonian

The Hamiltonian during the FSLG pulse sequence looks similar to the one given in Eq. (161) except that the rf phase $\phi(t)$ and the rf offset $\Delta(t)$ become time-dependent

$$\begin{aligned} H(t) &= H_{\mathrm{rf}}(t) + H_{\mathrm{int}} \\ &= \underbrace{\Delta(t)\, I_z + \omega_{\mathrm{nut}}\, R_z\big(\phi(t)\big)\, I_x\, R_z\big(-\phi(t)\big)}_{H_A(t)} + \underbrace{\omega_j^{\mathrm{CS}}\, T_{10}^{j} + \omega_k^{\mathrm{CS}}\, T_{10}^{k}}_{H_B^{\mathrm{CS}}}, \\ &\quad + \underbrace{\omega_{jk}^{\mathrm{DD}}\, T_{20}^{jk}}_{H_B^{\mathrm{DD}}}, \end{aligned} \tag{179}$$

where $H_A(t)$ periodic in time with the period $T = 2\tau_c$:

$$H_A(t + 2\tau_c) = H_A(t). \tag{180}$$

The piecewise time-independent Hamiltonian $H_A(t)$ is given by:

$$\begin{aligned} H_A(t) &= \begin{cases} \Delta\, I_z + \omega_{\mathrm{nut}} I_x & \text{for} \quad t_0 \le t < t_1 \\ -\Delta\, I_z - \omega_{\mathrm{nut}} I_x & \text{for} \quad t_1 \le t \le t_2 \end{cases} \\ &= \begin{cases} \omega_{\mathrm{eff}}\, R_y(\theta)\, I_z\, R_y(-\theta) & \text{for} \quad t_0 \le t < t_1 \\ -\omega_{\mathrm{eff}}\, R_y(\theta)\, I_z\, R_y(-\theta) & \text{for} \quad t_1 \le t \le t_2, \end{cases} \end{aligned} \tag{181}$$

where we note that $H_A(t)$ during the time interval $[t_1, t_2]$ is identical to $H_A(t)$ during $[t_0, t_1[$ except that ω_{ref} is replaced by $-\omega_{\mathrm{ref}}$, i. e. the sign of the effective field has been inverted.

3.3.2. Rf propagator and interaction frame Hamiltonian

Given $H_A(t)$ in Eq. (181) it is now straightforward to determine the rf propagator based on the previous result shown in Eq. (164):

$$U_A(t, t_0) = \begin{cases} R_y(\theta) R_z\big(\omega_{\mathrm{eff}}(t - t_0)\big) R_y(-\theta) & \text{for} \quad t_0 \le t < t_1 \\ R_y(\theta) R_z\big(-\omega_{\mathrm{eff}}(t - t_1)\big) R_y(-\theta) & \text{for} \quad t_1 \le t \le t_2 \end{cases} \tag{182}$$

At this stage it is worthwhile to pause and consider the time symmetry of the propagator $U_A(t, t_0)$. Consider a small duration τ such that $0 < \tau < \tau_c$, then the propagator $U_A(t, t_0)$ at time point $t = t_0 + \tau$ following from Eq. (182) is given by:

$$U_A(t_0 + \tau, t_0) = R_y(\theta) R_z\big(\omega_{\mathrm{eff}}\,\tau\big) R_y(-\theta) \tag{183}$$

Furthermore, the propagator $U_A(t, t_0)$ at time point $t = t_2 - \tau$ following from Eq. (182) can be determined:

$$\begin{aligned} U_A(t_2 - \tau, t_0) &= R_y(\theta) R_z\big(-\omega_{\mathrm{eff}}(t_2 - \tau - t_1)\big) R_y(-\theta) \\ &= R_y(\theta) R_z(-\omega_{\mathrm{eff}}\,\tau_c) R_z\big(\omega_{\mathrm{eff}}\,\tau\big) R_y(-\theta) \\ &= R_y(\theta) R_z\big(\omega_{\mathrm{eff}}\,\tau\big) R_y(-\theta) \\ &= U_A(t_0 + \tau, t_0), \end{aligned} \tag{184}$$

which implies that the propagator $U_A(t, t_0)$ is symmetric over the time interval $[t_0, t_2]$, which will impose the same time symmetry on the interaction frame Hamiltonians:

$$\tilde{H}_B(t_0 + \tau) = \tilde{H}_B(t_2 - \tau) \tag{185}$$

$$\tilde{H}_B^{\mathrm{DD}}(t_0 + \tau) = \tilde{H}_B(t_2 - \tau) \tag{186}$$

$$\tilde{H}_B^{\mathrm{CS}}(t_0 + \tau) = \tilde{H}_B(t_2 - \tau), \tag{187}$$

where the expressions for the interaction frame Hamiltonians the time point $t = t_0 + \tau$ can be found in Eqs. (168), (169) and (170).

3.3.3. First and higher order average Hamiltonians

Using the symmetry property in Eqs. (185)–(187) it is straightforward to show that average Hamiltonian over the complete FSLG basic building block of duration $T = 2\tau_c$ is identical to the one for a single LG element of duration τ_c:

$$\begin{aligned} \bar{H}_B^{(1)} &= \frac{1}{T}\int_{t_0}^{t_2} \mathrm{d}t\; \tilde{H}_B(t) \\ &= \frac{1}{2\tau_c}\Big(\int_{t_0}^{t_1} \mathrm{d}t\; \tilde{H}_B(t) + \int_{t_1}^{t_2} \mathrm{d}t\; \tilde{H}_B(t)\Big) \\ &= \frac{1}{2\tau_c}\Big(\int_{0}^{\tau_c} \mathrm{d}\tau\; \tilde{H}_B(t_0 + \tau) + \int_{0}^{\tau_c} \mathrm{d}\tau\; \tilde{H}_B(t_2 - \tau)\Big) \\ &= \frac{1}{\tau_c}\int_{0}^{\tau_c} \mathrm{d}\tau\; \tilde{H}_B(t_0 + \tau) \end{aligned} \tag{188}$$

Therefore, the first order average Hamiltonian of the homonuclear dipolar coupling $\bar{H}_B^{\mathrm{DD}(1)}$ and the chemical shift interaction $\bar{H}_B^{\mathrm{CS}(1)}$ are identical to Eqs. (174) and (175), respectively, leading to total first average Hamiltonian under the FSLG homonuclear decoupling sequence:

$$\begin{aligned} \bar{H}_B^{(1)} &= \bar{H}_B^{\mathrm{CS}(1)} \\ &= R_y(\theta)\Big(\sum_{l=j,k} \frac{1}{\sqrt{3}}\, \omega_l^{\mathrm{CS}}\, T_{10}^{l}\Big) R_y(-\theta), \end{aligned} \tag{189}$$

which is identical to the previous result for the LG sequence in Eq. (175). More importantly, as the interaction frame Hamiltonian is symmetric over the time interval $[t_0, t_2]$, see Eq. (185), all even order average Hamiltonian terms vanish, as discussed in section I-3.1:

$$\bar{H}_B^{(n)} = 0 \qquad \text{for all even } n = 2, 4, 6, \ldots \tag{190}$$

This is a significant improvement compared to the original, basic LG homonuclear decoupling sequence as can be seen in the results of numerical simulations of the two-^{1}H spin system in KHM under FSLG irradiation shown in Fig. 12(C), (F), (I) and (L). The results shown in panels (C) and (F) were simulated solely including the isotropic chemical shift, and including the full chemical shift tensor, respectively. As expected from first order average Hamiltonian theory these spectra appear identical to the spectra simulated for the basic LG sequence shown in panels (B) and (E),

More importantly, when the homonuclear dipolar ^{1}H···^{1}H coupling is included in the simulations, the results shown in Fig. 12(I) and (L) for the FSLG sequence are identical to the ones shown in panels (C) and (F), for which the homonuclear dipolar coupling was not included in the simulations. This demonstrates impressively the removal especially of the terms in the second order average Hamiltonian according to Eq. (190) that were the cause of the second order lineshapes in the results shown for the basic LG sequences in panels (H) and (K).

Furthermore, the results shown on panel (L) of Fig. 12 illustrate why homonuclear decoupling sequences have been combined with MAS (CRAMPS), as the CSA powder pattern lineshape limits the resolution in the ^{1}H spectrum. CRAMPS on the other hand combines the homonuclear decoupling of the rf pulse sequence with the averaging of the MAS and results in isotopic ^{1}H lines, where the final resolution is limited by the homogeneity of the rf field and higher order cross term in the average Hamiltonian [108,109].

In addition to the above mentioned excellent comparison study and detailed experimental protocol of various homonuclear decoupling sequences [96], readers are encouraged to consult for further reading the 2016 review of Mote et al. on five decades of homonuclear decoupling in solid-state NMR [110]. Recently, Tognetti et al. have performed CRAMPS experiment at 60 kHz spinning frequency employing the PMLG sequence [111]. Quantifying different polymorphs and solvatomorphs of active pharmaceutical ingredients (APIs) in pharmaceutical formulations is frequently done by ^{13}C solid-state NMR, however Wong et al. introduced the CRAMPS-MAR technique [112], employing CRAMPS together with mixture analysis using references (MAR) [113], in which the spectrum of a mixture is fitted as a linear combination of the pure component spectra. Finally, Nishiyama et al. [114] and Schröder et al. [115] have reviewed the recent progress in ultrafast magic-angle spinning (up to 200 kHz), allowing directly detected high-resolution ^{1}H spectra without employing homonuclear decoupling pulse sequences.

4. Concluding remarks

In this second part of our *Introduction to average Hamiltonian theory* we applied average Hamiltonian theory to two seminal rf pulse sequences in solid-state NMR: (i) The REDOR heteronuclear dipolar recoupling sequence under MAS conditions, where we could show that in the case of rf pulses with finite duration, starting with arbitrary rf phases and the requirement of a first order average Hamiltonian solely proportional to heteronuclear longitudinal two-spin order ($2I_zS_z$) will lead to solutions including the XY and MLEV type phase schemes. (ii) The LG homonuclear dipolar decoupling sequence under static conditions and its improved successors, the FFLG and FSLG sequences, where we showed how making the basic pulse sequence building blocks in the FFLG and FSLG sequence time-symmetric leads to improved performance as all even order average Hamiltonian terms vanish.

Finally, Part III of this *Introduction to average Hamiltonian theory* will cover rotor-synchronized, symmetry-based decoupling and recoupling rf pulse sequences denoted CN_n^ν and RN_n^ν in MAS NMR. These sequences are described by three symmetry numbers, N, n, and ν, which can be chosen according to simple theorems linking the basic rf pulse building block, the timings and rf phases such that only certain terms are symmetry-allow in the average Hamiltonian [14,16,57,116–119]. This will simplify the rational design of recoupling and decoupling sequences with certain properties compared to having to start with arbitrary rf phases as was done for the REDOR sequence in Section 2.4.

Acknowledgements

I am grateful to Malcolm Levitt for introducing me to average Hamiltonian theory during my time as Ph.D. student in his laboratory. As this paper is based on educational lectures given at conferences and summerschools, I would like to thank some of the other lectures, specifically Marc Baldus, Matthias Ernst, Bob Griffin, Beat Meier, Niels Nielsen, Shimon Vega and Thomas Vosegaard for valuable comments and suggestions.

Declaration of competing interest

The authors declare that they have no known competing financial interests or personal relationships that could have appeared to influence the work reported in this paper.

Appendix A. Analytical expressions for rotary resonance recoupling

In this Appendix we derive the analytical form of the S-spin signal intensity in a powdered sample as a function of the duration τ of a constant rf field at the R^3 $n = 1$ resonance condition, i. e. REDOR with pulse fraction $f = 1$, $S(\tau, 1)$, shown in Eq. (85). For this, the powder averaging Eq. (83) has to be performed analytically using Eq. (36):

$$\begin{aligned} S(\tau,1) &= \frac{1}{4\pi}\int_0^{2\pi} \mathrm{d}\gamma_{PR}^{IS} \int_0^{\pi} \mathrm{d}\beta_{PR}^{IS}\, \sin\beta_{PR}^{IS}\, \cos\Big(\frac{1}{2\sqrt{2}}\, b_{IS}\, \sin\big(2\beta_{PR}^{IS}\big)\,\tau\Big) \\ &= \frac{1}{2}\int_0^{\pi} \mathrm{d}\beta_{PR}^{IS}\, \sin\beta_{PR}^{IS}\, \cos\Big(\frac{1}{2\sqrt{2}}\, b_{IS}\, \sin\big(2\beta_{PR}^{IS}\big)\,\tau\Big), \end{aligned} \tag{A.1}$$

where the integral in the last line can be solved with the help of Eq. 6. in section 3.715 of Ref. [51]:

$$\int_0^{\pi} \mathrm{d}x\, \sin(ax)\cos(z\sin x) = -a(1-\cos a\pi)\, s_{-1,a}(z), \tag{A.2}$$

where $s_{\nu,\mu}(z)$ denotes the Lommel function with in general integer or fractional parameter ν and μ and in general complex argument z [51]. Using suitable substitutions this leads to the final result shown in Eq. (85):

$$S(\tau,1) = -\frac{1}{4}\, s_{-1,1/2}\Big(\frac{1}{2\sqrt{2}}\, b_{IS}\,\tau\Big). \tag{A.3}$$

Although the Lommel function $s_{\nu,\mu}(z)$ has currently been implemented for example in the Python library *mpath* [120] and is expected to be integrated into Mathematica in the future, it can be straightforwardly implemented exploiting its connection to the generalized hypergeometric function:

$$s_{\mu,\nu}(z) = \frac{z^{\mu+1}}{(\mu-\nu+1)(\mu+\nu+1)}\, {}_1F_2\Big(1; \frac{\mu-\nu+3}{2}, \frac{\mu+\nu+3}{2}; -\frac{z^2}{4}\Big), \tag{A.4}$$

where ${}_pF_q(\mathbf{a};\mathbf{b};z)$ is the generalized hypergeometric function [51] of the complex variable z with tuples $\mathbf{a}$ and $\mathbf{b}$ of length p and q, respectively. Therefore, Eq. (85) maybe written as:

$$S(\tau,1) = {}_1F_2\Big(1; \frac{3}{4}, \frac{5}{4}; -\frac{1}{32} b_{IS}^2 \tau^2\Big). \tag{A.5}$$

Furthermore, the Lommel function $s_{-1,\nu}(z)$ can be expressed using both the Anger and Weber functions $\mathbf{J}_\nu(z)$ and $\mathbf{E}_\nu(z)$ [51]:

$$s_{-1,\nu}(z) = -\frac{\pi}{2\nu\sin\nu\pi}\big\{\mathbf{J}_\nu(z) + \mathbf{J}_{-\nu}(z)\big\} \tag{A.6}$$

$$s_{-1,\nu}(z) = -\frac{\pi}{2\nu(1-\cos\nu\pi)}\big\{\mathbf{E}_\nu(z) - \mathbf{E}_{-\nu}(z)\big\}, \tag{A.7}$$

leading to the following expressions for Eq. (85):

$$S(\tau,1) = \frac{\pi}{4}\left\{\mathbf{J}_{1/2}\Big(\frac{1}{2\sqrt{2}}\, b_{IS}\,\tau\Big) + \mathbf{J}_{-1/2}\Big(\frac{1}{2\sqrt{2}}\, b_{IS}\,\tau\Big)\right\} \tag{A.8}$$

$$S(\tau,1) = \frac{\pi}{4}\left\{\mathbf{E}_{1/2}\Big(\frac{1}{2\sqrt{2}}\, b_{IS}\,\tau\Big) - \mathbf{E}_{-1/2}\Big(\frac{1}{2\sqrt{2}}\, b_{IS}\,\tau\Big)\right\} \tag{A.9}$$

Finally, the special case of the Lommel function $s_{-1,1/2}(z)$ can be expressed with the help of the Fresnel cosine and sine integrals [121, 122]:

$$s_{-1,1/2}(z) = -2\sqrt{\frac{2\pi}{z}}\left\{\sin z\, S\Big(\sqrt{\frac{2z}{\pi}}\Big) + \cos z\, C\Big(\sqrt{\frac{2z}{\pi}}\Big)\right\}, \tag{A.10}$$

where $S(z)$ and $C(z)$ are the normalized Fresnel cosine and sine integrals [50]:

$$S(z) = \int_0^z \mathrm{d}t\, \sin\Big(\frac{\pi}{2}t^2\Big) \tag{A.11}$$

$$C(z) = \int_0^z \mathrm{d}t\, \cos\Big(\frac{\pi}{2}t^2\Big). \tag{A.12}$$

It follows, the signal intensity Eq. (85) maybe written as:

$$S(\tau,1) = \frac{1}{2}\sqrt{\frac{2\pi}{z}}\left\{\sin z\, S\Big(\sqrt{\frac{2z}{\pi}}\Big) + \cos z\, C\Big(\sqrt{\frac{2z}{\pi}}\Big)\right\} \tag{A.13}$$

with

$$z = \frac{1}{2\sqrt{2}}\, b_{IS}\,\tau. \tag{A.14}$$

Pileio et al. have used the Fresnel cosine and sine integrals to express the double-quantum filtered efficiency as a function of the duration of the application of a γ-encoded homonuclear dipolar recoupling sequence [59], resulting in an expression similar to Eq. (A.13). However, arguably, the use of the Lommel function leads to a significantly more elegant expression Eq. (85).

Appendix B. Second order average Hamiltonian under Lee-Goldburg homonuclear decoupling

In this Appendix we derive the second order average Hamiltonian for the LG homonuclear decoupling sequence applied to a two-spin system consisting of spins I_j and I_k. In a first step the internal Hamiltonian in general can be written as

$$\begin{aligned} H_{\text{int}} &= \sum_{\Lambda,\lambda} H^{\Lambda}_{\lambda 0} \\ &= \sum_{\Lambda\lambda} \omega^{\Lambda}\, T^{\Lambda}_{\lambda 0}, \end{aligned} \tag{B.1}$$

where the sum is taken over the spin interactions Λ and the corresponding ranks λ of the irreducible spherical spin tensors. In Eq. (161) we have considered the chemical shift interaction and the homonuclear dipolar coupling, i.e. $\Lambda = \text{CS}, \text{DD}$, and the corresponding ranks of the spin tensors are $\lambda = 1, 2$, respectively.

Similarly, the interaction frame Hamiltonian can be written as

$$\begin{aligned} \tilde{H}_B(t) &= R_y(\theta)\Bigg(\sum_{\Lambda,\lambda,\mu} \tilde{H}^{\Lambda}_{\lambda\mu}(t)\Bigg) R_y(-\theta) \\ &= R_y(\theta)\Bigg(\sum_{\Lambda,\lambda,\mu} \tilde{\omega}^{\Lambda}_{\lambda\mu}(t)\, T^{\Lambda}_{\lambda\mu}\Bigg) R_y(-\theta), \end{aligned} \tag{B.2}$$

where we have defined the interaction frame frequencies

$$\tilde{\omega}^{\Lambda}_{\lambda\mu}(t) = \omega^{\Lambda}\, d^{(\lambda)}_{\mu 0}(-\theta)\, \exp\big(\mathrm{i}\,\mu\,\omega_{\text{eff}}(t - t_0)\big), \tag{B.3}$$

and sum over μ takes all possible values $\mu = -\lambda, -\lambda+1, \ldots, \lambda$ for each rank λ. As a result, Eq. (B.2) together with (B.3) generalize Eqs. (169) and (170), which were given separately for the homonuclear dipolar coupling and the chemical shift interaction, respectively.

The first order average Hamiltonian can be written as

$$\begin{aligned} \bar{H}^{(1)}_B &= R_y(\theta)\Bigg(\sum_{\Lambda,\lambda,\mu} \bar{H}^{\Lambda}_{\lambda\mu}\Bigg) R_y(-\theta) \\ &= R_y(\theta)\Bigg(\sum_{\Lambda,\lambda,\mu} \bar{\omega}^{\Lambda}_{\lambda\mu}\, T^{\Lambda}_{\lambda\mu}\Bigg) R_y(-\theta) \end{aligned} \tag{B.4}$$

where the time-independent amplitude $\bar{\omega}^{\Lambda}_{\lambda\mu}$ is defined as

$$\bar{\omega}^{\Lambda}_{\lambda\mu} = \omega^{\Lambda}\, \kappa_{\lambda\mu}, \tag{B.5}$$

and $\kappa_{\lambda\mu}$ is the scaling factor of the first order average Hamiltonian term with the spin rank λ and spin component μ, which is a product of two components:

$$\kappa_{\lambda\mu} = d^{(\lambda)}_{\mu 0}(-\theta)\; \mathcal{I}_{\mu}, \tag{B.6}$$

where I_μ is the integral solved in Eq. (173):

$$\begin{aligned} \mathcal{I}_{\mu} &= \frac{1}{T}\int_0^T \mathrm{d}t'\; \exp\big(\mathrm{i}\,\mu\,\omega_{\text{eff}}\,t'\big) \\ &= \delta_{\mu 0}, \end{aligned} \tag{B.7}$$

where $\delta_{\mu\mu'}$ is the Kronecker δ-symbol [28]. As discussed in Section 3.2.4, $\kappa_{20} = 0$ and $\kappa_{10} = 1/\sqrt{3}$ at the magic angle $\theta = \arctan\sqrt{2}$.

Table B.1
The values of the scaling factor $\kappa^{\lambda_2\mu_2}_{\lambda_1\mu_1}$ in Eq. (B.10) for the cross terms $\Lambda_2 \times \Lambda_1$ in the second order average Hamiltonian Eq. (B.8).

μ_2	$\text{CS}_j \times \text{CS}_j$			$\text{DD}_{jk} \times \text{CS}_j$			$\text{DD}_{jk} \times \text{DD}_{jk}$				
	μ_1			μ_1			μ_1				
	-1	0	1	-1	0	1	-2	-1	0	1	2
-2				0	$1/(6\sqrt{2})$	0	0	0	0	0	$-1/12$
-1	0	1/3	1/3	0	1/3	1/3	0	0	0	1/3	0
0	$-1/3$	0[a]	$-1/3$	0	0	0	0	0	0	0	0
1	$-1/3$	1/3	0	$-1/3$	1/3	0	0	$-1/3$	0	0	0
2				0	$-1/(6\sqrt{2})$	0	1/12	0	0	0	0

[a] Set to 0 as $[T^j_{10}, T^j_{10}] = 0$.

The second order average Hamiltonian in Eq. (178) can be written as

$$\begin{aligned} \bar{H}^{(2)}_B &= R_y(\theta)\Bigg(\sum_{\substack{\Lambda_2,\lambda_2,\mu_2 \\ \Lambda_1,\lambda_1,\mu_1}} \bar{H}^{\Lambda_2\times\Lambda_1}_{\substack{\lambda_2\mu_2 \\ \lambda_1\mu_1}}\Bigg) R_y(-\theta) \\ &= R_y(\theta)\Bigg(\sum_{\substack{\Lambda_2,\lambda_2,\mu_2 \\ \Lambda_1,\lambda_1,\mu_1}} \bar{\omega}^{\Lambda_2\times\Lambda_1}_{\substack{\lambda_2\mu_2 \\ \lambda_1\mu_1}}\, [T^{\Lambda_2}_{\lambda_2\mu_2}, T^{\Lambda_1}_{\lambda_1\mu_1}]\Bigg) R_y(-\theta) \end{aligned} \tag{B.8}$$

where the sum is taken over all second order cross terms between a term of interaction Λ_2 with quantum numbers (λ_2, μ_2), and that of interaction Λ_1 with quantum numbers (λ_1, μ_1). The time-independent amplitudes $\bar{\omega}^{\Lambda}_{\lambda\mu}$ are defined as

$$\bar{\omega}^{\Lambda_2\times\Lambda_1}_{\substack{\lambda_2\mu_2 \\ \lambda_1\mu_1}} = \frac{\omega^{\Lambda_2}\,\omega^{\Lambda_1}}{2\,\omega_{\text{eff}}}\; \kappa_{\substack{\lambda_2\mu_2 \\ \lambda_1\mu_1}} \tag{B.9}$$

and $\kappa_{\substack{\lambda_2\mu_2 \\ \lambda_1\mu_1}}$ is the scaling factor of the second order cross term between interactions with the quantum numbers (λ_2, μ_2) and (λ_1, μ_1), respectively:

$$\kappa_{\substack{\lambda_2\mu_2 \\ \lambda_1\mu_1}} = d^{(\lambda_2)}_{\mu_2 0}(-\theta) d^{(\lambda_1)}_{\mu_1 0}(-\theta)\; \mathcal{I}_{\mu_2\mu_1}, \tag{B.10}$$

where $\mathcal{I}_{\mu_2\mu_1}$ is the following integral:

$$\begin{aligned} \mathcal{I}_{\mu_2\mu_1} &= \frac{2\,\omega_{\text{eff}}}{2\mathrm{i}T}\int_0^T \mathrm{d}t' \int_0^{t'} \mathrm{d}t''\; \exp\big\{\mathrm{i}\,\omega_{\text{eff}}\,(\mu_2\,t' + \mu_1\,t'')\big\} \\ &= \begin{cases} -\mathrm{i}\,\pi & \text{for} \quad \mu_2 = \mu_1 = 0 \\ & \qquad\quad (\mu_2 = 0 \quad\;\; \text{and} \quad \mu = \mu_1 \neq 0) \\ 1/\mu & \text{for} \quad \text{or} \quad (\mu = \mu_2 \neq 0 \quad \text{and} \quad \mu_1 = 0) \\ & \qquad\quad \text{or} \quad (\mu = \mu_2 = -\mu_1 \quad \text{and} \quad \mu \neq 0) \end{cases} \end{aligned} \tag{B.11}$$

Table B.1 lists the values of the scaling factor $\kappa_{\substack{\lambda_2\mu_2 \\ \lambda_1\mu_1}}$ in Eq. (B.10) for different cross terms $\Lambda_2 \times \Lambda_1$ of the spin interactions Λ_2 and Λ_1 in the second order average Hamiltonian for $\theta = \arctan\sqrt{2}$.

The elements in Table B.1 that do not vanish correspond to the cross term that contribute to the second order average Hamiltonian in Eqs. (178) and (B.8). Notably, most cross terms between the homonuclear dipolar coupling and itself vanish, except for $\mu 2 = -\mu 1 \neq 0$. Overall, more non-vanishing cross terms between the chemical shift interaction and the dipolar interaction can be found. The same holds true for cross term of the chemical shift interaction with itself. This explains why the second-order lineshapes visible in panels (H) and (K) of Fig. 12, resulting from numerical simulations of the LG sequence in KHM, are mostly the results of commutators between the chemical shift interaction and the homonuclear dipolar coupling.

From Eq. (B.9) it follows that the amplitudes $\bar{\omega}^{\Lambda_2\times\Lambda_1}_{\substack{\lambda_2\mu_2 \\ \lambda_1\mu_1}}$ of the second order terms are not only proportional to the scaling factor $\kappa_{\substack{\lambda_2\mu_2 \\ \lambda_1\mu_1}}$ listed

in Table B.1, but also proportional to the product of the interaction frequencies $\omega^{\Lambda_2}\,\omega^{\Lambda_1}$, and inversely proportional to the effective nutation frequency ω_{eff} during the homonuclear decoupling sequence. The latter implies that increasing the amplitude of the rf field (together with the rf resonance offset) will decrease the size of the terms in the second order average Hamiltonian.

Appendix C. The nuclear spin Hamiltonian

As discussed in detail in section I-2.1 the evolution of the state vector of a nuclear spin system is governed by the time-dependent Schrödinger equation (I-1). The time-dependent nuclear spin Hamiltonian may be written as a sum over different spin interactions Λ

$$H(t) = \sum_{\Lambda} H^{\Lambda}(t). \tag{C.1}$$

The contributions Λ to the nuclear spin Hamiltonian relevant for NMR experiments are in detail presented in Refs. [107,123–126]. In the following, only interactions Λ in systems of coupled spins-1/2 are considered.

C.1. Cartesian representation

The Hamiltonian for the spin interaction Λ may be expressed with the help of a second rank cartesian tensor $\mathbb{A}^{\Lambda}$ in the following way:

$$\begin{aligned} H^{\Lambda}(t) &= C^{\Lambda}\,(\mathbf{X}^{\Lambda})^{T}\cdot\mathbb{A}^{\Lambda}\cdot\mathbf{Y}^{\Lambda} \\ &= C^{\Lambda}\begin{pmatrix} X_x^{\Lambda} & X_y^{\Lambda} & X_z^{\Lambda}\end{pmatrix}\cdot\begin{pmatrix} A_{xx}^{\Lambda} & A_{xy}^{\Lambda} & A_{xz}^{\Lambda}\\ A_{yx}^{\Lambda} & A_{yy}^{\Lambda} & A_{yz}^{\Lambda}\\ A_{zx}^{\Lambda} & A_{zy}^{\Lambda} & A_{zz}^{\Lambda}\end{pmatrix}\cdot\begin{pmatrix} Y_x^{\Lambda}\\ Y_y^{\Lambda}\\ Y_z^{\Lambda}\end{pmatrix}, \end{aligned} \tag{C.2}$$

where $\mathbf{X}$ and $\mathbf{Y}$ are vector operators of the interacting physical quantities. These can be two nuclear spins, e.g. denoted $\mathbf{I}$ and $\mathbf{S}$, or one nuclear spin and an external magnetic field $\mathbf{B}$. The constant C^{Λ} is characteristic for the interaction Λ.

C.2. Spherical representation

The components of the second rank cartesian tensor $\mathbb{A}^{\Lambda}$ can be decomposed into a *scalar*, $\mathscr{A}_0^{\Lambda}$, an *antisymmetric* first rank tensor, $\mathscr{A}_1^{\Lambda}$ and a traceless, *symmetric* second rank tensor, $\mathscr{A}_2^{\Lambda}$. The three resulting tensors $\mathscr{A}_l^{\Lambda}$ are the called *irreducible spherical tensors* of ranks $l = 0, 1, 2$ with corresponding cartesian tensors $\mathbb{A}_l^{\Lambda}$, which relate as

$$\mathbb{A}^{\Lambda} = \mathbb{A}_0^{\Lambda} + \mathbb{A}_1^{\Lambda} + \mathbb{A}_2^{\Lambda}. \tag{C.3}$$

The exact form of a tensor depends upon the coordinate system or *reference frame* it is expressed in. Consider two reference frames F and F', which are related to each other by rotations. The rotations from frame, F to F' can be described by three Euler angles $\Omega_{FF'} = \{\alpha_{FF'}, \beta_{FF'}, \gamma_{FF'}\}$. An irreducible spherical tensor $\mathscr{A}_l^{\Lambda}$ of rank l is composed of $(2l+1)$ components $\mathscr{A}_{lq}^{\Lambda}$, where $q = -l, -l+1, \ldots, l$. Irreducible spherical tensors are *defined* as transforming in the following way under rotations of the coordinate system:

$$\left[\mathscr{A}_{lq}^{\Lambda}\right]^{F'} = \sum_{q'=-l}^{l}\left[\mathscr{A}_{lq'}^{\Lambda}\right]^{F} D^{(l)}_{q'q}(\Omega_{FF'}), \tag{C.4}$$

where $D^{(l)}_{q'q}$ is a Wigner D-matrix element [25,28].

The Hamiltonian for the spin interaction Λ may be expressed by a sum over scalar products of two irreducible spherical tensors, in the following way [107]:

$$H^{\Lambda} = C^{\Lambda}\sum_{l=0}^{2}\sum_{q=-l}^{l}(-1)^{q}\left[\mathscr{A}_{lq}^{\Lambda}\right]^{F}\left[\mathscr{T}_{l-q}^{\Lambda}\right]^{F}. \tag{C.5}$$

$\mathscr{A}_l^{\Lambda}$ is called a *spatial tensor*. $\mathscr{T}_{lq}^{\Lambda}$ is the component q of the irreducible spherical tensor of rank l, built from the two vector operators $\mathbf{X}$ and $\mathbf{Y}$ in Eq. (C.2) [107]. If $\mathbf{X}$ and $\mathbf{Y}$ are both spin operators, $\mathscr{T}_l^{\Lambda}$ is called a *spin tensor*. If one of $\mathbf{X}$ or $\mathbf{Y}$ is a spin operator and the other is an external magnetic field, $\mathscr{T}_l^{\Lambda}$ is called a *spin-field tensor*.

The exact form of the tensor elements depend upon the chosen reference frame F, whereas the scalar product of both tensors is independent of the choice of F. The complete list of components $\mathscr{A}_{lq}^{\Lambda}$ and $\mathscr{T}_{lq}^{\Lambda}$ for $l = 0, 1$ and 2 for the different spin interactions can be found in Ref. [107], where Table C.3 shows the components for $l = 0$ and 2 for spin-1/2 nuclei discussed in more detail in Sections Appendices C.5–C.9.

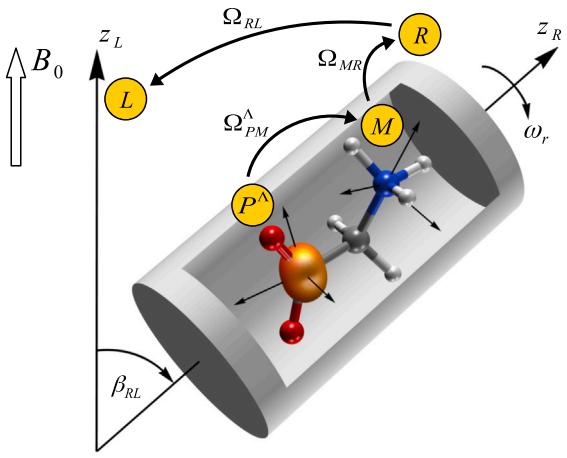

Fig. C.1. The relevant reference frames and transformations in MAS NMR: The principal axis system P^{Λ} of the spin interaction Λ, the molecular frame M, the rotor frame R and the laboratory frame L are depicted together with the Euler angles Ω^{Λ}_{PM}, Ω_{MR} and Ω_{RL} relating the respective reference frames.

C.3. Reference frames in solid state NMR

An overview over the relevant reference frames in solid state NMR is given in Fig. C.1. The *principal axis system* (PAS) of an interaction Λ, denoted P^{Λ}, is defined as the reference frame where the cartesian tensor $\mathbb{A}_2^{\Lambda}$ belonging to the second rank spatial tensor $\mathscr{A}_2^{\Lambda}$ is diagonal. The *molecular frame*, denoted M, is a reference frame fixed on the molecule and may be chosen arbitrarily. The *rotor frame*, denoted R, is a reference frame in which the z_R-axis coincides with the rotor axis. We note that here as shown in Fig. C.1 the molecular frame has been introduced as an additional intermediate step compared to Fig. 1. Finally, the *laboratory frame*, denoted L, is a reference frame in which the z_L-axis points in the direction of the external magnetic field.

Since the tensors $\mathscr{T}_l^{\Lambda}$ are usually expressed in the laboratory frame L of the experiment, it is necessary to transform the spatial tensors from the PAS to the laboratory frame:

$$\left[\mathscr{A}_{lq}^{\Lambda}\right]^{L} = \sum_{q'=-l}^{l}\left[\mathscr{A}_{lq'}^{\Lambda}\right]^{P} D^{(l)}_{q'q}(\Omega^{\Lambda}_{PL}), \tag{C.6}$$

where $\Omega^{\Lambda}_{PL} = \{\alpha^{\Lambda}_{PL}, \beta^{\Lambda}_{PL}, \gamma^{\Lambda}_{PL}\}$ are the Euler angles relating the PAS of the interaction Λ to the laboratory frame. Eq. (C.5) becomes:

$$H^{\Lambda} = C^{\Lambda}\sum_{l=0}^{2}\sum_{q,q'=-l}^{l}(-1)^{q}\left[\mathscr{A}_{lq'}^{\Lambda}\right]^{P} D^{(l)}_{q'q}(\Omega^{\Lambda}_{PL})\left[\mathscr{T}_{l-q}^{\Lambda}\right]^{L}. \tag{C.7}$$

C.4. High field approximation

It proves to be useful to divide the nuclear spin Hamiltonian into the part describing the interaction with the rf field and a part describing the internal spin interactions and the interaction with the static field. The total spin Hamiltonian at time point t may be written as

$$H(t) = H_{\text{rf}}(t) + H_{\text{int}}(t), \tag{C.8}$$

Table C.1
Single-spin and two-spin irreducible spherical tensor operators $T^{j}_{\lambda\mu}$ and $T^{jk}_{\lambda\mu}$.

Spin rank λ	Spin component μ	Single spin j		Two spins j,k	
0	0	T^{j}_{00}	$\frac{1}{\sqrt{2}}\mathbb{1}_j$	T^{jk}_{00}	$-\frac{1}{\sqrt{3}}\mathbf{I}_j\cdot\mathbf{I}_k$
1	0	T^{j}_{10}	I_{jz}	T^{jk}_{10}	$\frac{1}{2\sqrt{2}}\left(I^+_jI^-_k-I^-_jI^+_k\right)$
1	±1	$T^{j}_{1\pm1}$	$\mp\frac{1}{\sqrt{2}}I^{\pm}_j$	$T^{jk}_{1\pm1}$	$\frac{1}{2}\left(I^{\pm}_jI_{kz}-I_{jz}I^{\pm}_k\right)$
2	0	T^{j}_{20}	$\frac{1}{\sqrt{6}}\left(3I^2_{jz}-I_j(I_j+1)\right)$	T^{jk}_{20}	$\frac{1}{\sqrt{6}}\left(3I_{jz}I_{kz}-\mathbf{I}_j\cdot\mathbf{I}_k\right)$
2	±1	$T^{j}_{2\pm1}$	$\mp\frac{1}{2}\left(I^{\pm}_jI_{jz}+I_{jz}I^{\pm}_j\right)$	$T^{jk}_{2\pm1}$	$\mp\frac{1}{2}\left(I^{\pm}_jI_{kz}+I_{jz}I^{\pm}_k\right)$
2	±2	$T^{j}_{2\pm2}$	$\frac{1}{2}\left(I^{\pm}_j\right)^2$	$T^{jk}_{2\pm2}$	$\frac{1}{2}I^{\pm}_jI^{\pm}_k$

Table C.2
The space and spin parts for a list of spin interactions.

Interaction	Λ	Space part					Spin part
		F	$[A^{\Lambda}_{00}]^F$	$[A^{\Lambda}_{20}]^F$	$[A^{\Lambda}_{2\pm1}]^F$	$[A^{\Lambda}_{2\pm2}]^F$	
Zeeman	Z	L	ω_0	–	–	–	T^{j}_{10}
isotropic shift	CS	L	$\omega_0\delta^{\rm iso}_j$	–	–	–	T^{j}_{10}
Zeeman and isotropic shift in rotating frame	Z,CS	L	$\Omega^{\rm iso}_j$	–	–	–	T^{j}_{10}
CSA	CS	P	–	$\omega_0(\delta^P_{zz}-\delta^{\rm iso}_j)$	0	$-\frac{\eta}{\sqrt{6}}[A_{20}]^P$	T^{j}_{10}
Homonuclear dipolar coupling	DD_{jk}	P	–	$\sqrt{6}\,b_{jk}$	0	0	T^{jk}_{20}
Homonuclear isotropic J-coupling	J_{jk}	L	$-\sqrt{3}\,2\pi J$	–	–	–	T^{jk}_{00}
Heteronuclear dipolar coupling	DD_{IS}	P	–	$2\,b_{IS}$	0	0	$T^{I}_{10}T^{S}_{10}$
Heteronuclear isotropic J-coupling	J_{IS}	L	$2\pi J$	–	–	–	$T^{I}_{10}T^{S}_{10}$

where the internal spin Hamiltonian $H_{\rm int}(t)$ is time dependent if the molecules in the sample move or the whole sample is moved, while the rf spin Hamiltonian $H_{\rm int}(t)$ is time dependent because of the modulations of the rf fields. In a spin system containing two spin species I and S, the internal Hamiltonian may be divided further:

$$H_{\rm int}(t) = H^{I}_{\rm int}(t) + H^{S}_{\rm int}(t) + H^{IS}_{\rm int}(t), \tag{C.9}$$

where $H^{I}_{\rm int}(t)$ and $H^{S}_{\rm int}(t)$ describe all homonuclear spin interactions of spins I and S respectively. The term $H^{IS}_{\rm int}(t)$ describes the heteronuclear interactions between spins of species I and S.

In high-field NMR of spin-½ nuclei, the internal spin Hamiltonian in Eq. (C.9) may be simplified by neglecting terms which do not commute with I_z and S_z. The remaining terms are referred to as *secular* terms, whereas the neglected terms are called *non-secular* terms. The neglecting of non-secular terms is called the *secular* or *high-field approximation* [32,127,128].

Since it is possible to rotate the spin angular momenta by external rf fields, the internal Hamiltonians will no longer be written in terms of components $\mathscr{T}^{\Lambda}_{lq}$ of the spin or spin-field tensors, but in terms of components $T^{\Lambda}_{\lambda\mu}$ of pure irreducible spherical spin tensors T^{Λ}_{λ}, which are defined in Table C.1. This is allowed because the external magnetic field is constant and not subject to rotations. The ranks l and λ are *not necessarily* the same. In addition, spatial tensors A^{Λ}_{l} are defined, which are related to the spatial tensors $\mathscr{A}^{\Lambda}_{l}$ by numerical factors. Table C.2 contains the relevant tensor components of A^{Λ}_{l} for different spin interactions in the high-field approximation and Table C.3 shows the relationship of the spatial tensors A^{Λ}_{l} and $\mathscr{A}^{\Lambda}_{l}$ and the relationships of the spin tensor components $T^{\Lambda}_{\lambda0}$ and the components $\mathscr{T}^{\Lambda}_{l0}$ of the spin or spin-field tensors.

The internal Hamiltonians for homonuclear spin interactions for spins I and S may, in the high field approximation, be written as

$$H^{I}_{\rm int}(t) = \sum_{\Lambda_I,l,\lambda_I} H^{\Lambda_I}_{l\,\lambda_I0}(t) \tag{C.10}$$

$$H^{S}_{\rm int}(t) = \sum_{\Lambda_S,l,\lambda_S} H^{\Lambda_S}_{l\,\lambda_S0}(t), \tag{C.11}$$

where

$$H^{\Lambda}_{l\,\lambda0}(t) = \sum_{q=-l}^{l}\left[A^{\Lambda}_{lq}\right]^P D^{(l)}_{q0}(\Omega^{\Lambda}_{PL})\,T^{\Lambda}_{\lambda0}. \tag{C.12}$$

The term $H^{\Lambda}_{l\lambda0}(t)$ transforms as an irreducible spherical tensor of rank l for spatial rotations and rank λ for spin rotations.

The internal Hamiltonians for heteronuclear spin interactions for spins I and S may, in the high field approximation, be written as

$$H^{IS}_{\rm int}(t) = \sum_{\Lambda_{IS},l,\lambda_I,\lambda_S} H^{\Lambda_{IS}}_{l\,\lambda_I0\,\lambda_S0}(t), \tag{C.13}$$

where the terms $H^{\Lambda_{IS}}_{l\,\lambda_I0\,\lambda_S0}(t)$ may be written in terms of products of the components of two irreducible spherical spin tensors, $T^{\Lambda_I}_{\lambda_I0}\,T^{\Lambda_S}_{\lambda_S0}$, for the spin species I and S respectively:

$$H^{\Lambda_{IS}}_{l\,\lambda_I0\,\lambda_S0}(t) = \sum_{q=-l}^{l}\left[A^{\Lambda_{IS}}_{lq}\right]^P D^{(l)}_{q0}(\Omega^{\Lambda_{IS}}_{PL})\,T^{\Lambda_I}_{\lambda_I0}\,T^{\Lambda_S}_{\lambda_S0}. \tag{C.14}$$

The term $H^{\Lambda_{IS}}_{l\,\lambda_I0\,\lambda_S0}(t)$ transforms as an irreducible spherical tensor of rank l for spatial rotations, rank λ_I for I-spin rotations and rank λ_S for S-spin rotations.

C.5. Zeeman interaction

The Hamiltonian of the Zeeman interaction of the I-spin nuclear magnetic moments with an external magnetic field $\mathbf{B}_0 = B_0\,\mathbf{e}_{z_L}$ is given by

$$H^{\rm Z}_I = -\boldsymbol{\mu}\cdot\mathbf{B}_0 \tag{C.15}$$

$$= -\gamma_I\,\mathbf{I}^T\cdot\mathbb{1}\cdot\mathbf{B}_0 \tag{C.16}$$

$$= -\gamma_I\,B_0\,I_z \tag{C.17}$$

$$= \omega_0\,I_z \tag{C.18}$$

Table C.3
Relationships between the spatial tensor components A^{Λ}_{lq} and $\mathscr{A}^{\Lambda}_{lq}$, and the spin tensor components $T^{\Lambda}_{\lambda 0}$ and the spin or spin-field tensor components $\mathscr{T}^{\Lambda}_{\lambda 0}$.

Interaction	Λ	C^{Λ}	Space part	Spin or spin-field part
Zeeman	Z	$-\gamma_S$	$[\mathscr{A}^{\Lambda}_{00}]^L = -\frac{\sqrt{3}}{\omega_0}[A^{\Lambda}_{00}]^L$	$[\mathscr{T}^{\Lambda}_{00}]^L = -\frac{1}{\sqrt{3}} B_0 T^j_{10}$
isotropic shift	CS	$-\gamma_S$	$[\mathscr{A}^{\Lambda}_{00}]^L = -\frac{\sqrt{3}}{\omega_0}[A^{\Lambda}_{00}]^L$	$[\mathscr{T}^{\Lambda}_{00}]^L = -\frac{1}{\sqrt{3}} B_0 T^j_{10}$
CSA	CS	$-\gamma_S$	$[\mathscr{A}^{\Lambda}_{2q}]^P = \frac{\sqrt{3}}{\sqrt{2}\,\omega_0}[A^{\Lambda}_{2q}]^P$	$[\mathscr{T}^{\Lambda}_{20}]^L = \sqrt{\frac{2}{3}} B_0 T^j_{10}$
Homonuclear dipolar coupling	DD_{jk}	1	$[\mathscr{A}^{\Lambda}_{2q}]^P = [A^{\Lambda}_{2q}]^P$	$[\mathscr{T}^{\Lambda}_{20}]^L = T^{jk}_{20}$
Homonuclear isotropic J-coupling	J_{jk}	2π	$[\mathscr{A}^{\Lambda}_{00}]^L = \frac{1}{2\pi}[A^{\Lambda}_{00}]^L$	$[\mathscr{T}^{\Lambda}_{00}]^L = T^{jk}_{00}$
Heteronuclear dipolar coupling	DD_{IS}	1	$[\mathscr{A}^{\Lambda}_{2q}]^P = \sqrt{\frac{3}{2}}[A^{\Lambda}_{2q}]^P$	$[\mathscr{T}^{\Lambda}_{20}]^L = \frac{1}{\sqrt{6}}\left(2\,T^I_{10}\,T^S_{10} + T^I_{1-1}\,T^S_{11} + T^I_{11}\,T^S_{1-1}\right)$
Heteronuclear isotropic J-coupling	J_{IS}	2π	$[\mathscr{A}^{\Lambda}_{00}]^L = -\frac{\sqrt{3}}{2\pi}[A^{\Lambda}_{00}]^L$	$[\mathscr{T}^{\Lambda}_{00}]^L = -\frac{1}{\sqrt{3}}\left(T^I_{10}\,T^S_{10} - T^I_{1-1}\,T^S_{11} - T^I_{11}\,T^S_{1-1}\right)$

$$= \sum_j [A^{\mathrm{Z}}_{00}]^L\, T^j_{10}, \tag{C.19}$$

where $\omega_0 = -\gamma_I B_0$ is the Larmor frequency of the spin species I, and the sum is taken over all spins I_j. Table C.2 lists the component $[A^{\mathrm{Z}}_{00}]^L$.

C.6. Interaction with rf fields

During an rf pulse, the oscillating transverse magnetic field at time point t is given by

$$\mathbf{B}_{\mathrm{rf}}(t) = B_{\mathrm{rf}} \cos(\omega_{\mathrm{ref}} t + \phi)\, \mathbf{e}_{x_L}, \tag{C.20}$$

where ω_{ref} is the spectrometer reference frequency and ϕ is the rf phase, taking into account the sign of the gyromagnetic ratio [129,130]. The reference frequency is defined as having the same sign as the Larmor frequency, ω_0, of the irradiated spin species [129,130]. The oscillating rf field may be decomposed into two counter-rotating parts. If $\omega_{\mathrm{ref}} \approx \omega_0$, only the resonant part, rotating in the same sense as the Larmor precession, has a significant influence on the nuclear spins.

The Hamiltonian of the interaction of the S-spin nuclear magnetic moments with the resonant part of the oscillating transverse magnetic field is

$$H_{\mathrm{rf}}(t) = -\frac{1}{2}\gamma_S B_{\mathrm{rf}}\big(\cos(\omega_{\mathrm{ref}} t + \phi) S_x + \sin(\omega_{\mathrm{ref}} t + \phi) S_y\big). \tag{C.21}$$

The oscillatory time-dependence of the nuclear spin Hamiltonian may be removed by transforming it into the *rotating frame*, the reference frame rotating with the frequency ω_{ref} around the z-axis in the static laboratory frame [31,32,127,128]. The resulting nuclear spin Hamiltonian is usually denoted $\tilde{H}$ but this notation is used in this series of *Introduction to Average Hamiltonian Theory* [1, this work] for the Hamiltonian in the interaction frame of the rf field. Therefore, from now on, all Hamiltonians are written in the rotating laboratory frame without a change in notation. The rf Hamiltonian in the rotating frame becomes:

$$\begin{aligned} H_{\mathrm{rf}}(t) &= \omega_{\mathrm{nut}}(I_x \cos\phi + I_y \sin\phi) \\ &= \omega_{\mathrm{nut}}\; R_z(\phi)\; I_x\; R_z(-\phi), \end{aligned} \tag{C.22}$$

as previously presented in Eq. (I-16) in section I-2.4, where ω_{nut} is the nutation frequency of the rf field, defined as

$$\omega_{\mathrm{nut}} = |\frac{1}{2}\gamma_I B_{\mathrm{rf}}|. \tag{C.23}$$

The transformation of the nuclear spin Hamiltonian into the rotating frame results in an additional term $-\omega_{\mathrm{ref}} I_z$, which might be included into the Zeeman interaction:

$$H^{\mathrm{Z}}_I = \Omega_0\, I_z, \tag{C.24}$$

where the frequency offset Ω_0 is defined as

$$\Omega_0 = \omega_0 - \omega_{\mathrm{ref}}. \tag{C.25}$$

C.7. Chemical shift interaction

The interaction of a nuclear spin I_j with the magnetic field induced by the external fields in the electron clouds of the molecule can be described by the chemical shift tensor $\mathbb{\delta}^j$:

$$H^{\mathrm{CS}}_j = -\gamma_I\, \mathbf{I}^T \cdot \mathbb{\delta}^j \cdot \mathbf{B}_0. \tag{C.26}$$

The *deshielding* convention [32] is used for the chemical shift tensor. The cartesian tensor $\mathbb{\delta}^j$ may be decomposed into irreducible spherical tensors of rank $l = 0, 1, 2$, with the corresponding cartesian tensors $\mathbb{\delta}^j_l$, as outlined in general in Eq. (C.3). The rank 0 part is the *isotropic chemical shift*. The rank 1 part is the antisymmetric chemical shift, which can be ignored in the high-field approximation. The rank 2 part is the *chemical shift anisotropy* (CSA). The sum of the cartesian tensors for the isotropic chemical shift and the CSA, $\mathbb{\delta}^j_0 + \mathbb{\delta}^j_2$, is diagonal in its own PAS. The diagonal elements are called the *principal values* or *principal components* of the chemical shift tensor.

In the *Haeberlen* convention [11,131] the principal components in the deshielding convention are labelled δ^j_{XX}, δ^j_{YY} and δ^j_{ZZ} and ordered according to

$$|\delta^j_{ZZ} - \delta^j_{\mathrm{iso}}| \geq |\delta^j_{XX} - \delta^j_{\mathrm{iso}}| \geq |\delta^j_{YY} - \delta^j_{\mathrm{iso}}|, \tag{C.27}$$

where the isotropic chemical shift is given by

$$\delta^j_{\mathrm{iso}} = \frac{1}{3}(\delta^j_{XX} + \delta^j_{YY} + \delta^j_{ZZ}). \tag{C.28}$$

The CSA is associated with an anisotropic chemical shift $\delta^j_{\mathrm{aniso}}$, the corresponding frequency $\omega^j_{\mathrm{aniso}}$ and an *asymmetry parameter* η, defined as

$$\delta^j_{\mathrm{aniso}} = \delta^j_{ZZ} - \delta^j_{\mathrm{iso}}, \qquad \omega^j_{\mathrm{aniso}} = \omega_0\, \delta^j_{\mathrm{aniso}} \tag{C.29}$$

and

$$\eta^j = \frac{\delta^j_{YY} - \delta^j_{XX}}{\delta^j_{\mathrm{aniso}}}. \tag{C.30}$$

The chemical shift Hamiltonian in the high-field approximation is given by

$$H^{\mathrm{CS}}_j = \left([A^{\mathrm{CS}}_{00}]^L + [A^{\mathrm{CS}}_{20}]^L\right) I_{jz} \tag{C.31}$$

$$= \left([A^{\mathrm{CS}}_{00}]^L + [A^{\mathrm{CS}}_{20}]^L\right) T^j_{10}, \tag{C.32}$$

where $[A^{\mathrm{CS}}_{00}]^L$ (in the laboratory frame) and $[A^{\mathrm{CS}}_{20}]^P$ (in the PAS) are listed in Table C.2.

The Zeeman Hamiltonian for spin I_j in the rotating frame may be combined with the chemical shift Hamiltonian, defining both an absolute isotropic chemical shift frequency

$$\omega_j^{\text{iso}} = \omega_0(1 + \delta_{\text{iso}}^j), \tag{C.33}$$

and a relative isotropic chemical shift frequency with respect to the spectrometer reference frequency

$$\Omega_j^{\text{iso}} = \omega_j^{\text{iso}} - \omega_{\text{ref}}. \tag{C.34}$$

The combined Hamiltonian has the same form as Eq. (C.31),

$$H_j^{\text{Z,CS}} = \left([A_{00}^{\text{Z,CS}}]^L + [A_{20}^{\text{CS}}]^L\right) T_{10}^j, \tag{C.35}$$

where $[A_{00}^{\text{Z,CS}}]^L$ can be found in Table C.2.

Alternatively, in the *Mehring* convention [107] the three principal components of the chemical shift tensor are labelled δ_{11}, δ_{11} and δ_{33} and ordered according to

$$\delta_{11}^j \geq \delta_{22}^j \geq \delta_{33}^j, \tag{C.36}$$

where it follows that the isotropic chemical shift is given by

$$\delta_{\text{iso}}^j = \frac{1}{3}(\delta_{11}^j + \delta_{22}^j + \delta_{33}^j). \tag{C.37}$$

When discussing the chemical shift tensor as a whole and the resulting spectral lineshapes in static powdered samples, it has been proven to be useful to follow the Maryland convention [131–133] and define the span Ω_{s}^j and skew κ^j:

$$\Omega_{\text{s}}^j = \delta_{11}^j - \delta_{33}^j \tag{C.38}$$

$$\kappa^j = 3\,\frac{\delta_{22}^j - \delta_{\text{iso}}^j}{\Omega_{\text{s}}^j}. \tag{C.39}$$

The Maryland convention is useful when discussing the chemical shift tensor as a whole including describing the experimental powder lineshapes and the result of quantum chemical calculations. However, as seen above the Haeberlen convention is more applicable when discussing the isotropic and anisotropic part (CSA) of the chemical shift tensor separately.

C.8. Direct dipole–dipole interaction

C.8.1. Homonuclear direct dipolar couplings

The direct homonuclear dipolar coupling between two spins I_j and I_k can be described by the traceless symmetric cartesian tensor $\mathbb{D}_{jk}$:

$$H_{jk}^{\text{DD}} = \mathbf{I}_j^T \cdot \mathbb{D}_{jk} \cdot \mathbf{I}_k. \tag{C.40}$$

In the high-field approximation, the Hamiltonian of the direct dipolar coupling may be written as

$$H_{jk}^{\text{DD}} = [A_{20}^{\text{DD}_{jk}}]^L\, T_{20}^{jk} \tag{C.41}$$

$$= \omega_{jk}^{\text{DD}}\, T_{20}^{jk} \tag{C.42}$$

$$= \omega_{jk}^{\text{DD}}\, \frac{1}{\sqrt{6}} \left(2I_{jz}I_{kz} - \frac{1}{2}\left(I_j^- I_k^+ + I_j^+ I_k^-\right)\right), \tag{C.43}$$

where $[A_{20}^{\text{DD}_{jk}}]^P$ (in the PAS) is given in Table C.2. The homonuclear dipolar coupling constant is defined as

$$b_{jk} = -\frac{\mu_0}{4\pi}\,\frac{\gamma_I^2 \hbar}{r_{jk}^3}, \tag{C.44}$$

where r_{jk} is the spin–spin internuclear distance. For example, a ^{13}C–^{13}C distance of 152.2 pm corresponds to a dipolar coupling constant of $b_{jk}/2\pi = -2155$ Hz, and a ^{1}H···^{1}H distance of 177.0 pm corresponds to a dipolar coupling of $b_{jk}/2\pi = -21.662$ kHz. See also Fig. 1.

C.8.2. Heteronuclear direct dipolar couplings

The direct heteronuclear dipolar coupling between two spins I and S is correspondingly given by

$$H_{IS}^{\text{DD}} = \mathbf{I}^T \cdot \mathbb{D}_{IS} \cdot \mathbf{S}. \tag{C.45}$$

In the high-field approximation, this reduces to

$$H_{IS}^{\text{DD}} = [A_{20}^{\text{DD}_{IS}}]^L\, T_{10}^I T_{10}^S \tag{C.46}$$

$$= \omega_{IS}^{\text{DD}}\, 2I_zS_z, \tag{C.47}$$

where in the definition of $[A_{20}^{\text{DD}_{IS}}]^P$ (in the PAS), given in Table C.2, the factor of 2 had been included in $[A_{20}^{\text{DD}_{IS}}]^P$. However, as shown in the last line of Eq. (C.46), the factor of 2 is often kept together with the spin operator I_zS_z, as it is part of the cyclic commutation relationship $[2I_zS_z, I_x] = \text{i}2I_yS_z$, which causes a Hamiltonian proportional to the heteronuclear longitudinal two-spin order operator $2I_zS_z$ to induce a rotation in the $(I_x, 2I_yS_z)$-plane of the $(I_x, 2I_yS_z, 2I_zS_z)$ operator subspace [31,32]. In this case the dipolar coupling frequency ω_{IS}^{DD} does not include the factor 2. The heteronuclear dipolar coupling constant is defined as

$$b_{IS} = -\frac{\mu_0}{4\pi}\,\frac{\gamma_I\gamma_S\hbar}{r_{IS}^3}. \tag{C.48}$$

For example, a ^{13}C–^{1}H distance of 109.0 pm corresponds to a dipolar coupling constant of $b_{IS}/2\pi = -23.328$ kHz. A ^{13}C–^{15}N distance of 145.0 pm corresponds to a dipolar coupling constant of $b_{IS}/2\pi = 1005$ Hz. See also Fig. 1.

C.9. Indirect dipole–dipole interaction

C.9.1. Homonuclear *J*-couplings

The electron mediated homonuclear J-coupling between two spins I_j and I_k can be described by the cartesian tensor $\mathbb{J}_{jk}$:

$$H_{jk}^J = 2\pi\, \mathbf{I}_j^T \cdot \mathbb{J}_{jk} \cdot \mathbf{I}_k. \tag{C.49}$$

The cartesian tensor $\mathbb{J}_{jk}$ may be decomposed into irreducible spherical tensors of rank $l = 0, 1, 2$.

The rank 0 part is the *isotropic* J-coupling. The Hamiltonian for the isotropic J-coupling is

$$H_{jk}^J = 2\pi\, J_{jk}\, \mathbf{I}_j \cdot \mathbf{I}_k \tag{C.50}$$

$$= [A_{00}^{J_{jk}}]^L\, T_{00}^{jk}, \tag{C.51}$$

where J_{jk} is the homonuclear isotropic J-coupling constant which is given in Hz. $[A_{00}^{J_{jk}}]^L$ is given in Table C.2.

The rank 1 part is the antisymmetric J-coupling, which is usually ignored. The rank 2 part is the anisotropic J-coupling, which may be described by an anisotropic J-coupling constant and an asymmetry parameter. The coupling constant is usually of the same order of magnitude as the isotropic J-coupling constant. The corresponding irreducible spin tensor component for the anisotropic J-coupling is the same as for the direct homonuclear dipolar coupling, T_{20}^{jk}.

C.9.2. Heteronuclear *J*-couplings

The heteronuclear J-coupling between two spins I and S is correspondingly given by

$$H_{IS}^J = \mathbf{I}^T \cdot \mathbb{J}_{IS} \cdot \mathbf{S}. \tag{C.52}$$

The Hamiltonian for the isotropic J-coupling in the high-field approximation is

$$H_{IS}^J = 2\pi\, J_{IS}\, I_zS_z \tag{C.53}$$

$$= [A_{00}^{J_{IS}}]^L\, T_{10}^I T_{10}^S, \tag{C.54}$$

where J_{IS} is the heteronuclear isotropic J-coupling and $[A_{00}^{J_{IS}}]^L$ is given in Table C.2.

C.10. Magic-angle spinning

For the description of MAS experiments, the transformation of the irreducible spherical spatial tensors A_l^Λ from the PAS to the laboratory frames is done in several steps, as shown in Fig. C.1.

In the first step, the tensors for different spin interactions Λ are transformed into the molecular frame. The Euler angles $\Omega_{PM}^\Lambda = \{\alpha_{PM}^\Lambda, \beta_{PM}^\Lambda, \gamma_{PM}^\Lambda\}$ describe the relative orientation of the PAS of the interaction Λ and the molecule-fixed frame.

$$[A_{l0}^\Lambda]^L = \sum_{m',m''=-l}^{l} [A_{lm''}^\Lambda]^P D_{m''m'}^{(l)}(\Omega_{PM}^\Lambda) D_{m'0}^{(l)}(\Omega_{ML}), \tag{C.55}$$

where the Euler angles $\Omega_{ML} = \{\alpha_{ML}, \beta_{ML}, \gamma_{ML}\}$ describe the relative orientation of the molecular frame to the laboratory frame. Since, in a powdered sample, each crystallite is randomly oriented with respect to the laboratory frame, the Euler angles Ω_{ML} are random variables.

In MAS NMR the transformation from the molecular frame to the laboratory frame is further divided. The interaction tensors are first transformed into the rotor frame. This transformation is described by the Euler angles $\Omega_{MR} = \{\alpha_{MR}, \beta_{MR}, \gamma_{MR}\}$, which are random variables in a powdered sample. In the last step, the interactions are transformed from the rotor frame to the laboratory frame:

$$[A_{l0}^\Lambda]^L = \sum_{m,m',m''=-l}^{l} [A_{lm''}^\Lambda]^P D_{m''m'}^{(l)}(\Omega_{PM}^\Lambda) D_{m'm}^{(l)}(\Omega_{MR}) D_{m0}^{(l)}(\Omega_{RL}), \tag{C.56}$$

Assume that the sample is rotated at the magic angle, $\beta_{RL} = \arctan\sqrt{2}$, with the angular frequency ω_r and that α_{RL}^0 defines the position of the rotor at time point $t = 0$. The Euler angles relating the rotor and the laboratory frame are at time point t conventionally given by

$$\Omega_{RL}(t) = \{\alpha_{RL}, \beta_{RL}, \gamma_{RL}\} = \{\alpha_{RL}^0 - \omega_r t, \arctan\sqrt{2}, 0\}. \tag{C.57}$$

Using the definition of the Wigner matrices [25,28], the interaction tensor in the laboratory frame may be written as

$$\begin{aligned}\omega_\Lambda(t) &= [A_{l0}^\Lambda]^L \\ &= \sum_{m=-l}^{l} [A_{lm}^\Lambda]^R d_{m0}^{(l)}(\beta_{RL}) \exp\{\mathrm{i}m(\omega_r t - \alpha_{RL}^0)\},\end{aligned} \tag{C.58}$$

where $[A_{lm}^\Lambda]^R$ is the interaction tensor in the rotor frame:

$$[A_{lm}^\Lambda]^R = \sum_{m',m''=-l}^{l} [A_{lm''}^\Lambda]^P D_{m''m'}^{(l)}(\Omega_{PM}^\Lambda) D_{m'm}^{(l)}(\Omega_{MR}). \tag{C.59}$$

Note that for exact magic-angle spinning, $d_{00}^2(\beta_{RL}) = 0$, i. e., the zeroth component of a rank 2 spatial interaction tensor is zero.

The homonuclear part of the internal Hamiltonian under MAS at time point t may be written:

$$H_{\mathrm{int}}(t) = \sum_{\Lambda,l,m,\lambda} H_{lm\lambda 0}^\Lambda(t), \tag{C.60}$$

where

$$H_{lm\lambda\mu}^\Lambda(t) = \omega_{lm}^\Lambda \exp\{\mathrm{i}m\omega_r t\} T_{\lambda\mu}^\Lambda, \tag{C.61}$$

and

$$\omega_{lm}^\Lambda = \left[A_{lm}^\Lambda\right]^R d_{m0}^{(l)}(\beta_{RL}) \exp\{-\mathrm{i}m\alpha_{RL}^0\}. \tag{C.62}$$

The heteronuclear part of the internal Hamiltonian under MAS at time point t may be written:

$$H_{\mathrm{int}}^{IS}(t) = \sum_{\Lambda,l,m,\lambda_I,\lambda_S} H_{lm\,\lambda_I 0\,\lambda_S 0}^\Lambda(t), \tag{C.63}$$

where

$$H_{lm\,\lambda_I\mu_I\,\lambda_S\mu_S}^{\Lambda_{IS}}(t) = \sum_{\substack{\Lambda_{IS},l,m,\\ \lambda_I,\mu_I,\lambda_S,\mu_S}} \omega_{lm}^{\Lambda_{IS}} \exp\{\mathrm{i}m\omega_r t\} T_{\lambda_I\mu_I}^{\Lambda_I} T_{\lambda_S\mu_S}^{\Lambda_S}, \tag{C.64}$$

and

$$\omega_{lm}^{\Lambda_{IS}} = \left[A_{lm}^{\Lambda_{IS}}\right]^R d_{m0}^{(l)}(\beta_{RL}) \exp\{-\mathrm{i}m\alpha_{RL}^0 t\}. \tag{C.65}$$

Data availability

Data will be made available on request.

References

[1] A. Brinkmann, Introduction to average Hamiltonian theory. I. Basics, Concepts Magn. Reson. A 45A (6) (2016) e21414, http://dx.doi.org/10.1002/cmr.a.21414.

[2] T. Gullion, J. Schaefer, Rotational-echo double-resonance NMR, J. Magn. Reson. 81 (1) (1989) 196–200, http://dx.doi.org/10.1016/0022-2364(89)90280-1.

[3] T. Gullion, J. Schaefer, Detection of weak heteronuclear dipolar coupling by rotational-echo double-resonance nuclear magnetic resonance, in: W.S. Warren (Ed.), Advances in Magnetic Resonancce, vol. 13, Academic Press, San Diego, USA, 1989, pp. 57–83.

[4] W.I. Goldburg, M. Lee, Nuclear magnetic resonance line narrowing by a rotating rf field, Phys. Rev. Lett. 11 (6) (1963) 255–258, http://dx.doi.org/10.1103/PhysRevLett.11.255.

[5] M. Lee, W.I. Goldburg, Nuclear-magnetic-resonance line narrowing by a rotating rf field, Phys. Rev. 140 (4A) (1965) A1261–A1271, http://dx.doi.org/10.1103/PhysRev.140.A1261.

[6] M. Mehring, J.S. Waugh, Magic-angle NMR experiments in solids, Phys. Rev. B 5 (9) (1972) 3459–3471, http://dx.doi.org/10.1103/PhysRevB.5.3459.

[7] J.D. Ellett, M.G. Gibby, U. Haeberlen, L. Huber, M. Mehring, A. Pines, J. Waugh, Spectrometers for multiple-pulse NMR, in: J.S. Waugh (Ed.), Advances in Magnetic and Optical Resonance, vol. 5, Academic Press, New York, USA, 1971, pp. 117–176, http://dx.doi.org/10.1016/B978-0-12-025505-4.50009-0.

[8] A. Bielecki, A.C. Kolbert, M.H. Levitt, Frequency-switched pulse sequences: Homonuclear decoupling and dilute spin NMR in solids, Chem. Phys. Lett. 155 (4–5) (1989) 341–346, http://dx.doi.org/10.1016/0009-2614(89)87166-0.

[9] M.H. Levitt, A.C. Kolbert, A. Bielecki, D.J. Ruben, High-resolution ^{1}H NMR in solids with frequency-switched multiple-pulse sequences, Solid State Nucl. Magn. Reson. 2 (4) (1993) 151–163, http://dx.doi.org/10.1016/0926-2040(93)90021-E.

[10] U. Haeberlen, J.S. Waugh, Coherent averaging effects in magnetic resonance, Phys. Rev. 175 (2) (1968) 453–467, http://dx.doi.org/10.1103/PhysRev.175.453.

[11] U. Haeberlen, High Resolution NMR in Solids. Selective Averaging, in: Advances in Magnetic Resonance, Supplement 1, Academic Press, New York, USA, 1976.

[12] A.E. Bennett, R.G. Griffin, S. Vega, Recoupling of homo- and heteronuclear and heteronuclear dipolar interactions in rotating solids, NMR Basic Princ. Prog. 33 (1994) 1–77, http://dx.doi.org/10.1007/978-3-642-79127-7_1.

[13] S. Dusold, A. Sebald, Dipolar recoupling under magic-angle spinning conditions, Ann. Rep. NMR Spectrosc. 41 (2000) 185–264, http://dx.doi.org/10.1016/S0066-4103(00)41010-0.

[14] M.H. Levitt, Symmetry-based pulse sequences in magic-angle spinning solid-state NMR, EMagRes (2007) http://dx.doi.org/10.1002/9780470034590.emrstm0551.

[15] G. De Paëpe, Dipolar recoupling in magic angle spinning solid-state nuclear magnetic resonance, Annu. Rev. Phys. Chem. 63 (1) (2012) 661–684, http://dx.doi.org/10.1146/annurev-physchem-032511-143726.

[16] M. Edén, Advances in symmetry-based pulse sequences in magic-angle spinning solid-state NMR, EMagRes 2 (3) (2013) 351–364, http://dx.doi.org/10.1002/9780470034590.emrstm1326.

[17] Y. Ji, L. Liang, X. Bao, G. Hou, Recent progress in dipolar recoupling techniques under fast MAS in solid-state NMR spectroscopy, Solid State Nucl. Magn. Reson. 112 (2021) 101711, http://dx.doi.org/10.1016/j.ssnmr.2020.101711.

[18] L. Liang, Y. Ji, K. Chen, P. Gao, Z. Zhao, G. Hou, Solid-state NMR dipolar and chemical shift anisotropy recoupling techniques for structural and dynamical studies in biological systems, Chem. Rev. 122 (10) (2022) 9880–9942, http://dx.doi.org/10.1021/acs.chemrev.1c00779.

[19] V. Ladizhansky, R.S. Palani, M. Mardini, R.G. Griffin, Dipolar recoupling in rotating solids, Chem. Rev. 124 (22) (2024) 12844–12917, http://dx.doi.org/10.1021/acs.chemrev.4c00373.

[20] S. Vega, Floquet theory, EMagRes (2007) http://dx.doi.org/10.1002/9780470034590.emrstm0167.

[21] A.D. Bain, R.S. Dumont, Introduction to floquet theory: The calculation of spinning sideband intensities in magic-angle spinning NMR, Concepts Magn. Reson. 13 (3) (2001) 159–170, http://dx.doi.org/10.1002/cmr.1006.

[22] K.L. Ivanov, K.R. Mote, M. Ernst, A. Equbal, P.K. Madhu, Floquet theory in magnetic resonance: Formalism and applications, Prog. Nucl. Magn. Reson. Spectrosc. 126–127 (2021) 17–58, http://dx.doi.org/10.1016/j.pnmrs.2021.05.002.

[23] P. Madhu, N.D. Kurur, Fer expansion for effective propagators and Hamiltonians in NMR, Chem. Phys. Lett. 418 (1) (2006) 235–238, http://dx.doi.org/10.1016/j.cplett.2005.10.134.

[24] K. Takegoshi, N. Miyazawa, K. Sharma, P.K. Madhu, Comparison among Magnus/Floquet/Fer expansion schemes in solid-state NMR, J. Chem. Phys. 142 (13) (2015) 134201, http://dx.doi.org/10.1063/1.4916324.

[25] M. Edén, Computer simulations in solid-state NMR. I. Spin dynamics theory, Concepts Magn. Reson. A 17A (1) (2003) 117–154, http://dx.doi.org/10.1002/cmr.a.10061.

[26] M. Edén, Computer simulations in solid-state NMR. II. Implementations for static and rotating samples, Concepts Magn. Reson. A 18A (1) (2003) 1–23, http://dx.doi.org/10.1002/cmr.a.10064.

[27] M. Edén, Computer simulations in solid-state NMR. III. Powder averaging, Concepts Magn. Reson. A 18A (1) (2003) 24–55, http://dx.doi.org/10.1002/cmr.a.10065.

[28] D.A. Varshalovich, A.N. Moskalev, V.K. Khersonskii, Quantum Theory of Angular Momentum, World Scientific, Singapore, 1988.

[29] O.N. Antzutkin, Sideband manipulation in magic-angle-spinning nuclear magnetic resonance, Prog. Nucl. Magn. Reson. Spectrosc. 35 (3) (1999) 203–266, http://dx.doi.org/10.1016/S0079-6565(99)00010-2.

[30] M.M. Maricq, J.S. Waugh, NMR in rotating solids, J. Chem. Phys. 70 (7) (1979) 3300–3316, http://dx.doi.org/10.1063/1.437915.

[31] R.R. Ernst, G. Bodenhausen, A. Wokaun, Principles of Nuclear Magnetic Resonance in One and Two Dimensions, in: International Series of Monographs on Chemistry, number 14, Oxford University Press, Oxford, UK, 1997.

[32] M.H. Levitt, Spin Dynamics: Basics of Nuclear Magnetic Resonance, second ed., Wiley, Chichester, England, 2008.

[33] G.E. Pake, Nuclear resonance absorption in hydrated crystals: Fine structure of the proton line, J. Chem. Phys. 16 (4) (1948) 327–336, http://dx.doi.org/10.1063/1.1746878.

[34] Wolfram Research Inc., Mathematica, Wolfram Research Inc., Champaign, Illinois, 2024, https://www.wolfram.com/mathematica.

[35] C. Bengs, M.H. Levitt, SpinDynamica: Symbolic and numerical magnetic resonance in a Mathematica environment, Magn. Reson. Chem. 56 (6) (2017) 374–414, http://dx.doi.org/10.1002/mrc.4642.

[36] S.R. Hartmann, E.L. Hahn, Nuclear double resonance in the rotating frame, Phys. Rev. 128 (5) (1962) 2042–2053, http://dx.doi.org/10.1103/PhysRev.128.2042.

[37] A. Pines, M.G. Gibby, J.S. Waugh, Proton-enhanced NMR of dilute spins in solids, J. Chem. Phys. 59 (2) (1973) 569–590, http://dx.doi.org/10.1063/1.1680061.

[38] J. Schaefer, E.O. Stejskal, Carbon-13 nuclear magnetic resonance of polymers spinning at the magic angle, J. Am. Chem. Soc. 98 (4) (1976) 1031–1032, http://dx.doi.org/10.1021/ja00420a036.

[39] E.O. Stejskal, J. Schaefer, J.S. Waugh, Magic-angle spinning and polarization transfer in proton-enhanced NMR, J. Magn. Reson. 28 (1) (1977) 105–112, http://dx.doi.org/10.1016/0022-2364(77)90260-8.

[40] T.G. Oas, R.G. Griffin, M.H. Levitt, Rotary resonance recoupling of dipolar interactions in solid-state nuclear magnetic resonance spectroscopy, J. Chem. Phys. 89 (2) (1988) 692–695, http://dx.doi.org/10.1063/1.455191.

[41] M.H. Levitt, T.G. Oas, R.G. Griffin, Rotary resonance recoupling in heteronuclear spin pair systems, Isr. J. Chem. 28 (4) (1988) 271–282, http://dx.doi.org/10.1002/ijch.198800039.

[42] A. Naito, K. Nishimura, S. Kimura, S. Tuzi, M. Aida, N. Yasuoka, H. Saitô, Determination of the three-dimensional structure of a new crystalline form of *N*-acetyl-Pro-Gly-Phe as revealed by ^{13}C REDOR, X-Ray diffraction, and molecular dynamics calculation, J. Phys. Chem. 100 (36) (1996) 14995–15004, http://dx.doi.org/10.1021/jp960179t.

[43] C.P. Jaroniec, B.A. Tounge, C.M. Rienstra, J. Herzfeld, R.G. Griffin, Recoupling of heteronuclear dipolar interactions with rotational-echo double-resonance at high magic-angle spinning frequencies, J. Magn. Reson. 146 (1) (2000) 132–139, http://dx.doi.org/10.1006/jmre.2000.2128.

[44] K. Saalwächter, R. Graf, H.W. Spiess, Recoupled polarization transfer heteronuclear ^{1}H–^{13}C multiple-quantum correlation in solids under ultra-fast MAS, J. Magn. Reson. 140 (2) (1999) 471–476, http://dx.doi.org/10.1006/jmre.1999.1856.

[45] K. Saalwächter, R. Graf, H.W. Spiess, Recoupled polarization-transfer methods for solid-state ^{1}H–^{13}C heteronuclear correlation in the limit of fast MAS, J. Magn. Reson. 148 (2) (2001) 398–418, http://dx.doi.org/10.1006/jmre.2000.2259.

[46] M.G. Jain, K.R. Mote, J. Hellwagner, G. Rajalakshmi, M. Ernst, P.K. Madhu, V. Agarwal, Measuring strong one-bond dipolar couplings using REDOR in magic-angle spinning solid-state NMR, J. Chem. Phys. 150 (13) (2019) 134201, http://dx.doi.org/10.1063/1.5088100.

[47] K.T. Mueller, Analytic solutions for the time evolution of dipolar-dephasing NMR signals, J. Magn. Reson. A 113 (1) (1995) 81–93, http://dx.doi.org/10.1006/jmra.1995.1059.

[48] K.T. Mueller, T.P. Jarvie, D.J. Aurentz, B.W. Robert, The REDOR transform: direct calculation of internuclear couplings from dipolar-dephasing NMR data, Chem. Phys. Lett. 242 (6) (1995) 535–542, http://dx.doi.org/10.1016/0009-2614(95)00773-W.

[49] F.G. Vogt, D.J. Aurentz, K.T. Mueller, Determination of internuclear distances from solid-state nuclear magnetic resonance: dipolar transforms and regularization methods, Mol. Phys. 95 (5) (1998) 907–919, http://dx.doi.org/10.1080/002689798166530.

[50] M. Abramowitz, I.A. Stegun (Eds.), Handbook of Mathematical Functions, Dover Publications, New York, USA, 1965.

[51] D. Zwillinger, V. Moll, I. Gradshteyn, I. Ryzhik (Eds.), Table of Integrals, Series, and Products, eighth ed., Academic Press, Boston, USA, 2014, pp. 1014–1059, http://dx.doi.org/10.1016/B978-0-12-384933-5.00009-6.

[52] K.J. MacKenzie, M.E. Smith, Experimental approaches, in: K.J. MacKenzie, M.E. Smith (Eds.), Multinuclear Solid-State NMR of Inorganic Materials, in: Pergamon Materials Series, vol. 6, Pergamon, New York, USA, 2002, pp. 111–197, http://dx.doi.org/10.1016/S1470-1804(02)80004-9.

[53] C.P. Jaroniec, Dipolar recoupling: Heteronuclear, EMagRes (2009) http://dx.doi.org/10.1002/9780470034590.emrstm1011.

[54] A. Goldbourt, Distance measurements to quadrupolar nuclei: Evolution of the rotational echo double resonance technique, Magn. Reson. Chem. 59 (9–10) (2021) 908–919, http://dx.doi.org/10.1002/mrc.5150.

[55] A.A. Shcherbakov, J. Medeiros-Silva, N. Tran, M.D. Gelenter, M. Hong, From angstroms to nanometers: Measuring interatomic distances by solid-state NMR, Chem. Rev. 122 (10) (2022) 9848–9879, http://dx.doi.org/10.1021/acs.chemrev.1c00662.

[56] N.C. Nielsen, H. Bildsøe, H.J. Jakobsen, M.H. Levitt, Double-quantum homonuclear rotary resonance: Efficient dipolar recovery in magic-angle spinning nuclear magnetic resonance, J. Chem. Phys. 101 (3) (1994) 1805–1812, http://dx.doi.org/10.1063/1.467759.

[57] A. Brinkmann, M.H. Levitt, Symmetry principles in the nuclear magnetic resonance of spinning solids: Heteronuclear recoupling by generalized Hartmann–Hahn sequences, J. Chem. Phys. 115 (1) (2001) 357–384, http://dx.doi.org/10.1063/1.1377031.

[58] C. Martineau, B. Bouchevreau, F. Taulelle, J. Trébosc, O. Lafon, J.-P. Amoureux, High-resolution through-space correlations between spin-1/2 and half-integer quadrupolar nuclei using the MQ-*D*-R-INEPT NMR experiment, Phys. Chem. Chem. Phys. 14 (19) (2012) 7112–7119, http://dx.doi.org/10.1039/c2cp40344g.

[59] G. Pileio, M. Concistrè, N. McLean, A. Gansmüller, R.C. Brown, M.H. Levitt, Analytical theory of γ-encoded double-quantum recoupling sequences in solid-state nuclear magnetic resonance, J. Magn. Reson. 186 (1) (2007) 65–74, http://dx.doi.org/10.1016/j.jmr.2007.01.009.

[60] T. Gullion, D.B. Baker, M.S. Conradi, New, compensated Carr–Purcell sequences, J. Magn. Reson. 89 (3) (1990) 479–484, http://dx.doi.org/10.1016/0022-2364(90)90331-3.

[61] M.J. Lizak, T. Gullion, M.S. Conradi, Measurement of like-spin dipole couplings, J. Magn. Reson. 91 (2) (1991) 254–260, http://dx.doi.org/10.1016/0022-2364(91)90190-5.

[62] T. Gullion, J. Schaefer, Elimination of resonance offset effects in rotational-echo, double-resonance NMR, J. Magn. Reson. 92 (2) (1991) 439–442, http://dx.doi.org/10.1016/0022-2364(91)90286-3.

[63] T. Gullion, The effect of amplitude imbalance on compensated Carr–Purcell sequences, J. Magn. Reson. A 101 (3) (1993) 320–323, http://dx.doi.org/10.1006/jmra.1993.1050.

[64] H.Y. Carr, E.M. Purcell, Effects of diffusion on free precession in nuclear magnetic resonance experiments, Phys. Rev. 94 (3) (1954) 630–638, http://dx.doi.org/10.1103/PhysRev.94.630.

[65] S. Meiboom, D. Gill, Modified spin-echo method for measuring nuclear relaxation times, Rev. Sci. Instrum. 29 (8) (1958) 688–691, http://dx.doi.org/10.1063/1.1716296.

[66] M.H. Levitt, R. Freeman, Composite pulse decoupling, J. Magn. Reson. 43 (3) (1981) 502–507, http://dx.doi.org/10.1016/0022-2364(81)90066-4.

[67] M.H. Levitt, R. Freeman, T. Frenkiel, Broadband heteronuclear decoupling, J. Magn. Reson. 47 (2) (1982) 328–330, http://dx.doi.org/10.1016/0022-2364(82)90124-X.

[68] M.H. Levitt, R. Freeman, T. Frenkiel, Supercycles for broadband heteronuclear decoupling, J. Magn. Reson. 50 (1) (1982) 157–160, http://dx.doi.org/10.1016/0022-2364(82)90042-7.

[69] M.H. Levitt, R. Freeman, T. Frenkiel, Broadband decoupling in high-resolution nuclear magnetic resonance spectroscopy, in: J.S. Waugh (Ed.), Advances in Magnetic Resonance, vol. 11, Academic Press, New York, USA, 1983, pp. 47–110.

[70] A.A. Maudsley, Modified Carr-Purcell-Meiboom-Gill sequence for NMR fourier imaging applications, J. Magn. Reson. 69 (3) (1986) 488–491, http://dx.doi.org/10.1016/0022-2364(86)90160-5.

[71] C.P. Jaroniec, B.A. Tounge, J. Herzfeld, R.G. Griffin, Frequency selective heteronuclear dipolar recoupling in rotating solids: Accurate ^{13}C–^{15}N distance measurements in uniformly ^{13}C, ^{15}N-labeled peptides, J. Am. Chem. Soc. 123 (15) (2001) 3507–3519, http://dx.doi.org/10.1021/ja003266e.

[72] M.G. Munowitz, R.G. Griffin, Two-dimensional nuclear magnetic resonance in rotating solids: An analysis of line shapes in chemical shift-dipolar spectra, J. Chem. Phys. 76 (6) (1982) 2848–2858, http://dx.doi.org/10.1063/1.443386.

[73] M. Munowitz, W.P. Aue, R.G. Griffin, Two-dimensional separation of dipolar and scaled isotropic chemical shift interactions in magic angle NMR spectra, J. Chem. Phys. 77 (4) (1982) 1686–1689, http://dx.doi.org/10.1063/1.444064.

[74] M.G. Jain, G. Rajalakshmi, V. Agarwal, P. Madhu, K.R. Mote, On the direct relation between REDOR and DIPSHIFT experiments in solid-state NMR, J. Magn. Reson. 308 (2019) 106563, http://dx.doi.org/10.1016/j.jmr.2019.07.050.

[75] M.G. Jain, G. Rajalakshmi, P.K. Madhu, V. Agarwal, K.R. Mote, Overcoming prohibitively large radiofrequency demands for the measurement of internuclear distances with solid-state NMR under fast magic-angle spinning, J. Phys. Chem. B 124 (8) (2020) 1444–1451, http://dx.doi.org/10.1021/acs.jpcb.9b11849.

[76] I. Schnell, K. Saalwächter, ^{15}N–^{1}H bond length determination in natural abundance by inverse detection in fast-MAS solid-state NMR spectroscopy, J. Am. Chem. Soc. 124 (37) (2002) 10938–10939, http://dx.doi.org/10.1021/ja026657x.

[77] P. Schanda, B.H. Meier, M. Ernst, Quantitative analysis of protein backbone dynamics in microcrystalline ubiquitin by solid-state NMR spectroscopy, J. Am. Chem. Soc. 132 (45) (2010) 15957–15967, http://dx.doi.org/10.1021/ja100726a.

[78] P. Schanda, B.H. Meier, M. Ernst, Accurate measurement of one-bond H–X heteronuclear dipolar couplings in MAS solid-state NMR, J. Magn. Reson. 210 (2) (2011) 246–259, http://dx.doi.org/10.1016/j.jmr.2011.03.015.

[79] A. Brinkmann, A.P.M. Kentgens, Sensitivity enhancement and heteronuclear distance measurements in biological ^{17}O solid-state NMR, J. Phys. Chem. B 110 (32) (2006) 16089–16101, http://dx.doi.org/10.1021/jp062809p.

[80] A. Brinkmann, A.P.M. Kentgens, Proton selective ^{17}O–^{1}H distance measurements in fast magic-angle-spinning solid-state NMR spectroscopy for the determination of hydrogen bond lengths, J. Am. Chem. Soc. 128 (46) (2006) 14758–14759, http://dx.doi.org/10.1021/ja065415k.

[81] J.S. Waugh, L.M. Huber, U. Haeberlen, Approach to high-resolution NMR in solids, Phys. Rev. Lett. 20 (5) (1968) 180–182, http://dx.doi.org/10.1103/PhysRevLett.20.180.

[82] P. Mansfield, Symmetrized pulse sequences in high resolution NMR in solids, J. Phys. C 4 (11) (1971) 1444–1452, http://dx.doi.org/10.1088/0022-3719/4/11/020.

[83] P. Mansfield, M.J. Orchard, D.C. Stalker, K.H.B. Richards, Symmetrized multipulse nuclear-magnetic-resonance experiments in solids: Measurement of the chemical-shift shielding tensor in some compounds, Phys. Rev. B 7 (1) (1973) 90–105, http://dx.doi.org/10.1103/PhysRevB.7.90.

[84] W.-K. Rhim, D.D. Elleman, R.W. Vaughan, Analysis of multiple pulse NMR in solids, J. Chem. Phys. 59 (7) (1973) 3740–3749, http://dx.doi.org/10.1063/1.1680545.

[85] D.P. Burum, W.K. Rhim, Analysis of multiple pulse NMR in solids. III, J. Chem. Phys. 71 (2) (1979) 944–956, http://dx.doi.org/10.1063/1.438385.

[86] D.P. Burum, M. Linder, R.R. Ernst, Low-power multipulse line narrowing in solid-state NMR, J. Magn. Reson. 44 (1) (1981) 173–188, http://dx.doi.org/10.1016/0022-2364(81)90200-6.

[87] J. Ashida, D. Rice, Frequency-switched decoupling methods for solids NMR on UNITY *INOVA* and UNITY*plus*, Magn. Moments 8 (1) (1996) 19–20, a Varian publication.

[88] B.M. Fung, K. Ermolaev, Y. Yu, ^{13}C NMR of liquid crystals with different proton homonuclear dipolar decoupling methods, J. Magn. Reson. 138 (1) (1999) 28–35, http://dx.doi.org/10.1006/jmre.1999.1723.

[89] E. Vinogradov, P.K. Madhu, S. Vega, High-resolution proton solid-state NMR spectroscopy by phase-modulated Lee–Goldburg experiment, Chem. Phys. Lett. 314 (5–6) (1999) 443–450, http://dx.doi.org/10.1016/S0009-2614(99)01174-4.

[90] M.E. Halse, L. Emsley, Improved phase-modulated homonuclear dipolar decoupling for solid-state NMR spectroscopy from symmetry considerations, J. Phys. Chem. A 117 (25) (2013) 5280–5290, http://dx.doi.org/10.1021/jp4038733.

[91] M.E. Halse, J. Schlagnitweit, L. Emsley, High-resolution ^{1}H solid-state NMR spectroscopy using windowed LG4 homonuclear dipolar decoupling, Isr. J. Chem. 54 (1–2) (2014) 136–146, http://dx.doi.org/10.1002/ijch.201300101.

[92] B.C. Gerstein, R.G. Pembleton, R.C. Wilson, L.M. Ryan, High resolution NMR in randomly oriented solids with homonuclear dipolar broadening: Combined multiple pulse NMR and magic angle spinning, J. Chem. Phys. 66 (1) (1977) 361–362, http://dx.doi.org/10.1063/1.433638.

[93] D. Sakellariou, A. Lesage, P. Hodgkinson, L. Emsley, Homonuclear dipolar decoupling in solid-state NMR using continuous phase modulation, Chem. Phys. Lett. 319 (3–4) (2000) 253–260, http://dx.doi.org/10.1016/S0009-2614(00)00127-5.

[94] A. Lesage, D. Sakellariou, S. Hediger, B. Eléna, P. Charmont, S. Steuernagel, L. Emsley, Experimental aspects of proton NMR spectroscopy in solids using phase-modulated homonuclear dipolar decoupling, J. Magn. Reson. 163 (1) (2003) 105–113, http://dx.doi.org/10.1016/S1090-7807(03)00104-6.

[95] B. Elena, G. de Paëpe, L. Emsley, Direct spectral optimisation of proton–proton homonuclear dipolar decoupling in solid-state NMR, Chem. Phys. Lett. 398 (4–6) (2004) 532–538, http://dx.doi.org/10.1016/j.cplett.2004.09.122.

[96] F.M. Paruzzo, L. Emsley, High-resolution ^{1}H NMR of powdered solids by homonuclear dipolar decoupling, J. Magn. Reson. 309 (2019) 106598, http://dx.doi.org/10.1016/j.jmr.2019.106598.

[97] F. Fillaux, N. Leygue, J. Tomkinson, A. Cousson, W. Paulus, Structure and dynamics of the symmetric hydrogen bond in potassium hydrogen maleate: a neutron scattering study, Chem. Phys. 244 (2) (1999) 387–403, http://dx.doi.org/10.1016/S0301-0104(99)00153-6.

[98] A. Achlama (Chmelnick), U. Kohlschütter, U. Haeberlen, Proton shielding tensors in potassium hydrogen maleate, Chem. Phys. 7 (2) (1975) 287–293, http://dx.doi.org/10.1016/0301-0104(75)87010-8.

[99] D.H. Brouwer, M. Horvath, Minimizing the effects of RF inhomogeneity and phase transients allows resolution of two peaks in the ^{1}H CRAMPS NMR spectrum of adamantane, Solid State Nucl. Magn. Reson. 71 (2015) 30–40, http://dx.doi.org/10.1016/j.ssnmr.2015.10.005.

[100] S. Hayashi, K. Hayamizu, Chemical shift standards in high-resolution solid-state NMR (1) ^{13}C, ^{29}Si, and ^{1}H nuclei, Bull. Chem. Soc. Jpn. 64 (2) (1991) 685–687, http://dx.doi.org/10.1246/bcsj.64.685.

[101] R.P. Young, C.R. Lewis, C. Yang, L. Wang, J.K. Harper, L.J. Mueller, TensorView: A software tool for displaying NMR tensors, Magn. Reson. Chem. 57 (5) (2019) 211–223, http://dx.doi.org/10.1002/mrc.4793.

[102] D.M. Grant, Chemical shift tensors, EMagRes (2007) http://dx.doi.org/10.1002/9780470034590.emrstm0074.

[103] M. Bak, N.C. Nielsen, SIMPSON: A general simulation program for solid-state NMR spectroscopy, J. Magn. Reson. 147 (2) (2000) 296–330, http://dx.doi.org/10.1006/jmre.2000.2179.

[104] T. Vosegaard, Z. Tošner, N.C. Nielsen, Numerical simulations in solid-state NMR with simpson, EMagRes (2010) http://dx.doi.org/10.1002/9780470034590.emrstm1097.

[105] Z. Tošner, R. Andersen, B. Stevensson, M. Edén, N.C. Nielsen, T. Vosegaard, Computer-intensive simulation of solid-state NMR experiments using SIMPSON, J. Magn. Reson. 246 (2014) 79–93, http://dx.doi.org/10.1016/j.jmr.2014.07.002.

[106] D.L. Bryce, Tensor interplay, EMagRes (2008) http://dx.doi.org/10.1002/9780470034590.emrstm1039.

[107] M. Mehring, Principles of High Resolution NMR in Solids, second ed., Springer-Verlag, Berlin, Germany, 1983.

[108] K. Aebischer, M. Ernst, Residual proton line width under refocused frequency-switched Lee–Goldburg decoupling in MAS NMR, Phys. Chem. Chem. Phys. 25 (17) (2023) 11959–11970, http://dx.doi.org/10.1039/D3CP00414G.

[109] J. Hellwagner, L. Grunwald, M. Ochsner, D. Zindel, B.H. Meier, M. Ernst, Origin of the residual line width under frequency-switched Lee–Goldburg decoupling in MAS solid-state NMR, Magn. Reson. 1 (1) (2020) 13–25, http://dx.doi.org/10.5194/mr-1-13-2020.

[110] K.R. Mote, V. Agarwal, P. Madhu, Five decades of homonuclear dipolar decoupling in solid-state NMR: Status and outlook, Prog. Nucl. Magn. Reson. Spectrosc. 97 (2016) 1–39, http://dx.doi.org/10.1016/j.pnmrs.2016.08.001.

[111] J. Tognetti, W.T. Franks, J.R. Lewandowski, S.P. Brown, Optimisation of ^{1}h PMLG homonuclear decoupling at 60 kHz MAS to enable ^{15}N–^{1}H through-bond heteronuclear correlation solid-state NMR spectroscopy, Phys. Chem. Chem. Phys. 24 (34) (2022) 20258–20273, http://dx.doi.org/10.1039/D2CP01041K.

[112] Y.T.A. Wong, R.L.E.G. Aspers, M. Uusi-Penttilä, A.P.M. Kentgens, Rapid quantification of pharmaceuticals via ^{1}H solid-state NMR spectroscopy, Anal. Chem. 94 (48) (2022) 16667–16674, http://dx.doi.org/10.1021/acs.analchem.2c02905.

[113] D. Stueber, Z.E.X. Dance, Component quantification in solids with the mixture analysis using references method, Anal. Chem. 92 (16) (2020) 11095–11102, http://dx.doi.org/10.1021/acs.analchem.0c01045.

[114] Y. Nishiyama, G. Hou, V. Agarwal, Y. Su, A. Ramamoorthy, Ultrafast magic angle spinning solid-state NMR spectroscopy: Advances in methodology and applications, Chem. Rev. 123 (3) (2023) 918–988, http://dx.doi.org/10.1021/acs.chemrev.2c00197.

[115] N. Schröder, E. Bartalucci, T. Wiegand, Probing noncovalent interactions by fast magic-angle spinning NMR at 100 kHz and more, ChemPhysChem 25 (20) (2024) e202400537, http://dx.doi.org/10.1002/cphc.202400537.

[116] Y.K. Lee, N.D. Kurur, M. Helmle, O.G. Johannessen, N.C. Nielsen, M.H. Levitt, Efficient dipolar recoupling in the NMR of rotating solids. A sevenfold symmetric radiofrequency pulse sequence, Chem. Phys. Lett. 242 (3) (1995) 304–309, http://dx.doi.org/10.1016/0009-2614(95)00741-L.

[117] M. Edén, M.H. Levitt, Pulse sequence symmetries in the nuclear magnetic resonance of spinning solids: Application to heteronuclear decoupling, J. Chem. Phys. 111 (4) (1999) 1511–1519, http://dx.doi.org/10.1063/1.479410.

[118] A. Brinkmann, M. Edén, M.H. Levitt, Synchronous helical pulse sequences in magic-angle spinning nuclear magnetic resonance: Double quantum recoupling of multiple-spin systems, J. Chem. Phys. 112 (19) (2000) 8539–8554, http://dx.doi.org/10.1063/1.481458.

[119] M. Carravetta, M. Edén, X. Zhao, A. Brinkmann, M.H. Levitt, Symmetry principles for the design of radiofrequency pulse sequences in the nuclear magnetic resonance of rotating solids, Chem. Phys. Lett. 321 (3–4) (2000) 205–215, http://dx.doi.org/10.1016/S0009-2614(00)00340-7.

[120] The mpmath development team, mpmath: a Python library for arbitrary-precision floating-point arithmetic (version 1.3.0), 2023, http://mpmath.org/.

[121] B.J. Laurenzi, Special values of the Lommel functions and associated integrals, 2019, http://dx.doi.org/10.48550/arXiv.1901.03384, arXiv.

[122] W. Magnus, F. Oberhettinger, R.P. Soni, Formulas and Theorems for the Special Functions of Mathematical Physics, first ed., in: Grundlehren der Mathematischen Wissenschaften, vol. 52, Springer-Verlag, Berlin Heidelberg, Germany, 1966, http://dx.doi.org/10.1007/978-3-662-11761-3.

[123] S.A. Smith, W.E. Palke, J.T. Gerig, The Hamiltonians of NMR. Part I, Concepts Magn. Reson. 4 (2) (1992) 107–144, http://dx.doi.org/10.1002/cmr.1820040202.

[124] S.A. Smith, W.E. Palke, J.T. Gerig, The Hamiltonians of NMR. Part II, Concepts Magn. Reson. 4 (3) (1992) 181–204, http://dx.doi.org/10.1002/cmr.1820040302.

[125] S.A. Smith, W.E. Palke, J.T. Gerig, The Hamiltonians of NMR. Part III, Concepts Magn. Reson. 5 (2) (1993) 151–177, http://dx.doi.org/10.1002/cmr.1820050204.

[126] S.A. Smith, W.E. Palke, J.T. Gerig, The Hamiltonians of NMR. Part IV: NMR relaxation, Concepts Magn. Reson. 6 (2) (1994) 137–162, http://dx.doi.org/10.1002/cmr.1820060205.

[127] M. Edén, Zeeman truncation in NMR. I. The role of operator commutation, Concepts Magn. Reson. A 43 (4) (2014) 91–108, http://dx.doi.org/10.1002/cmr.a.21319.

[128] M. Edén, Zeeman truncation in NMR. II. Time averaging in the rotating frame, Concepts Magn. Reson. A 43 (4) (2014) 109–126, http://dx.doi.org/10.1002/cmr.a.21301.

[129] M.H. Levitt, The signs of frequencies and phases in NMR, J. Magn. Reson. 126 (2) (1997) 164–182, http://dx.doi.org/10.1006/jmre.1997.1161.

[130] M.H. Levitt, O.G. Johannessen, Signs of frequencies and phases in NMR: The role of radiofrequency mixing, J. Magn. Reson. 142 (1) (2000) 190–194, http://dx.doi.org/10.1006/jmre.1999.1929.

[131] R.K. Harris, E.D. Becker, S.M. Cabral de Menezes, P. Granger, R.E. Hoffman, K.W. Zilm, Further conventions for NMR shielding and chemical shifts (IUPAC recommendations 2008), Pure Appl. Chem. 80 (1) (2008) 59–84, http://dx.doi.org/10.1351/pac200880010059.

[132] J. Mason, Conventions for the reporting of nuclear magnetic shielding (or shift) tensors suggested by participants in the NATO ARW on NMR shielding constants at the University of Maryland, College Park, July 1992, Solid State Nucl. Magn. Reson. 2 (5) (1993) 285–288, http://dx.doi.org/10.1016/0926-2040(93)90010-K.

[133] C.J. Jameson, Reply to 'conventions for tensor quantities used in nuclear magnetic resonance, nuclear quadrupole resonance and electron spin resonance spectroscopy, Solid State Nucl. Magn. Reson. 11 (3) (1998) 265–268, http://dx.doi.org/10.1016/S0926-2040(98)00029-0.